12-16-2020 10:30 AM

Intensification of Clostridium pasteurianum Fermentation Producing n-Butanol From Glycerol using Microfiltration Cell Recycle

Colin W. Couper, *The University of Western Ontario*

Supervisor: Rehmann, Lars, *The University of Western Ontario*

A thesis submitted in partial fulfillment of the requirements for the Master of Engineering Science degree in Chemical and Biochemical Engineering

Abstract

This work demonstrates lab scale intensification of the fermentation of glycerol to 1-butanol using *Clostridum pasteurianum*, starting with simulation and comparison of different cell recycle arrangements, development of a cell recycle apparatus with an existing bioreactor, and demonstration of fermentation with the final system. Fermentations performed with the completed system showed that the cell recycle system was not significantly inhibitory to fermentation, and achieved a maximum apparent cell dry weight of 3.14g/L and a maximum butanol productivity of 1.16g/Lh.

Keywords

Butanol, glycerol, fermentation, biofuel, cell recycle, fed batch, microfiltration, simulation, intensification

Summary for Lay Audience

This thesis covers the development of a system for conversion of glycerol into butanol. The source of glycerol is intended to be crude glycerol, a byproduct of biodiesel production, and butanol can be used as a carbon-neutral replacement for gasoline, which unlike other biofuels does not require mixing or modification for current gasoline engines.

To produce butanol from glycerol the bacteria, *Clostridum pasteurianum*, was used. This organism produces a number of valuable compounds when grown on glycerol, one of which is butanol. These compounds are inhibitory to the organism, which slows fermentation and decreases productivity, so low glycerol concentrations are needed to prevent halting of fermentation. This, however, can result in low productivity, and intensification of the process by cell retention can be used to accommodate this low productivity by increasing dilution rate and thus volumetric productivity. In this case, this was performed using a cell recycle system which retains the cells in the bioreactor while process media can be continuously added and removed. In order to determine the best design of the cell recycle apparatus, simulations were performed and compared, then the system was built, demonstrated on water, and then multiple fermentations were performed demonstrating that the system does in fact intensity fermentation successfully, reaching cell concentrations that in other fermentations required four times greater glycerol concentration, and butanol productivity that in other fermentations required 50% greater glycerol concentration.

Co-Authorship Statement

This thesis was completed under the supervision of Dr Lars Rehmann.

Acknowledgments

I would like to thank Dr. Lars Rehmann for his patience, encouragement, and guidance during my studies at the University of Western Ontario. I have received a great deal of wisdom and support from Dr. Rehmann. I could not have completed this without his help, and I am extremely grateful.

I would also like to thank Dr. Erin Johnson and Dr. Garret Munch, who were partners in this project and mentors for me. They have been a great help on this project in every way possible both in and out of the lab.

I would also like to thank the many dear friends who have helped and supported me during my time at the University of Western Ontario.

Lastly, I would like to thank my family. My parents Ian and Jane Couper, and my brothers Jamie and Scott, for their love and support during this work.

Table of Contents

List of Tables

List of Figures

List of Equations

List of Appendices

Chapter 1

1 Introduction and Background

This chapter covers the value of using glycerol as an input to butanol production, and an introduction to fermentation basics, types of bioreactors and bioreactor setups, and intensification methods for bioreactors. This work is a part of a larger project of developing a system for the conversion of crude glycerol from biodiesel production to 1-butanol for use as a drop-in fuel or industrial solvent, outlined in Johnson et al, 2016 [1].

1.1 Value of Producing Butanol from Glycerol

1.1.1 Butanol: Characteristics, Production, Uses, and Market

Butanol also has uses as a reagent, solvent, and fuel. As fuel, butanol is considered a second-generation biofuel and has a number of advantages over ethanol, as it has a higher energy density, lower volatility, is less hygroscopic, and can be used directly in a gasoline engine without modification either blended or as pure butanol [2, 3].

Worldwide butanol production is currently sourced from petroleum, and the market size for n-butanol as a reagent and solvent is expected to grow at a CAGR of 6.5% and reach 6.74 billion USD by 2025 [4]. Production of biobutanol for use as a biofuel would be in addition to this already sizable market.

Butanol was originally produced industrially in an acetone-butanol-ethanol (ABE) fermentation, as these fermentations were done to produce acetone, and butanol was a by-product. ABE fermentations produce a lower product titer than other fermentations, as both acetone and butanol can be inhibitory, and require multiple steps to isolate the volatile products. Selected microorganisms known to produce of butanol are outlined in Table 1. Organisms that produce butanol only via genetic engineering, such as *Escherichia coli* (E. coli) and *Saccharomyces cerevisiae* (brewers and bakers yeast), are excluded.

Species	Products	Substrates	Source
Clostridium pasteruianum	1,3-propanediol (PDO), Butanol, Ethanol, Butyric Acid, Acetic Acid	Glucose, glycerol	[5]
Clostridium acetobutylicum	Acetone, Butanol, Ethanol,	Glucose	[6]
Clostridium beijerinckii	Acetone, Butanol, Ethanol	Glucose	[6]
Clostridium isopropylicum	Acetone, Butanol, Ethanol	Glucose, molasses	[6]
Clostridium saccharobutylicum	Acetone, Butanol, Ethanol, Butyric Acid, Acetic Acid	Pretreated algal biomass, glucose	[7]
Clostridium saccharoperbutylacetonicum	Acetone, Butanol, Ethanol	Glucose	[8]

Table 1: Industrially Relevant Microorganisms for Butanol production

A more recent approach uses a 1,3-propanediol-butanol-ethanol (PBE) fermentation, with glycerol as a substrate, which has benefits of simpler downstream processing and lower toxicity during fermentation due to the absence of acetone. A convenient source of glycerol is crude glycerol, a byproduct of biodiesel production [1].

1.1.2 Crude Glycerol: Characteristics, Uses, and Market

Glycerol can be cheaply sourced for butanol production as a byproduct of biodiesel production from triglycerides [1]. This is referred to as crude glycerol, as it is not fit for direct use in products but can be upgraded for uses in various markets. The quality of the input triglycerides limits the markets that the output crude glycerol can be sold to, that is to sell glycerol into a pharmaceutical market, the input triglyceride must be pharmaceutical grade. The same is true for food, or feed grade glycerol. An additional limitation is the quality of the biodiesel process, as greater contamination from undesirable byproducts limits the possible upgrading and the cost effectiveness of that upgrading, and because of this the characteristics of crude glycerol can vary widely depending on source. Ranges of crude glycerol characteristics can be seen in Table 2.

	pH	Density (g/cm^3)	Glycerol (%)	Moisture (%)	Ash (%)	Methanol (%)	MONG (%)
Min	2.0	1.07	38.4	0.0	0.0	<0.01	1.0
Max	10.8	1.26	96.5	16.1	29.4	13.94	57.0

Table 2 - Sample range of Crude Glycerol Characteristics. All percentage values are mass percent. MONG – Matter Organic, Non-Glycerol. Adapted from Hansen et al. **[9]**.

The worldwide glycerol market was worth 2.6 billion USD, is expected to reach 3.0 billion USD in 2020, and to continue growing at 4.0% from 2020 to 2027. The majority of this glycerol comes from biodiesel production (59%), however the greatest market demand is for refined glycerol, with 65% of revenue. The value of glycerol is highly dependent on the market it can be applied to, with food and pharmaceutical grade glycerol being the strictest [10].

Crude glycerol can alternatively be used as animal feed, or for production of chemicals such as citric acid, hydrogen, docosahexaenoic acid (DHA), and a variety of other products, in addition to producing 1,3-propanediol and butanol in *Clostridium pasteurianum* [11]. These uses still require pretreatment, where amount and degree of pretreatment varies.

Pretreatment of crude glycerol involves the removal of soaps, salts, methanol, water, and organic compounds other than glycerol. Methods of accomplishing glycerol include methods as simple as neutralizing with sulfuric or phosphoric acid, followed by centrifugation, to more complex procedures including multiple filtration steps or ion exchange, depending the quality of input crude glycerol and required quality of the output glycerol [12].

1.2 Research Objectives

i) Modelling and Comparison of Cell Recycle Configurations in General Fermentation

Generally, fermentations with cell recycle in the literature use a simple setup. This section investigates alternative arrangements, specifically two arrangements of Feed-and-Bleed, and demonstrates which are more productive, and how setups compare. We found that the Feed-and-Bleed system with Bioreactor Bleed has a benefit of 6% or 8% increase in productivity in the permeate stream compared to simple cell recycling, depending on the presence or absence of product inhibition, and 2% increased productivity when both outlet streams are combined, regardless of inhibition

ii) Design, Construction, and Integration of Benchtop Cell Recycle

Show considerations and design decisions for practical implementation of a cell recycle system. This includes development of a low-cost benchtop system with a minimal viable product approach using inexpensive materials, considerations for fluid transfer out of the reactor and through the membrane loop, demonstration of benchtop setup with DI water, and demonstration of main variables affecting permeate flow, membrane resistance, and flow limitations of the membrane,

iii) Demonstration of viability of cell recycle applied to *Clostridium pasteurianum*

Demonstrates that cells can grow in fed-batch arrangement with cell recycle apparatus attached, and similar results are produced in parallel fed-batch fermentations between arrangements with and without the cell recycle apparatus.

iv) Demonstration of increased cell concentration and productivity using cell recycle in continuous fermentation of *Clostridium pasteurianum*

Demonstrates effectiveness of cell recycle system at increasing cell concentration under low feed flow and low bleed flow, and increased butanol production with higher feed flow.

Chapter 2

2 Background and Literature Review

2.1.1 Basics of Cell Growth

Fermentation is the conversion of some substrate into a product by a microorganism, and the microorganism itself may be the product. The simplest example of a fermentation is a batch reactor with a single substrate and a single organism. This system follows a commonly used growth curve shown in Figure 1.

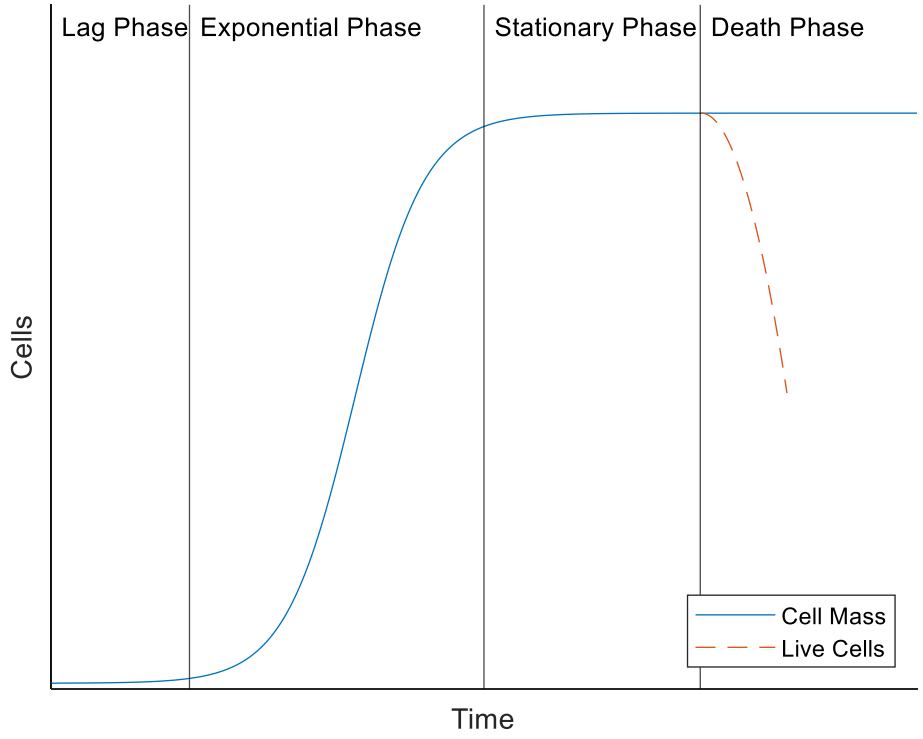

Figure 1: Arbitrary Growth Curve for a Batch System

The growth curve shown in Figure 1 follows the logistic curve initially proposed by Pierre Verhulst in 1845 [13, 14]. This was improved by Monod in 1942 by modelling the reaction rate using a function mirroring the Michaelis-Menten equation used for enzyme kinetics [15, 16, 14]. Differential equations defining reaction rates and mass balance in batch can be seen below in Table 3.

Reaction Name	Chemical Reaction	Rate Equation	
Enzyme reaction (Michaelis-Menten) [17]	$C_1 + E \rightarrow C_1E \rightarrow C_2E \rightarrow C_2 + E$	$\frac{dC_1}{dt} = -\frac{dC_2}{dt} = r_{max}\frac{C_1}{K_m + C_1};$	**2-1**
Biological Growth (Monod) [15]	$X_n + C_1 \rightarrow X_{n+1} + C_2$ $C_1 = S; C_2 = P$	$\frac{dX}{dt} = \mu X;\ \mu = \mu_{max}\frac{C_1}{K_s + C_1}$	**2-5**
		$\frac{dC_1}{dt} = -\frac{1}{Y_{XS}}\frac{dX}{dt}$	**2-6**
		$\frac{dC_2}{dt} = Y_{PS}\frac{dC_1}{dt}$	**2-7**
			2-8

Table 3: Reaction Rate Equations for Simple Chemical and Biological Systems. $\boldsymbol{C_1}$ refers to concentration reactant, $\boldsymbol{C_2}$ refers to concentration of product, $\boldsymbol{k}$ is a reaction constant, $\boldsymbol{r_{max}}$ is the maximum rate of reaction f given enzyme, $\mu_{\boldsymbol{max}}$ is the maximum specific growth rate for a given organism, $\boldsymbol{Y_{XS}}$ is the biomass yield per ur substrate (reactant), $\boldsymbol{Y_{PS}}$ is the product yield per unit substrate. These equations can all be further modified depending on the specific reactions.

Cell growth follows different kinetics than chemical reactions. The rate of reaction for biomass growth is the Monod equation, which follows a hyperbolic curve similar to the Michaelis-Menten equation. This curve can be seen in Figure 2.

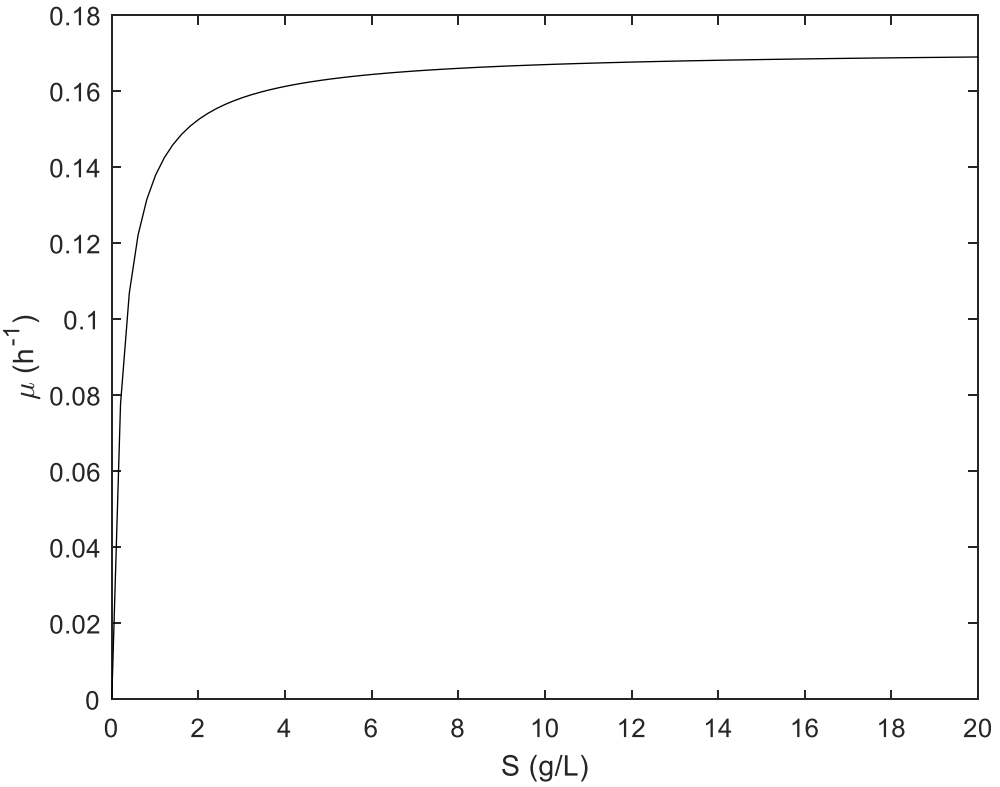

Figure 2: Specific growth rate vs substrate concentration from Monod Equation. μ=0.171, Ks=0.243.

Substrate consumption is directly proportional to biomass growth but adjusted by the yield of biomass per unit substrate, Y_{XS}. If the formation of a product is of interest, another yield constant is used to model this and can be based on biomass growth or substrate consumption (Y_{PS} or Y_{PX}). Substrate consumption is often preferred as the basis for product yield as substrate is often easier and more accurate to measure. In this work, all product formation is assumed to be growth associated. If product formation is metabolism associated and the majority of metabolic activity fuels biomass growth, then this assumption should also be appropriate. Monod kinetics can be expanded upon to include product inhibition, where the presence of a product slows growth, and substrate consumption from cell maintenance, but those are outside the scope of this work.

The Michaelis-Menten equation is derived from differential equations based on the interaction of substrate and enzyme in solution, whereas the Monod equation is empirical and relies on the assumption that the metabolism of a cell follows the same or similar kinetics as the enzymes it is made of. While the Monod equation does produce a

reasonable model of cellular growth, this model ignores the state of the cell, and cannot effectively model or predict lag, stationary, or death phases in batch. Additionally, the same organism in similar media may produce different kinetic parameters depending on the specifics of the fermentation. Mode of fermentation, that is batch, fed-batch, continuous, or other bioreactor arrangements, may produce different kinetic parameters as a result of the wide variety of variables that can affect the organism. Different concentrations of substrate, product, byproducts, cell remnants, other biomolecules, or other physical, chemical, or biological variables, can affect genetic response of the organism, inhibition or activation of enzymes and metabolic pathways, cell stress, and cell death, all in ways that can be difficult to predict, measure, or model. Microorganisms also go through different stages of growth and have complex physiological changes that are current areas of study [14].

All of these combined factors demonstrate the importance of understanding that Monod kinetic parameters, μ_{max} and K_s, are dependent on not just the organism but also on all other fermentation conditions, and that simulations of bioreactor systems should be viewed with skepticism and only considered a starting point for empirical verification. While this is true for any scientific endeavor, it is especially relevant in biological systems and fermentation as it is not immediately apparent that the reaction and characteristic parameters may change with a change in the system.

Monitoring cell growth is most directly measured by determining the number of cells using a cell count, where cells are placed on a counting chamber or hemocytometer, viewed under a microscope and manually counted. This method has the benefit of allowing for staining to indicate which cells are alive and dead. However, this method can have large variability between individual experimenters. An alternative to measuring the number of cells is measuring cell mass, which is approximated by cell dry weight (CDW). This method involves centrifuging or filtering a known volume of cell culture, washing with deionized water to remove media components other than cells, and then drying. Using cell dry weight does not give information for determining viability, but it is a more consistent method between experimenters [18].

2.1.2 Introduction to Bioreactors

A bioreactor is a vessel within which a biological reaction takes place, and can be categorized based on flows into, through, and out of the system, how it is mixed, and any special components that change the operation of the system. Which type of bioreactor and the degree and methods of control are based on the organism used and the goals of fermentation [19, 20].

The simplest type of bioreactor arrangement is the batch system, where media is put into a vessel, microorganisms are inoculated at the beginning of the fermentation, and fermentation broth is only removed after the reaction has finished. A fed-batch system is one where the initial volume of media in the bioreactor at the time of inoculation is low, and media is continuously added. Whether the rate of media addition changes depends on the specific fermentation, and may be periodically added instead of continuously added, which is referred to as charge batch. A system where media is continuously added while fermentation broth is continuously removed is called continuous, with the most common type being a Continuously Stirred-Tank Reactor (CSTR). A special case is a plug flow reactor (PFR) where the reactor is tubular and media flows through with either continuous addition of microorganisms at the beginning of the reactor, or microorganisms are immobilized within the reactor. These systems may or may not be mixed, or controlled for temperature and pH, depending on the needs and limitations of the systems. [19, 20]

Two important concepts for the economics of bioreactors are the yield of the reaction and the productivity of the reactor. The biological or biochemical yield is the change in the amount of the product of interest per unit substrate consumed. This could be biomass yield ($Y_{XS} = \frac{\Delta X}{\Delta S}, \frac{g\ biomass}{g\ substrate}$) or product yield ($Y_{PS} = \frac{\Delta P}{\Delta S}, \frac{g\ product}{g\ substrate}$). These values are needed for simulation of the bioreactor, however they can change in actual fermentation. For simplification of simulation they are assumed to be constant. [19, 20]

The second concept is productivity, which is dependent on the fermentation process. This is defined as the amount of a product produced in a given time and volume ($\frac{g}{L\ h}$). For

simple systems this can be simulated from the characteristics of the system, however for systems that require numerical analysis to solve the productivity must be determined from the output of the simulation [19, 20].

Parameter	Value
Maximum specific growth rate	$\mu_{max} = 0.171h^{-1}$
K_S	$K_S = 0.243g/L$
Biomass Yield	$Y_{XS} = 0.07$
Product Yield	$Y_{PS} = 0.29$
Inhibition Constant	$P_{Max} = 16g/L$
Total Volume	$V_{Total} = 5L$
Substrate Feed Concentration	$S_{in} = 20g/L$

Table 4: Parameters Used in Demonstration Simulations

2.1.3 Mass Balance and Models for Biological Systems

Mass and energy balance are foundational ideas in chemical engineering, describing the accumulation, change, and movement of mass for a system. A general mass balance is shown below. Energy balance is omitted as it is not the focus of this project, as the overall goal is to determine the feasibility of the system, not the cost effectiveness [19, 20].

$$\frac{d(VC)}{dt} = C_{system}\frac{dV}{dt} + V_{system}\frac{dC}{dt} = Q_{in}C_{in} + Q_{out}C_{out} + r_{reaction}V_{reactor}C_{reactor} \quad \textbf{2-9}$$

Applying this to biological systems gives the series of equations defining the systems for biomass (X), substrate (S), and product (P) and their solutions given in Table 5 below.

System	Differential Equations	
Batch	$\frac{dX}{dt} = \mu_{max}\left(\frac{S}{K_S + S}\right)X$	**2-1**
	$\frac{dS}{dt} = -\frac{1}{Y_{XS}}\frac{dX}{dt}$	**2-1**
	$\frac{dP}{dt} = Y_{PS}\frac{dS}{dt} = \frac{Y_{PS}}{Y_{XS}}\frac{dX}{dt}$	**2-1**
Fed-Batch	$\frac{dX}{dt} = \frac{Q_{in}(X_{in} - X)}{V} + \mu X$	**2-23**
	$\frac{dS}{dt} = \frac{Q_{in}(S_{in} - S)}{V} - \frac{1}{Y_{XS}}\mu X$	**2-21**
	$\frac{dP}{dt} = \frac{Y_{PS}}{Y_{XS}}\mu X$	**2-19**
	$\frac{dV}{dt} = Q_{in}$	**2-17**
Continuous	$\frac{dX}{dt} = \frac{Q_{in}(X_{in} - X)}{V} + \mu X = D(X_{in} - X) + \mu X$	**2-27**
	$\frac{dS}{dt} = \frac{Q_{in}(S_{in} - S)}{V} - \frac{1}{Y_{XS}}\mu X = D(S_{in} - S) - \frac{1}{Y_{XS}}\mu X$	**2-29**
	$\frac{dP}{dt} = \frac{Y_{PS}}{Y_{XS}}\mu X$	**2-25**

Table 5: Systems of Equations for Mass Balance on Biological Systems. X refers to biomass, S refers to substrate, P refers to product, $\boldsymbol{Y_{XS}}$ refers to biomass yield per unit substrate, $\boldsymbol{Y_{PS}}$ refers to product yield per unit substrate, μ is growth rate as defined by the Monod equation, μ_{max} is the specific growth rate, $\boldsymbol{K_S}$ is the half-velocity constant as used in the Monod equation, $\boldsymbol{Q_{in}}$ is feed flow rate, V is volume, D is dilution rate defined as $\boldsymbol{D = \frac{Q_{in}}{V}}$ **[19, 20].**

The batch system is the simplest of the three systems described in Table 5, however both fed-batch and continuous systems often start with a batch phase to produce an initial amount of biomass [19, 20]. A simulation of batch fermentation is shown in Figure 3 below.

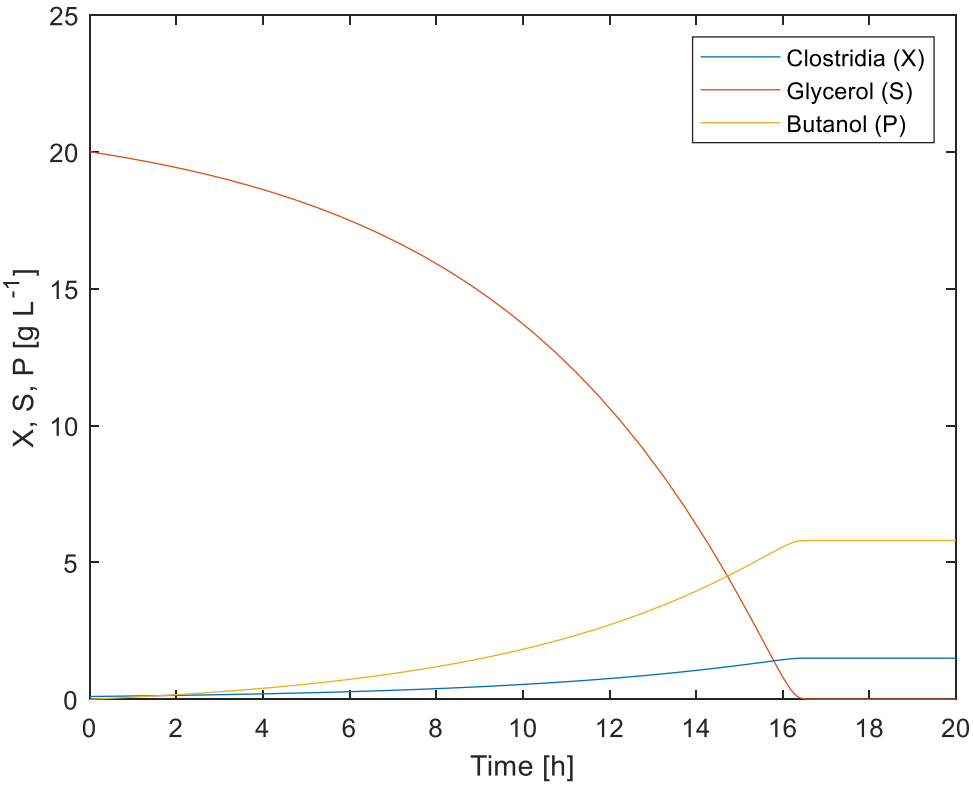

Figure 3: Simulation of Batch Fermentation of *Clostridium pasteurianum* Grown on Glycerol. Parameters for microbial growth can be found in Table 4. Equations for simulation can be found in Table 5.

For a batch system, productivity is defined by the time required to complete the fermentation, t_f, and the lag time required to clean and refill the bioreactor, t_l. This can all be summed into a single value for the time required to complete a single batch called cycle time ($t_c = t_f + t_l$). The productivity of a batch system is then the amount of biomass or product produced per cycle time, with batch productivity denoted by p_b. Assuming a batch reaction consumes all available substrate, this gives the equation for productivity below [19, 20].

$$p_{b,X} = \frac{Y_{XS}S_0}{t_c} \quad \textbf{2-31}$$

$$p_{b,P} = \frac{Y_{PS}S_0}{t_c} \quad \textbf{2-33}$$

Fed-batch fermentations are performed for a variety of reasons. In some cases, the goal of the fermentation is to maintain a low substrate concentration to encourage a particular metabolic pathway. The following simulation, shown in Figure 4 uses a low feed flow in order to draw out the duration of the fermentation, as this was done in the experiments discussed in Chapter 4, in order to demonstrate the viability of the cell recycle system [19, 20].

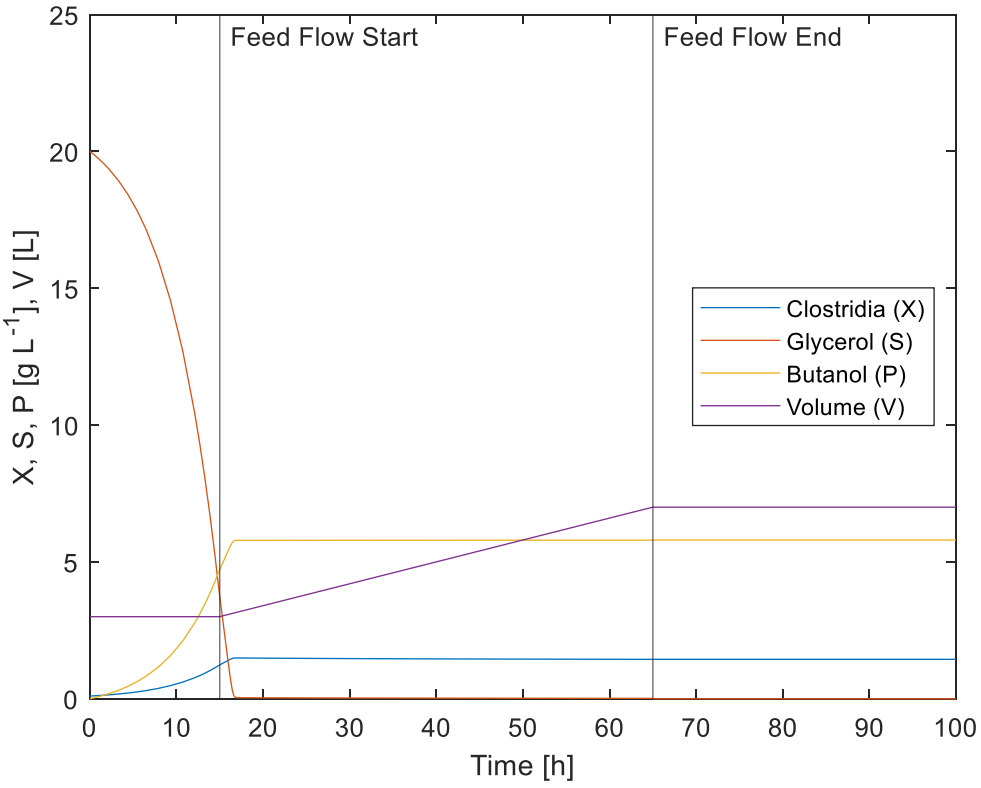

Figure 4: Fed-Batch Simulation of *Clostridium pasteurianum* Grown on Glycerol. This simulation used a flow rate of 0.08L/h, with an initial volume of 3L and final volume of 7L. Feed flow begins at 15h and ends at 65h. Parameters for microbial growth can be found in Table 4. Equations for simulation can be found in Table 5.

Productivity in fed-batch systems is defined by the same constants as a batch system. The only difference is operational, that the vessel is not completely filled prior to the beginning of reaction. Whether this increases or decreases productivity depends on the context. This could increase productivity if a very large vessel has to be filled by allowing fermentation to begin before the vessel is completely filled.

Continuous systems are used for higher productivity, as there is less downtime associated with cleaning, filling, emptying, or any other necessary non-fermentation activity. Similar to fed-batch, there is often a growth period at the beginning of fermentation followed by feed flow and then steady state [19, 20]. Simulations of a continuous fermentation at two feed flow rates are shown in Figure 5.

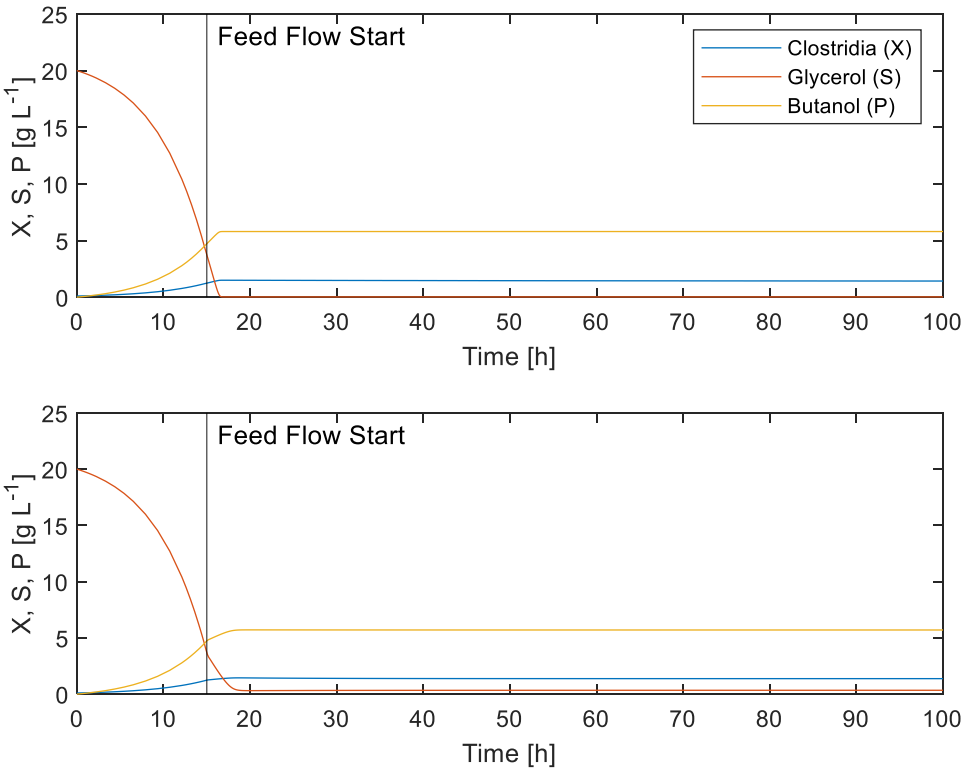

Figure 5: Simulations of Low and High Feed Flow Continuous Fermentations. These simulations used flow rates of 0.08L/h and 0.5L/h, with a volume of 5L. Feed flow begins at 15h. Parameters for microbial growth can be found in Table 4. Equations for simulation can be found in Table 5.

Here we can see when the feed flow begins at 15 hours into fermentation, biomass concentration increases slower as a result of the flow out of the bioreactor. The bioreactor

is reasonably close to steady state between 18 and 20 hours, and here substrate concentration is higher in the high flow condition, which means that substrate is leaving the bioreactor. This means that while production will be higher, the substrate yield, the efficiency of substrate dosed into bioreactor, is lower.

Productivity in continuous systems is defined by the flow out of the system, where biomass and product productivity are equal to dilution rate multiplied by the respective concentration [19, 20].

$$p_{c,X} = DX \quad \textbf{2-35}$$

$$p_{c,P} = DP \quad \textbf{2-37}$$

Continuous fermentations can be defined by dilution rate, and since we are rested in productivity, we can compare dilution rate vs productivity as seen Figure 6 below. **2-38**

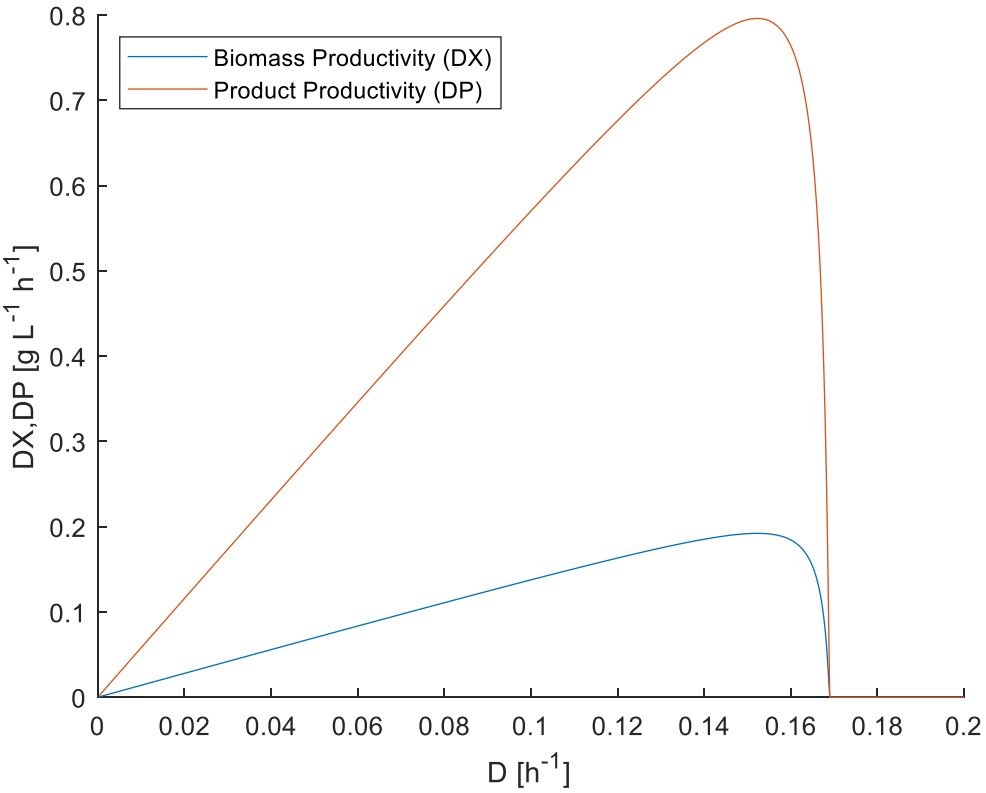

Figure 6: Dilution Rate (D) vs Productivity for Biomass (DX) and Product (DP) for Simulated Continuous Fermentation. Parameters for simulation can be found in Table 4. Equations for simulation can be found in Table 5.

There is an optimum dilution rate for determining maximum productivity of both biomass and product, since both are determined by the same kinetics. This optimum dilution rate is can be found by taking the derivative of the productivity, setting it to zero, and solving for D. The solution is given in the equation below.

$$D_{opt} = \mu_{max}\left(1 - \sqrt{\frac{K_S}{K_S + S_0}}\right) \qquad \textbf{2-39}$$

At this point, the concentration of substrate can be found, and then biomass and product concentrations can be determined from that. These are shown in the equations below [18].

$$S_{opt} = Y_{XS}S_0 \frac{\sqrt{\frac{K_s + S_0}{K_S}}}{\sqrt{\frac{K_s + S_0}{K_S}} + 1} \quad \textbf{2-43}$$

$$X_{opt} = Y_{XS}(S_0 - S_{opt}) \quad \textbf{2-41}$$

$$P_{opt} = Y_{PS}(S_0 - S_{opt}) \quad \textbf{2-45}$$

Despite the simplicity of a basic continuous system, the solutions to these important characteristics become quite complex. When dealing with more complicated systems that require numerical solutions these characteristics, like optimum dilution rates and the concentrations at those points, cannot be determined algebraically and must be taken from the simulations.

Productivity can be increase by retaining cells, which can be done by a variety of methods. This work is focused on filtration using hollow-fiber membranes, however other membrane types, centrifuges, and settling are among the methods than can be used to concentrate or retain cells.

2.1.4 Introduction to filtration

Filtration is the process of separating particles within a fluid from that fluid using a physical barrier. Filtration is categorized in at least three ways: by the direction of flow relative to the filter, the size of the pores in the filter, and the construction of the filter. The filter type of interest in this work are crossflow, hollow-fiber filters use for microfiltration. These filters are tubular, cross flow filters with pores between 0.1µm and 10µm. The pores are smaller on the side containing the particles and larger on the side with filtered fluid (permeate) in order to minimize fouling within the membrane [21].

At the beginning of operating a filter system with particles in solution, permeate flows at the same rate as it would for a particle free solution, however this quickly changes with the formation of a filter cake, a region of particles on the filter surface. In a solution with

no fouling, the rate of cake formation, and thus the rate of decrease in flux, initially changes linearly in direct proportion to transmembrane pressure and particle concentration, with smaller particles having higher rates. Over a longer duration, the flux decreases proportional to the inverse the square root of time ($\frac{1}{\sqrt{t}}$), and approaches zero over very long time frames [22]. Since filter cake is on the surface of the membrane it is affected by changes in the solution and flow conditions, which can help decrease cake thickness by flushing with high speed flow, backwashing, or flushing with particle free solution [23].

Fouling of membranes refers to components or particles which are embedded in the membrane which decrease flow. If this fouling is from inorganic material, this may also be referred to as scaling. This follows a similar pattern as filter cake formation, but less analytically predictable as fouling will depend on the interaction of media and cell components with the material the membrane is constructed from [23].

In ultrafiltration applications a phenomenon called concentration polarization occurs as a result of change in osmotic pressure on opposite sides of the membrane and on the surface of the membrane, which results in a significant decrease in filter effectiveness, however this is negligible for particles above 0.1µm [22]. The smallest bacteria, *Pelagibacter ubique*, has a minimum average diameter of 0.12µm along its shortest dimension, meaning that filtration effectiveness in cell culture applications should be limited only by the concentration of particles, filter cake formation, fouling of the membrane [24].

2.1.5 Mass Balance for Fermentations with Filtration

There are a wide variety of designs for fermentation systems for retaining cells, however bioreactors with external with cell recycle systems using cross flow filtration are the focus of this work. A basic cell recycle system can be seen in Figure 7 below.

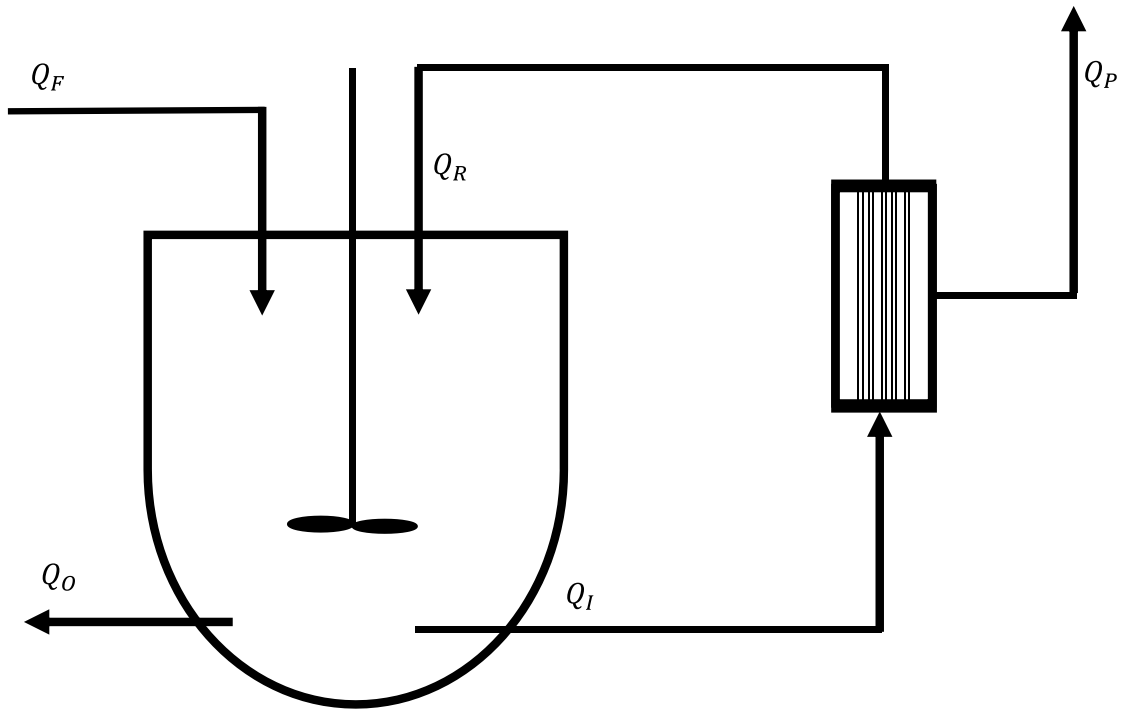

Figure 7: Basic Diagram of Continuous Cell Recycle. Flows are labelled with subscripts: $\boldsymbol{Q_F}$ is feed; $\boldsymbol{Q_O}$ is output from the bioreactor; $\boldsymbol{Q_I}$ is input to cell recycle; $\boldsymbol{Q_R}$ is membrane retentate (cell rich); $\boldsymbol{Q_P}$ is membrane permeate (cell fee).

For the system in Figure 7 to run at steady state, the volume and the reaction must be constant. For volume to be constant the feed flow must be equal to the sum of the bioreactor output and the permeate and the feed flow rate must be constant to ensure a constant substrate and biomass concentration in the reactor. This gives the base flow relationship for a bioreactor with recycle.

$$Q_F = Q_O + Q_P \qquad \textbf{2-47}$$

Flows can be related in two ways: by the recycle ratio, α, and cell concentration ratio C; or by the bleed ratio, β. The recycle ratio, α, is the proportion of feed flow rate that is returned to the bioreactor, and the cell concentration ratio is the proportion of the concentration of cells that are returned to the bioreactor. This gives relationships between flows in Figure 7 as shown in the equations below.

$$\alpha = \frac{Q_R}{Q_F} \quad \textbf{2-51}$$

$$Q_I = Q_R + Q_P = (1+\alpha)Q_F - Q_O \quad \textbf{2-49}$$

The recycle ratio, α, is commonly used when the cell separation mechanism only retains a portion of the cells, for example with a settling tank or centrifuge [20]. In these cases, an additional outflow/bleed stream (Q_O) is not required to maintain a steady state. However, in the case of microfiltration by size exclusion, all cells can be retained via the filter, and so the outflow Q_O is required for a steady state to be reached. It is then simpler to use the bleed ratio, β, which is defined below alongside its relationship to the flows shown in Figure 7 [19].

$$\beta = \frac{Q_O}{Q_F} \quad \textbf{2-53}$$

$$Q_P = (1-\beta)Q_F \quad \textbf{2-55}$$

So long as bleed flow is present, the relationship between recycle ratio, α, and bleed ratio, β, is shown below.

$$\frac{\alpha}{\beta} = \frac{Q_R}{Q_O} \quad \textbf{2-57}$$

Alternatively, by combining permeate and bleed flows a system with a bleed stream can be converted to a system without one. In this case, the relationship for finding recycle ratio, α, does not change. The relationship for converting from a system with a bleed line to one without it is given below, with the subscript α and β can be used to indicate variables from a system without and with a bleed line respectively.

$$\mathrm{Q}_{P,\alpha} = Q_{P,\beta} + Q_{O,\beta} \quad \textbf{2-59}$$

$$X_{P,\alpha} = \frac{Q_{P,\beta}X_{P,\beta} + Q_{O,\beta}X_{O,\beta}}{Q_{P,\beta} + Q_{O,\beta}} \quad \textbf{2-61}$$

In the case of size exclusion filtration where the average pore size is sufficiently small to retain all cells, then $X_{P,\beta} = 0$ and only the cells removed via the bleed line affect the calculation.

If the bleed flow is absent, using the recycle ratio makes for a simpler set of equations for defining mass balance. However, if bleed flow is present using the bleed ratio can be a simpler way to define the mass balance, especially when using size exclusion microfiltration where all cells are retained. In this work the bleed ratio is used as it is easier at laboratory scale to control volume using a bleed line, and size exclusion microfiltration with full cell retention is of interest.

The diagram in Figure 7 is for a simple cell recycle arrangement, with the outlet stream containing cells coming directly from the bioreactor. Alternative setups with outlet streams coming from the recirculation line can be built, however these require active control of the volume in the bioreactor using either constant monitoring or a feedback mechanism, whereas there are passive methods of ensuring constant volume when taking directly from the bioreactor. Passive volume control methods are discussed in Chapter 4.

In all cases, cell concentration ratio, C, represents the ratio of retained cells to cell concentration in the bioreactor, whether there is a bleed line or not. This is given below.

$$C = \frac{X_R}{X} \quad \textbf{2-63}$$

In a continuous reactor, the flow rate is expressed via the dilution rate, however with the cell recycle system retaining cells the dilution rate can be increased. In size exclusion microfiltration, cells are only removed via the bioreactor output Q_O**.** Using β and D, we can use this to determine the system of equations that describes the system, shown below.

$$\frac{dX}{dt} = \frac{Q_F}{V} X_{in} - \frac{Q_O}{V} X + \mu X = \mu X - \beta D X \quad \textbf{2-65}$$

$$\frac{dS}{dt} = \frac{Q_F}{V} S_{in} - \frac{Q_O}{V} S - \frac{Q_P}{V} S - \frac{1}{Y_{XS}} \mu X = D(S_{in} - S) - \frac{1}{Y_{XS}} \mu X \quad \textbf{2-67}$$

$$\frac{dP}{dt} = \frac{Q_F}{V} P_{in} - \frac{Q_O}{V} P - \frac{Q_P}{V} P + \frac{Y_{PS}}{Y_{XS}} \mu X = \frac{Y_{PS}}{Y_{XS}} \mu X - DP \quad \textbf{2-69}$$

$$\frac{dV}{dt} = 0 \quad \textbf{2-71}$$

Here, we can see that steady state solutions for biomass growth, $\mu = \beta D$, is based on membrane performance, with the maximum flow based on dilution rate being $D = \frac{\mu_{max}}{\beta}$, above which washout is guaranteed [18]. Alternatively, if the system if defined by α, the steady state cell concentration is adjusted by a factor of $1/[1 + \alpha(1 - C)]$, and the relation between growth rate and dilution rate is $\mu = [1 + \alpha(1 - C)]D$ [20].

Changes in product and substrate are only changed by changes in cell concentration and biomass growth. Since volume is constant ($\frac{dV}{dt} = 0$), flow in is equal to the sum of flows out ($Q_F = Q_P + Q_O$) and we can see that cells are retained and recycled, but substrate and product are not. For substrate to be recycled with the removal of product, *in situ* product removal is required, however those setups are outside of the scope of this work.

Productivity in cell recycle systems is dependent on the dilution rate and the degree of cell concentration, with cell concentration in turn being dependent on filter performance. Assuming that kinetic parameters stay the same and all streams leaving the bioreactor can be used, the optimum dilution rate for a cell recycle system is the dilution rate for a continuous system without cell recycle scaled proportional to the inverse of the bleed ratio with a higher productivity.

$$D_{opt,Cell\ Recycle} = \frac{D_{opt,Continious}}{\beta} \qquad \textbf{2-73}$$

An intuitive way to interpret this is using the Bleed Dilution Rate, βD, the dilution rate based on only the stream of flow leaving the bioreactor that contains cells, in which case the optimum bleed dilution rate is the same as the optimum dilution rate for a continuous bioreactor. This can be seen in Figure 8 below.

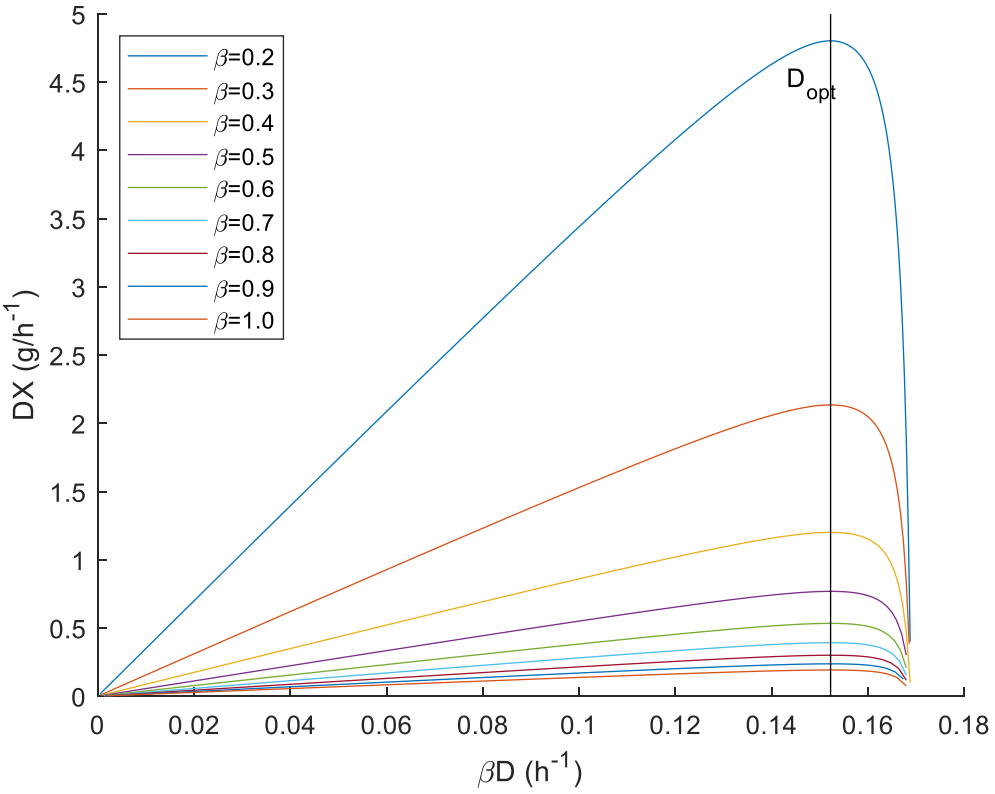

Figure 8: Cell Productivity (DX) vs Bleed Dilution Rate (βD) for a Simple Cell Recycle System. The vertical line represents the optimum dilution rate.

As can be seen in Figure 8, bleed ratio and cell productivity are inversely proportional to one another. This is due to both to the retention of cells and the amount that dilution rate can be increased with cell retention. Figure 9 better shows how decreasing β allows for a higher dilution rate, both for optimum production and before washout occurs.

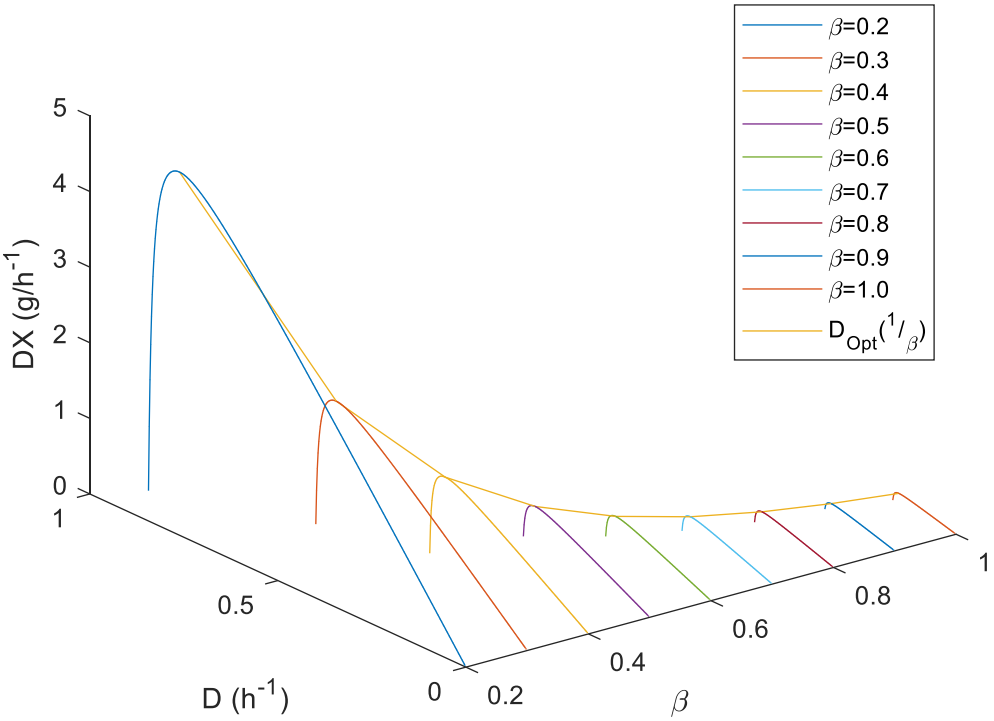

Figure 9: Cell Productivity vs Dilution Rate (D) and Bleed Ratio (β). D_{opt} used is the optimum dilution rate for a continuous system, and the curve shown is the optimum dilution rate for a simple cell recycle system.

The increase in cell concentration and dilution rate are also associated with an increase in product productivity, as there are more cells to perform fermentation. The same trend seen in Figure 8 and Figure 9 for cell productivity is true for product productivity, and can be seen in Figure 10 and Figure 11.

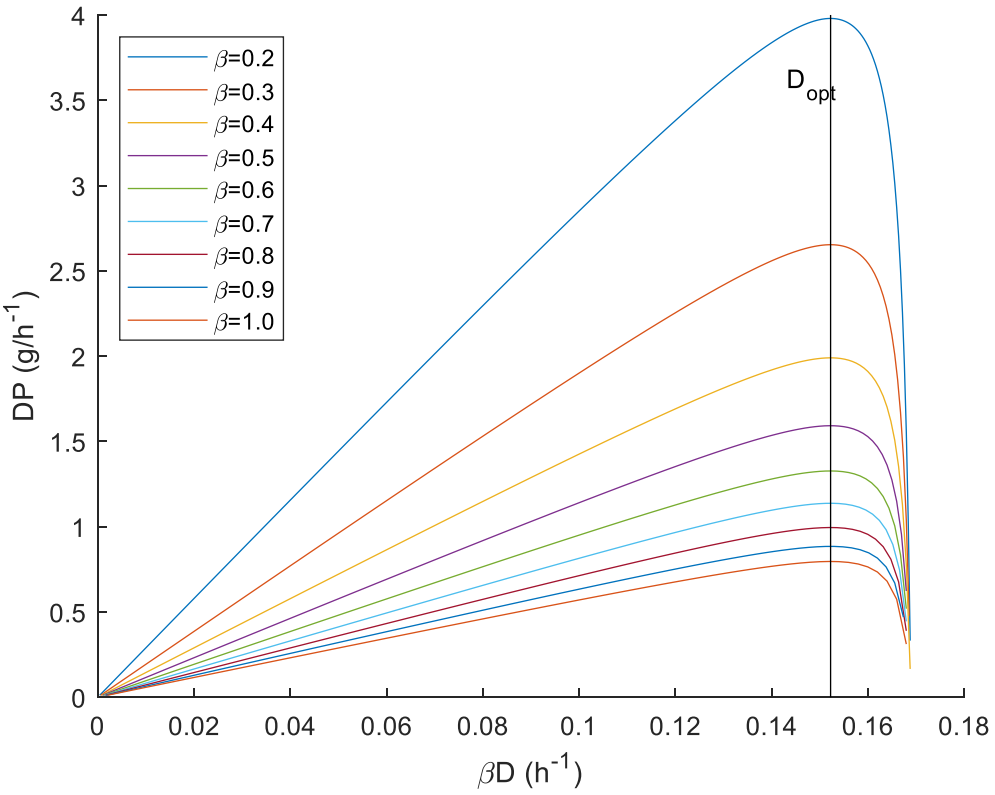

Figure 10: Product Productivity vs Bleed Dilution Rate. The vertical line represents the optimum dilution rate.

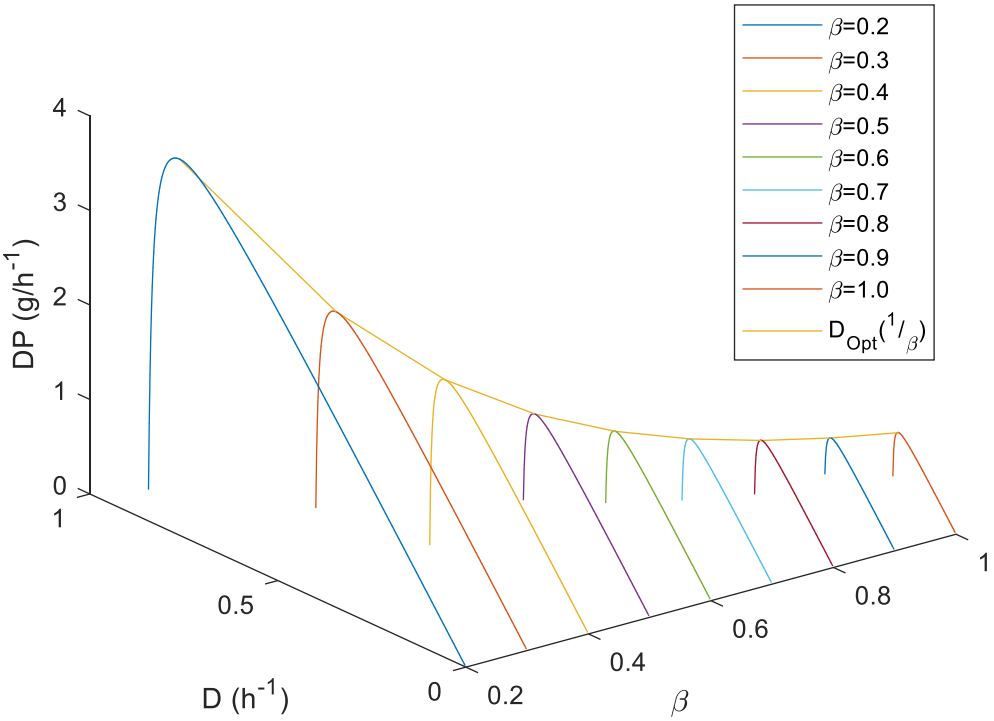

Figure 11: Product Productivity vs Dilution rate (D) and Bleed Ratio (β). D_{opt} used is the optimum dilution rate for a continuous system, and the curve shown is the optimum dilution rate for a simple cell recycle system.

It is important to note that in these cases productivity is assuming that flow streams are combined after leaving the bioreactor. If only the cell free line is usable for product extraction, productivity will need to be adjusted by the proportion of flow going to permeate $(1-\beta)$.

2.1.6 Filter Arrangements

There are also different arrangements for membranes, or any cell removal technology, to be attached to the bioreactors. Example the variety of membrane configurations can be seen in Figure 12 below.

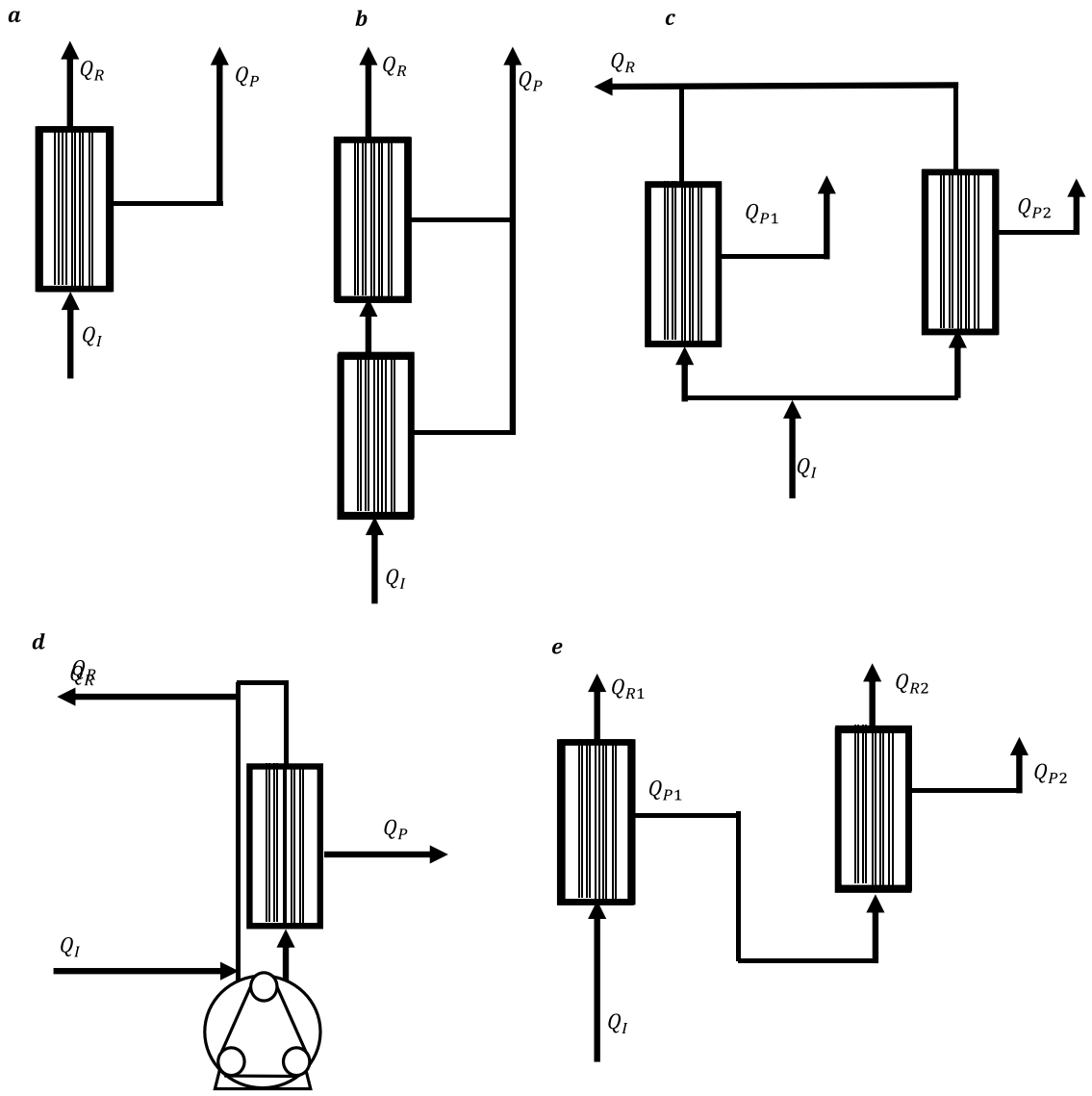

Figure 12: Cell Recycle Arrangements for External Membranes. a) Single pass, single module; b) Single pass, two modules with retentate in series; c) Single pass, two modules in parallel; d) Recirculating flow, single module, also called Feed-and-Bleed; e) Single pass, two modules with permeate flow in series. Subscripts for flows refer to input ($\boldsymbol{Q_I}$), permeate ($\boldsymbol{Q_P}$), or retentate ($\boldsymbol{Q_R}$), with numbers used for multiple flows. For the Feed-and-Bleed setup $\boldsymbol{Q_R}$ refers to the retentate return line going back to the bioreactor. Adapted from Groot et al **[25]**.

In Figure 12, arrangements *a* through *c* show basic variations on cell recycle setup, with *a* being the same as the arrangement in Figure 7. In *b*, the membranes are in series, however the effect of this can be accomplished by using a longer membrane, and in *c* the membranes in parallel can also be accomplished by using a membrane with a larger area.

The main difference between *a* and *c* will be how the flow is split between the two membranes.

Arrangements *d* and *e* in Figure 12 are distinct in that they cannot be accomplished by substituting different membranes. Arrangement *d* is referred to as closed-loop, single module, or Feed-and-Bleed [25, 23]. In *d*, the recirculation loop results in greater passes through the membrane before return to the bioreactor, which can accomplish a greater amount of separation and concentration of the fluid in the recirculation loop relative to the size of the system [25]. Additionally, arrangements *a* through *c* can have the single membrane replaced with a feed-and-bleed setup. The feed-and-bleed arrangement in *d* has been used in filtration systems for particle removal and desalination, but implementations have been limited to inorganic systems [23].

In *e*, the output of one membrane is used as the input to another membrane. This is particularly useful for minimizing fouling of membrane systems which require a high degree of filtration and begin with systems with high suspended solids and a wide variety of particles. One example of this is filtration of biomolecules from a microbial culture, as in the production of gluconic acid [26]. This arrangement can also be modified so that each membrane section uses a feed-and-bleed arrangement as shown in *d*.

2.1.7 Fermentations using *Clostridium pasteurianum*

Many fermentations have been performed with *Clostridium pasteurianum* since it was first isolated by Sergei Winogradsky in the late 1800s [27]. Notable work can be seen in Table 6 below.

Strain	Mode	Substrate	Source
DSM 525	Batch	20 g/L Glycerol	[28]
DSM 525	Batch	50 g/L Crude Glycerol	[29]
DSMZ 525	Batch	80g/L glycerol, 20g/L glucose	[30]
DSMZ 525 (GMO)	Batch	80 g/L glycerol	[31]
MBEL_GLY2 (GMO)	Batch	80 g/L glycerol	[32]
DSMZ 525	Batch	10 g/L glycerol	[33]
DSMZ 525	Batch with gas stripping	111 g/L glycerol and crude glycerol	[34]
DSMZ 525 (MNO6)	Batch with gas stripping	105 g/L crude glycerol	[35]
DSMZ 525	Repeated batch with immobilized cells	60 g/L glycerol	[36]
DSMZ 525	Fed-batch with gas stripping	80 g/L glycerol	[37]
CT7	Fed-batch with pervaporation	100 g/L glycerol	[38]
DSM 525	Continuous	30 g/L Glycerol	[5]
DSMZ 525	Continuous	10 g/L glycerol, D=0.07	[33]
DSMZ 525	Continuous, immobilized on corn stover	35 g/L Glycerol	[39]
MBEL_GLY2 (GMO)	Continuous with cell recycle	60 g/L Glycerol	[32]
DSMZ 525	Continuous with cell recycle	20 g/L Glycerol	This work
DSM 525	Batch	50 g/L Crude glycerol with 4 g/L butyrate	[29]
DSM 525	Batch	50 g/L Crude glycerol, 12 g/L Jerusalem Artichoke hydrolysate	[40]
DSMZ 525	Batch	50 g/L glycerol and 50 g/L biomass hydrolysate	[30]
CH4	Batch	60 g/L glycerol and 20 g/L glucose	[41]
CH4	Batch	60 g/L glycerol, 25 g/L bagasse hydrolysate	[41]

Table 6: Notable fermentations using *Clostridium pasteurianum*

Of all work found in the literature on *Clostridium pasteurianum*, only one work demonstrated fermentation with a cell recycle apparatus, and which used a mutant strain of *C. pasteurianum*.

Chapter 3

3 Modelling and Simulation of Bioreactor Systems with Cell Recycle

Traditionally, most industrial biological processes have been done in batch, as that is the simplest and easiest setup. However, low productivity fermentations require more involved designs to be used with bioreactors to be cost effective. The production of 1-butanol from glycerol by *Clostridium pasteurianum* is one of these processes. This chapter outlines modelling and simulation of a benchtop bioreactor with different cell recycle arrangements using MATLAB R2020a. Transient and steady-state solutions to single pass and two feed-and-bleed cell recycle arrangements are show. These simulations show similar results between arrangements, with the permeate stream of the Feed-and-Bleed system with Bioreactor Bleed having an increase in productivity of 8% without product inhibition, and 6% if product inhibition is taken into account. Total productivity increases by 2% both with and without product inhibition in the Feed-and-Bleed system with Bioreactor Bleed system. The Feed-and-Bleed system with recirculation loop bleed underperforms compared to the other arrangements in all cases. Considering how small the benefit of using the Feed-and-Bleed system with Bioreactor Bleed is, and the assumptions required for the Feed-and-Bleed system to work, initial work with cell recycle should use the simple, single pass arrangement before attempts are made at implementing a feed-and-bleed system.

3.1 Introduction and Background

There is a need for finding a use for crude glycerol produced from biodiesel processes, and the production of butanol via fermentation is one valuable route, as butanol can be used as a drop-in fuel, a reagent, and as solvent. Fermentations using *Clostridium pasteurianum* to produce butanol are slower than ethanol fermentations, so process intensification is required in order to minimize capital costs and make these fermentations industrially feasible [1].

Continuous fermentation has been performed on *Clostridium pasteurianum*, but because of the slow growth rate of the organism the productivity is limited. Additionally, further

steps with *in situ* extraction would benefit from removal of solids, decreasing fouling and increasing mass transfer of the extraction process and time between cleaning. Finding flow characteristics and estimated output are valuable for designing systems for maximizing productivity, contextualizing experimental work, and later designing and integrating *in situ* extraction [6].

By applying a cell recycle mechanism using microfiltration, downstream processes can be freed of cells and solids, decreasing the need for cleaning of those downstream processes and possibly increasing mass transfer by decreasing or eliminating fouling [1].

Previous work in process engineering for bioprocesses have been focused on ethanol production or have used assumptions to simplify systems so that explicit, algebraic solutions could be produced [25]. This work uses MATLAB to produce numerical solutions to systems of equations defining these bioreactor systems, allowing for concentrations of biomass, products, and media components to be determined from the model rather than assumed.

This chapter will cover simulation of three bioreactor configurations for design of a benchtop bioreactor system of *Clostridium pasteruianum* grown on glycerol, using numerical methods, minimizing the number of assumptions, and comparing conditions with and without inhibition. This work is the first to perform this process engineering for *Clostridium pasteurianum*, and expands process engineering for fermentation systems. The parameters used are based on growth of *Clostridium pasteurianum*, however kinetic constants are specific to fermentation conditions. Regardless, conclusions should generalize to any similar fermentation system.

3.2 Experimental Methods

Models were built based on mass balance for a single pass, single module system (simple cell recycle) and two closed loop, single module systems (feed-and-bleed with bioreactor bleed or recirculation loop bleed) to compare the productivity of these two systems. Figure 13 shows the description for the single pass, single module cell recycle, with equations for that system in Table 8, Figure 14 shows the description for the closed loop,

single module cell recycle with bioreactor bleed, with equations for that system in Table 9, and Figure 15 shows the description for the closed loop, single module cell recycle with recirculation loop bleed, with equations for that system in Table 10. Parameters for simulation can be found in Table 12. Solutions to these models were found in MATLAB 2020a using built-in functions ode45 and fsolve.

3.2.1 Bioreactor Models

Three bioreactor arrangements are investigated in this work: a single pass, single module cell recycle system (simple cell recycle), and two closed loop, single module systems (feed-and-bleed), all originally discussed in Groot et al [25].

In all models, feed flow (Q_F), outlet or bleed flow (Q_O), and permeate flow (Q_P), are based on dilution rate (D) and bleed-ratio (β), as shown below in Table 7. The reaction rate is based on Monod kinetics and dilution rate is based on total system volume. In order to be applicable to *Clostridium pasteurianum*, product inhibition needs to be taken into consideration, as butanol production has been shown to be inhibitory [1]. A simple product inhibition term is used here.

Parameter	Equation	
Dilution Rate	$D = \frac{Q_F}{V_{Total}}$	**3-1**
Bleed Ratio	$\beta = \frac{Q_O}{Q_F} = \frac{Q_O}{DV_{Total}}$	**3-3**
Permeate Flow	$Q_P = (1-\beta)Q_F = (1-\beta)DV_{Total}$	**3-5**
Monod Equation	$\mu_i = \mu_{max}\left(\frac{S_i}{K_S + S_i}\right)$	**3-7**
Monod Equation with Product Inhibition	$\mu_i = \mu_{max}\left(\frac{S_i}{K_S + S_i}\right)\left(1 - \frac{P_i}{P_{Max}}\right)$	**3-9**

Table 7: Flow Equations Common to Simple Cell Recycle and Feed-and-Bleed Systems

The single pass, single module cell recycle system is shown in Figure 13. In this system, cells are concentrated in the retentate line (Q_R) and returned directly to the bioreactor. The intake to the membrane (Q_I) has an assumed high flow to minimize fouling of the membrane, and this high flow implied that the membrane loop and the bioreactor can be assumed to be well-mixed and concentration of all species to be the same.

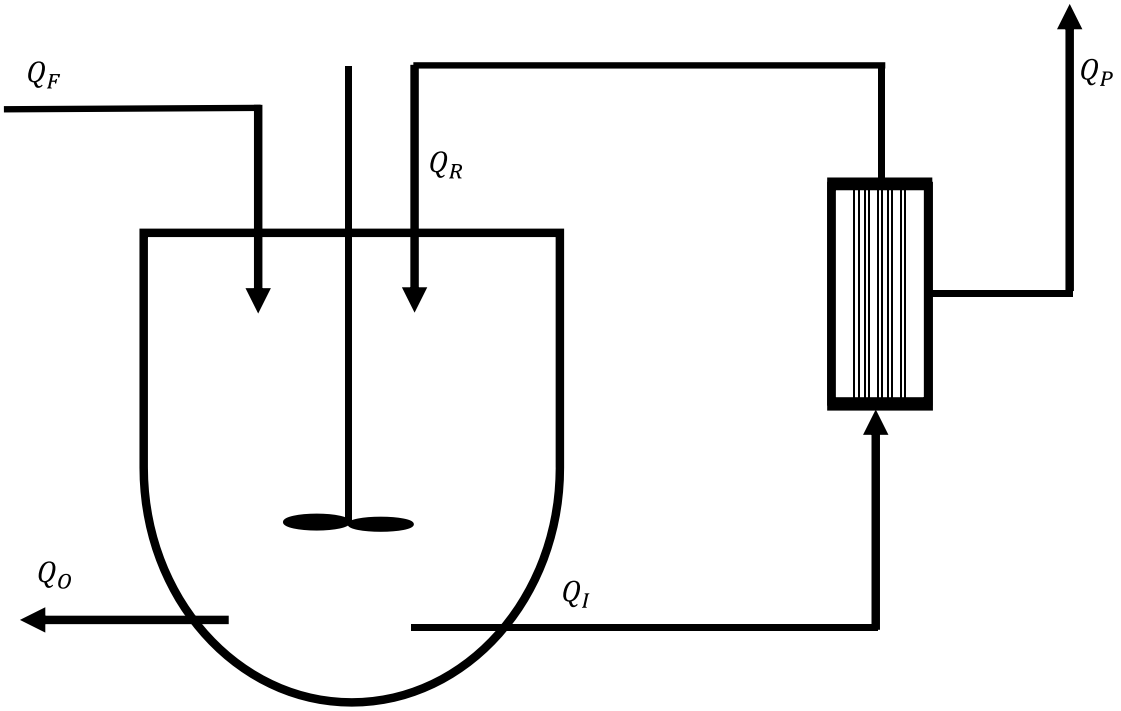

Figure 13: Diagram of Single Pass, Single Module Cell Recycle System. Flows are labelled with subscripts: $\boldsymbol{Q_F}$ is feed; $\boldsymbol{Q_O}$ is output from the bioreactor; $\boldsymbol{Q_I}$ is input to cell recycle; $\boldsymbol{Q_R}$ is membrane retentate (cell rich); $\boldsymbol{Q_P}$ is membrane permeate (cell fee).

The differential equations describing the single pass, single module system are based on Monod kinetics and a simple mass balance a single volume. These equations can be seen Table 8 below. When combined with the equations in Table 7, are determined by kinetic parameters (μ, Y_{XS}, Y_{PS}), substrate feed concentration (S_{in}), dilution rate (D), and bleed ratio (β).

Component	Equation	
Biomass	$\frac{dX}{dt} = \mu X - \beta DX$	**3-11**
Substrate	$\frac{dS}{dt} = D(S_{in} - S) - \frac{1}{Y_{XS}} \mu X$	**3-1**
Product	$\frac{dP}{dt} = \frac{Y_{PS}}{Y_{XS}} \mu X - DP$	**3-1**

Table 8: Equations defining the Single Module, Single Pass Cell Recycle System

A diagram of the closed loop, single module (or feed-and-bleed) with bioreactor cell bleed arrangement is shown in Figure 14. This system divides the same total volume into two sections: the bioreactor and the recirculation loop. Both sections are assumed to be well-mixed, and transfer between the two sections occurs in flows Q_I and Q_R, with Q_L being recirculation flow within the loop.

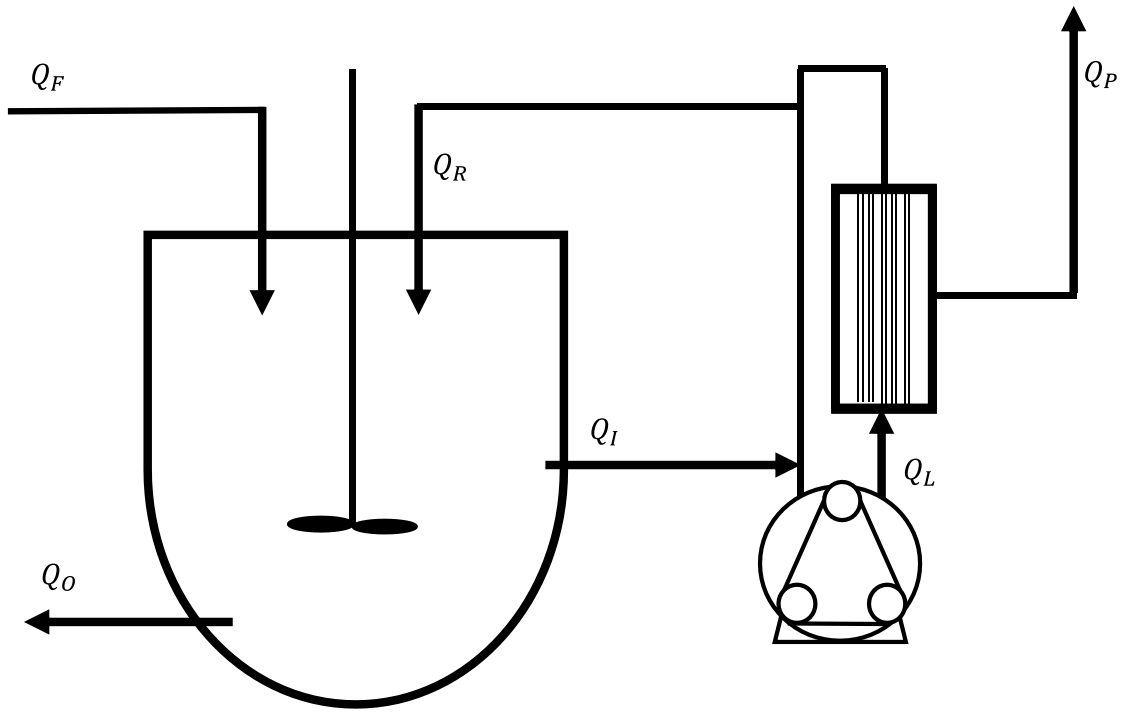

Figure 14: Diagram of Closed Loop, Single Module (Feed-and-Bleed) with Bioreactor Bleed Cell Recycle System. Flows are labelled with subscripts: $\boldsymbol{Q_F}$ is feed; $\boldsymbol{Q_O}$ is output from the bioreactor; $\boldsymbol{Q_I}$ is input to feed and bleed recirculation look; $\boldsymbol{Q_L}$ is the input to the membrane; $\boldsymbol{Q_R}$ is return to bioreactor from recirculation loop (cell rich); $\boldsymbol{Q_P}$ is membrane permeate (cell fee).

The differential equations describing the closed loop, single module system are based on Monod kinetics and a mass balance two volumes, the bioreactor (V_B) and the recirculation loop (V_L). These equations can be seen Table 8 below. When combined with the equations in Table 7, then these equations are determined by kinetic parameters (μ, Y_{XS}, Y_{PS}), substrate feed concentration (S_{in}), dilution rate (D), bleed ratio (β), and the flow between the loop and bioreactor (Q_I and Q_R).

Component	Equation	
Reactor Biomass	$\frac{dX_1}{dt} = \mu_1 X_1 - \frac{Q_O}{V_B} X_1 + \frac{Q_R}{V_B} X_2 - \frac{Q_I}{V_B} X_1$	**3-17**
Reactor Substrate	$\frac{dS_1}{dt} = Q_F S_{in} - \frac{Q_O}{V_B} S_1 - \frac{1}{Y_{XS}} \mu_1 X_1 + \frac{Q_R}{V_B} S_2 - \frac{Q_I}{V_B} S_1$	**3-19**
Reactor Product	$\frac{dP_1}{dt} = \frac{Y_{PS}}{Y_{XS}} \mu_1 X_1 - \frac{Q_O}{V_B} P_1 + \frac{Q_R}{V_B} P_2 - \frac{Q_I}{V_B} P_1$	**3-21**
Loop Biomass	$\frac{dX_2}{dt} = \mu_2 X_2 - \frac{Q_R}{V_L} X_2 + \frac{Q_I}{V_L} X_1$	**3-23**
Loop Substrate	$\frac{dS_2}{dt} = -\frac{1}{Y_{XS}} \mu_2 X_2 - \frac{Q_R}{V_L} S_2 + \frac{Q_I}{V_L} S_1 + \frac{Q_P}{V_L} S_2$	**3-25**
Loop Product	$\frac{dP_2}{dt} = \frac{Y_{PS}}{Y_{XS}} \mu_2 X_2 - \frac{Q_R}{V_L} P_2 + \frac{Q_I}{V_L} P_1 + \frac{Q_P}{V_L} P_2$	**3-27**
Loop Inlet Flow	$Q_I = Q_R + Q_P$	**3-29**

Table 9: Equations defining the Closed Loop, Single Module (Feed-and-Bleed) with Bioreactor Bleed Cell Recycle System

A diagram of the closed loop, single module (or feed-and-bleed) with recirculation loop cell bleed arrangement is shown in Figure 15.

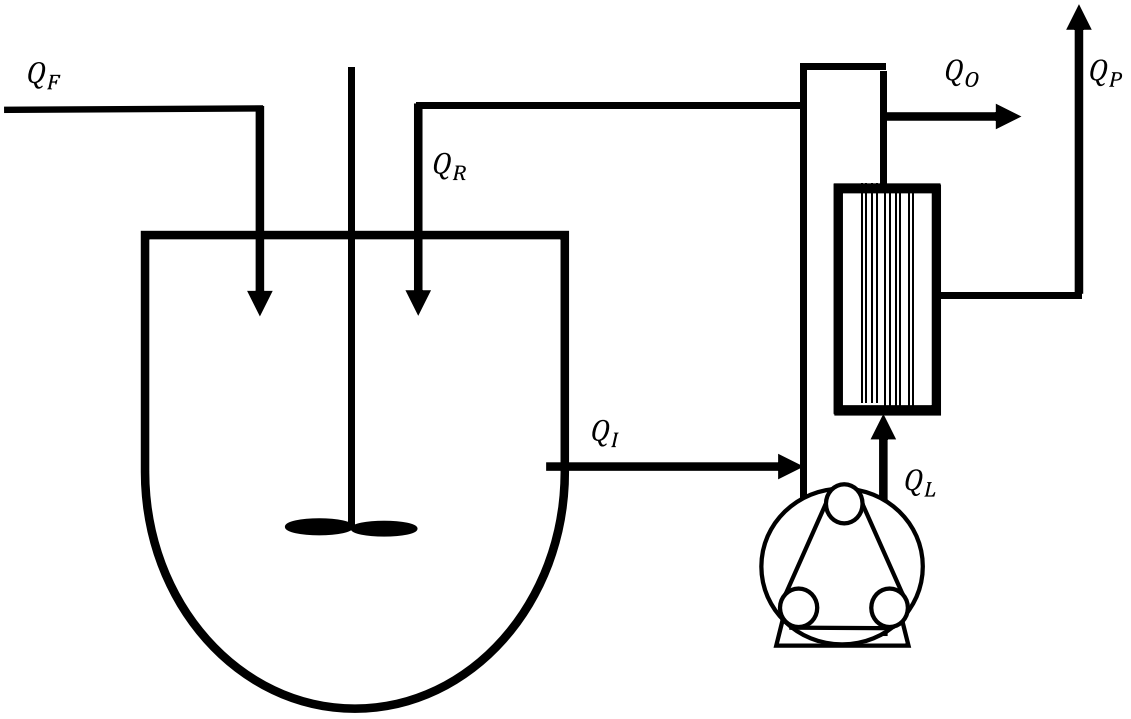

Figure 15: Diagram of Closed Loop, Single Module (Feed-and-Bleed) with Recirculation Bleed Cell Recycle System. Flows are labelled with subscripts: $\boldsymbol{Q_F}$ is feed; $\boldsymbol{Q_O}$ is output from the bioreactor; $\boldsymbol{Q_I}$ is input to feed and bleed recirculation look; $\boldsymbol{Q_L}$ is the input to the membrane; $\boldsymbol{Q_R}$ is return to bioreactor from recirculation loop (cell rich); $\boldsymbol{Q_P}$ is membrane permeate (cell fee).

This system operates the same as the feed and bleed with bioreactor bleed, with the exception that the bleed line has been moved to the recirculation loop, so media coming from the bleed line should have higher cell concentration and lower substrate compared to the bioreactor. However, this will impact the rest of the system, as fewer cells will be returned to the bioreactor. Equations defining the closed loop, single module system with recirculation bleed can be seen in Table 10 below.

Component	Equation	
Reactor Biomass	$\frac{dX_1}{dt} = \mu_1 X_1 + \frac{Q_R}{V_B} X_2 - \frac{Q_I}{V_B} X_1$	**3-33**
Reactor Substrate	$\frac{dS_1}{dt} = Q_F S_{in} - \frac{1}{Y_{XS}} \mu_1 X_1 + \frac{Q_R}{V_B} S_2 - \frac{Q_I}{V_B} S_1$	**3-35**
Reactor Product	$\frac{dP_1}{dt} = \frac{Y_{PS}}{Y_{XS}} \mu_1 X_1 - \frac{Q_O}{V_B} P_1 + \frac{Q_R}{V_B} P_2 - \frac{Q_I}{V_B} P_1$	**3-37**
Loop Biomass	$\frac{dX_2}{dt} = \mu_2 X_2 - \frac{Q_R}{V_L} X_2 + \frac{Q_I}{V_L} X_1 - \frac{Q_O}{V_L} X_2$	**3-31**
Loop Substrate	$\frac{dS_2}{dt} = -\frac{1}{Y_{XS}} \mu_2 X_2 - \frac{Q_R}{V_L} S_2 + \frac{Q_I}{V_L} S_1 + \frac{Q_P}{V_L} S_2 - \frac{Q_O}{V_L} S_2$	**3-39**
Loop Product	$\frac{dP_2}{dt} = \frac{Y_{PS}}{Y_{XS}} \mu_2 X_2 - \frac{Q_R}{V_L} P_2 + \frac{Q_I}{V_L} P_1 + \frac{Q_P}{V_L} P_2 - \frac{Q_O}{V_L} P_2$	**3-43**
Loop Inlet Flow	$Q_I = Q_R + Q_P + Q_O$	**3-41**

Table 10: Equations defining the Closed Loop, Single Module (Feed-and-Bleed) with Recirculation Loop Bleed Cell Recycle System

Assuming that size exclusion microfiltration is used, and that all cells are retained, then the response of the single pass, single module cell recycle is already known. Solutions to the optimum dilution rate for a continuous system are known, and the optimum dilution rate for a single pass, single module system is the optimum dilution rate for a continuous system scaled by 1/β. These solutions are shown below in Table 11.

Component	Equation	
Optimum Dilution Rate for Continuous	$D_{Opt,Continuous} = \mu_{max}\left(1 - \sqrt{\frac{K_S}{K_S + S_{in}}}\right)$	**3-45**
Optimum Dilution Rate for Cell Recycle	$D_{Opt,Simple\ \ Cell\ Recycle} = \frac{D_{Opt,Continuous}}{\beta}$	**3-47**

Table 11: Optimum Dilution Rates for Continuous and Simple Cell Recycle Systems

With the equations in Table 11, combined with all previous relationships, remaining parameters can be set to finish defining the system. The parameters used for simulation are given below in Table 12.

Parameter	Value
Maximum specific growth rate	$\mu_{max} = 0.171$
K_S	$K_S = 0.243$
Biomass Yield	$Y_{XS} = 0.07$
Product Yield	$Y_{PS} = 0.29$
Inhibition Constant	$P_{Max} = 16g/L$
Total Volume	$V_{Total} = 5L$
Bioreactor Volume for Feed-and-Bleed	$V_B = 3L$
Membrane Loop Volume	$V_L = 2L$
Membrane Loop Return Flow	$Q_R = 100mL/min$
Substrate Feed Concentration	$S_{in} = 20g/L$

Table 12: Parameters used in Simulation

3.2.2 Numerical and Computational Methods

Systems of equations developed based on Monod kinetics and mass balance were solved using two functions which are built into MATLAB 2020a: ode45 for transient solutions to systems of differential equations, and fsolve for finding steady state solutions to systems of equations.

The ode45 function was chosen as it can produce a more accurate answer, though at the expense of additional computation, than other solvers available. This function uses the Dormand-Prince method, a specific implementation of a Runge-Kutte method. Runge-Kutta methods are group of iterative methods used for solving time-dependent differential equations, and the Dormand-Prince method estimates the fourth and fifth order solutions and the difference between these two solutions is the error [42, 43]. When the error is below a set value the solution is effectively solved.

The fsolve function uses a trust-region-dogleg algorithm, based on the Powel method for finding a local minimum [44, 45]. Equations need to be set to zero to be solvable using this function, which is easily done when looking for steady state solutions where differential terms are zero.

3.3 Simulation of Bioreactor systems

In this section, three bioreactor configurations simulations, one simple cell recycle and two feed-and-bleed arrangements, are shown. Transient solutions and general trends between configurations for each system are given. Each system was simulated using simplified models and their assumptions. The goal of this section is to find which recycle configuration will work best for increasing butanol production in a glycerol fermentation using *Clostridium pasteurianum*.

Which kinetic parameters used for simulation depend on which organism the simulation is intended for, though any organism with similar characteristics should have similar results. Kinetic parameters given for the organisms will define optimum dilution rate, though since the Monod equation is empirical in nature, these constants cannot be assumed to strictly hold true to actual experiments, but are useful for comparison. This

work is intended to inform the construction of a bioreactor for *Clostridium pasteurianum*, and kinetic and flow parameters used in simulations can be found in Table 13 below.

Parameter	Value
β	0.7
$D_{Opt,Continuous}$	0.1523 h^{-1}
$D_{Opt,Simple\ Cell\ Recycle}$	0.2176 h^{-1}

Table 13: Kinetic parameters and assumed flows used for Simulation of *Clostridium pasteurianum* fermentations

In order to give a comparison of a low and high flow scenario, the optimum dilution rate for a continuous system is used as the low flow ($D_{Opt,Continuous} = 0.1523\ h^{-1}$), and for high flow rates, the optimum dilution rate for the cell recycle system is used ($\beta = 0.7, D = 0.2176\ h^{-1}$).

Additionally, solutions for these systems are limited to those where the concentration of biomass in the solution passing by the membrane is less than 6% solids (60g/L), and substrate concentration is greater than zero, to avoid starvation of the organism.

3.3.1 Simulations

Simulations are presented here under two conditions: low flow based on optimum dilution rate for a continuous reactor (D=0.1523h^{-1}); and high flow which is the continuous optimum rate adjusted by $\frac{1}{\beta}$, which is the optimum dilution rate for a simple cell recycle system without inhibition (D=0.2176h-1). Transient solutions can be seen below in Figure 16 and Figure 17.

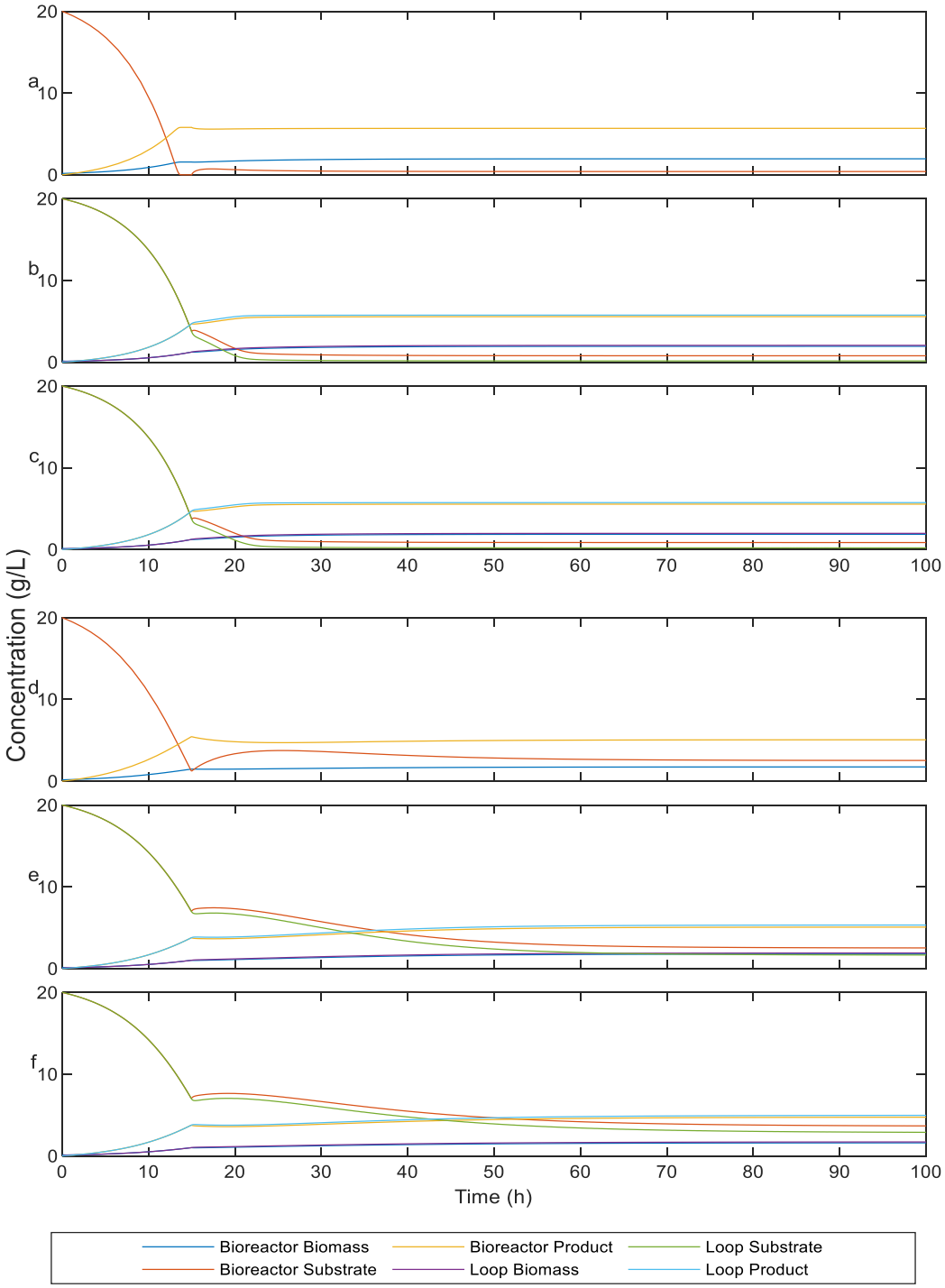

Figure 16: Transient Solutions for Cell Recycle Arrangements at Low Dilution Rate. Simulations a-c are without product inhibition, d-f are with product inhibition. a) and d): Simple Cell Recycle; b) and e) Feed-and-Bleed with outlet from bioreactor; c) and f) Feed-and-Bleed with outlet from recirculation loop. D=0.1523h^{-1}. Parameters for simulation can be found in Table 4. Feed flow begins at 15h. Substrate in the bioreactor is orange, substrate in the recirculation loop is purple; Biomass in the bioreactor is blue, biomass in the recirculation loop is green; Product in the bioreactor is yellow, product in the recirculation loop is red.

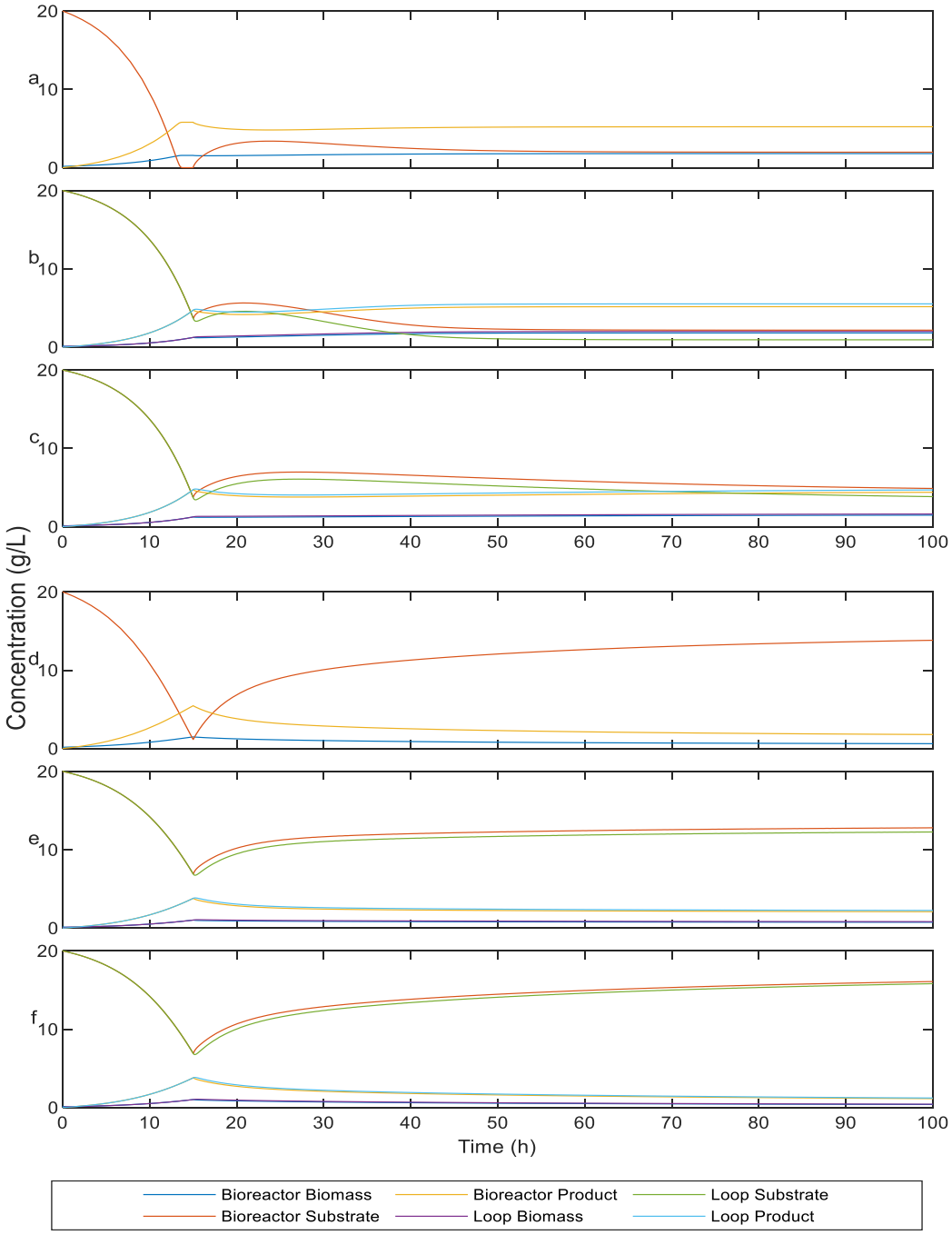

Figure 17: Transient Solutions for Cell Recycle Arrangements at High Dilution Rate. Simulations a-c are without product inhibition, d-f are with product inhibition. a) and d): Simple Cell Recycle; b) and e) Feed-and-Bleed with outlet from bioreactor; c) and f) Feed-and-Bleed with outlet from recirculation loop. D=0.2176h^{-1}. Parameters for simulation can be found in Table 4. Feed flow begins at 15h. Substrate in the bioreactor is orange, substrate in the recirculation loop is purple; Biomass in the bioreactor is blue, biomass in the recirculation loop is green; Product in the bioreactor is yellow, product in the recirculation loop is red.

From beginning of fermentation until the beginning of feed flow at 15 hours, the difference between the simple cell recycle and feed-and-bleed arrangements is distinct, especially at lower flow. The simple cell recycle system has significantly faster fermentation, and thus has a higher cell concentration and higher productivity when the feed flow is turned on. In the feed-and-bleed arrangements fermentation is slower as the biomass is all concentrated in the bioreactor at inoculation resulting in cells in the bioreactor being exposed to a slightly lower substrate concentration.

Once feed flow begins, substrate and product concentrations approach steady state before biomass in all systems, and in the feed-and-bleed arrangements the bioreactor and recirculation segments separate into distinct steady states. Under the high flow condition, all systems take longer to approach steady state. The difference in steady state concentration are shown in Figure 18 and Figure 19 below.

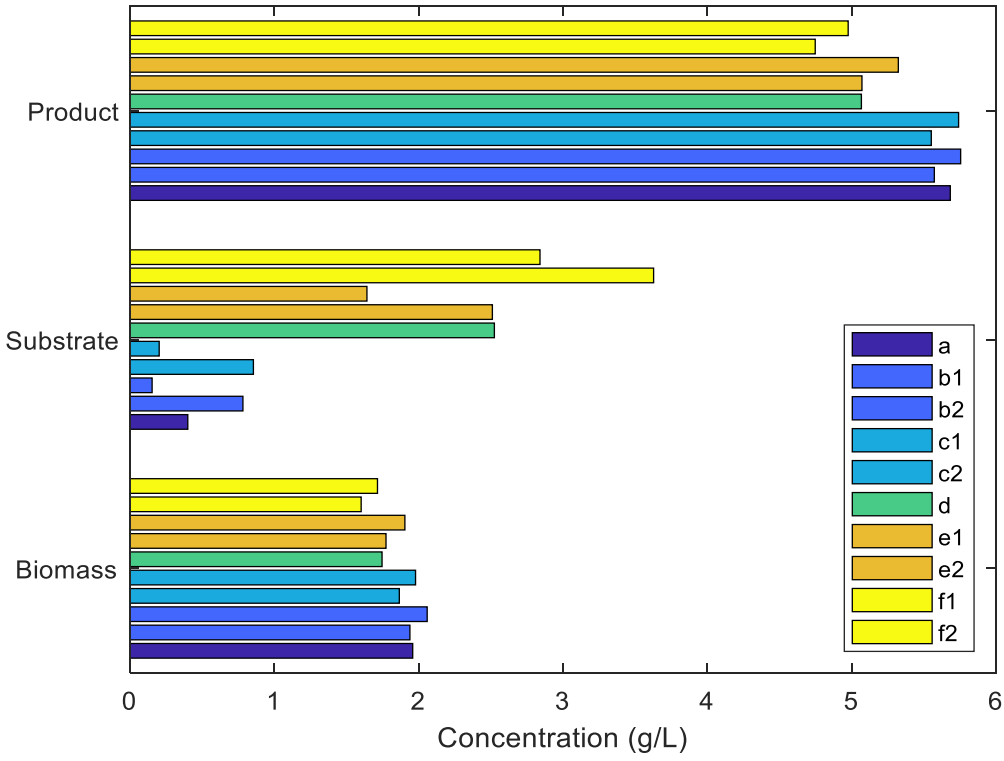

Figure 18: Steady State Concentrations of Biomass, Substrate, and Product for Cell Recycle Arrangements at Low Dilution Rate. Simulations a-c are without product inhibition, d-f are with product inhibition, 1 indicates bioreactor bleed and 2 indicates recirculation loop bleed for feed-and-bleed arrangements. a) and d): Simple Cell Recycle; b) and e) Feed-and-Bleed with outlet from bioreactor; c) and f) Feed-and-Bleed with outlet from recirculation loop. D=0.1523h^{-1}.

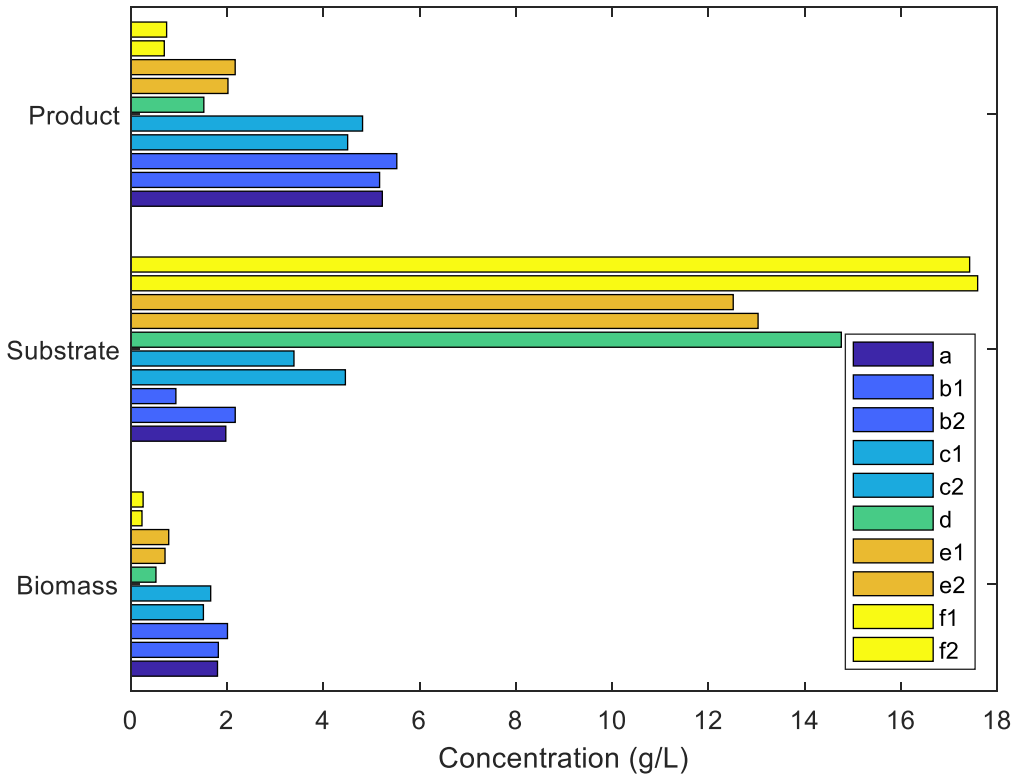

Figure 19: Steady State Concentrations of Biomass, Substrate, and Product for Cell Recycle Arrangements at High Dilution Rate. Simulations a-c are without product inhibition, d-f are with product inhibition, 1 indicates bioreactor bleed and 2 indicates recirculation loop bleed for feed-and-bleed arrangements. a) and d): Simple Cell Recycle; b) and e) Feed-and-Bleed with outlet from bioreactor; c) and f) Feed-and-Bleed with outlet from recirculation loop. D=0.2176h^{-1}.

Under the low flow condition shown in Figure 18 biomass concentrations in the bioreactor for Simple and Feed-and-Bleed with bioreactor bleed arrangements (Figure 18 a and b1; d and e1) are comparable, however the recirculation loop biomass concentration is slightly higher (Figure 18 b2, e2). For the Feed-and-Bleed arrangement with recirculation loop bleed (Figure 18 f1, f2), the biomass concentration in the bioreactor is lower than, and the concentration in the loop is comparable to, the concentration seen in the bioreactor in the simple cell recycle arrangement (a). The placement of the bleed line on the recirculation loop decreases the concentration of biomass in the loop, however product concentrations are very similar for both feed-and-bleed arrangements when product inhibition is not present. With product inhibition, these differences are exaggerated, and the Feed-and-Bleed arrangement with recirculation bleed (f) significantly underperforms compared to both other arrangements. When product

inhibition is not present, the performance difference is not clear from concentrations alone. Productivity from the permeate line, and total productivity throughout the entire system, is shown for each arrangement below in Figure 20 and Figure 21.

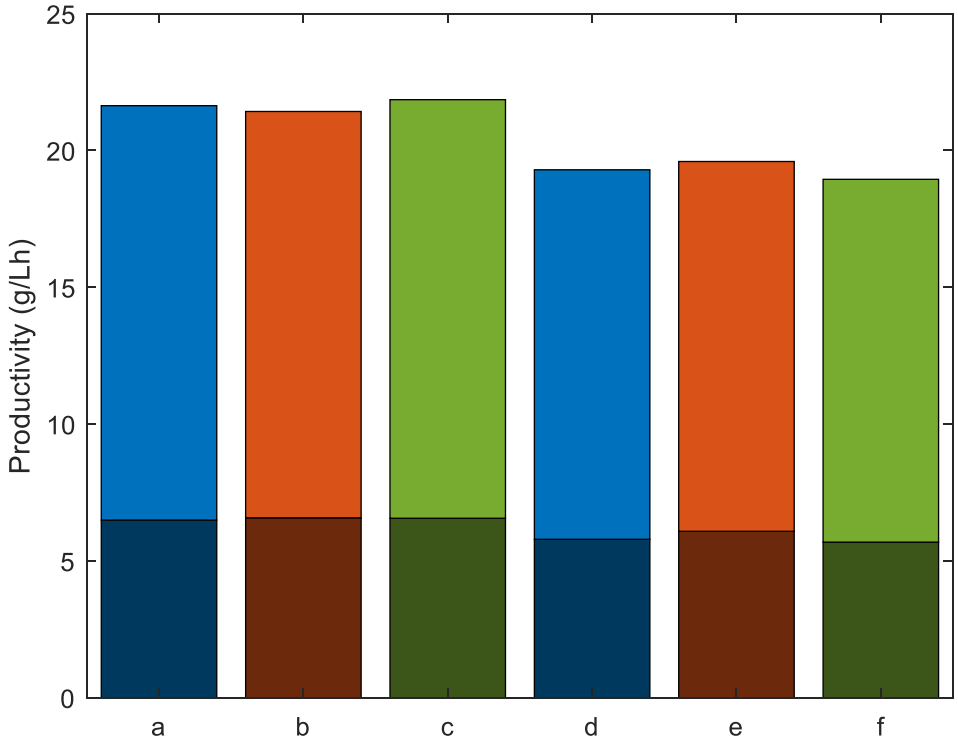

Figure 20: Steady State Product Productivity for Cell Recycle Arrangements at Low Dilution Rate. Simulations a-c are without product inhibition, d-f are with product inhibition. Dark bars represent permeate productivity, and light represent bleed line productivity, with each stack being total productivity. a) and d): Simple Cell Recycle; b) and e) Feed-and-Bleed with outlet from bioreactor; c) and f) Feed-and-Bleed with outlet from recirculation loop. $D=0.1523h^{-1}$.

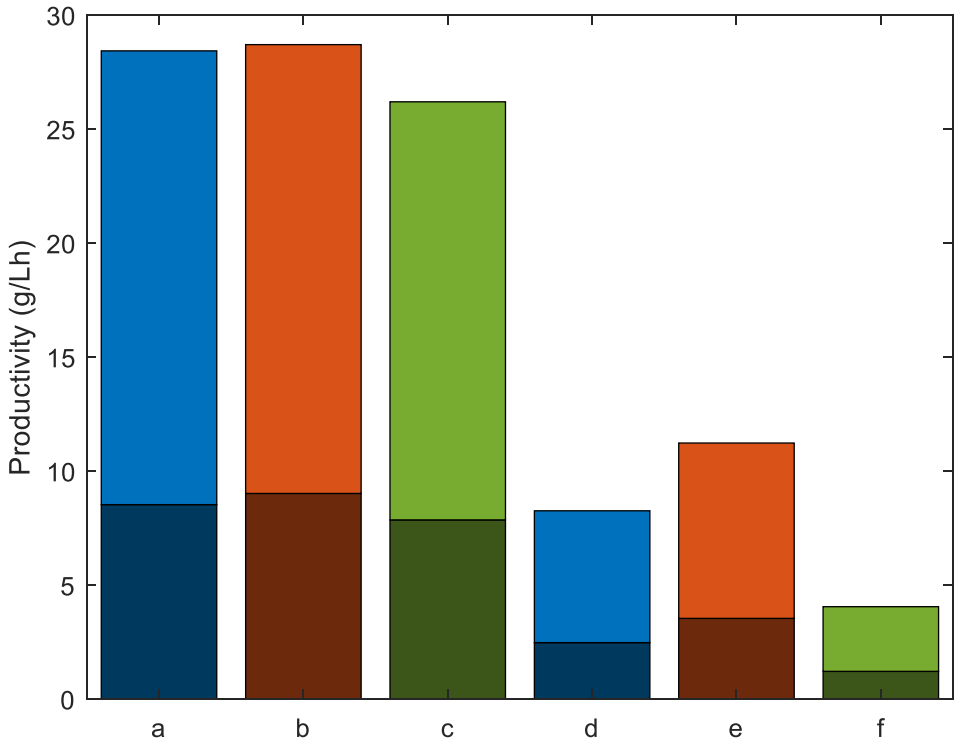

Figure 21: Steady State Product Productivity for Cell Recycle Arrangements at High Dilution Rate. Simulations a-c are without product inhibition, d-f are with product inhibition. Dark bars represent permeate productivity, and light represent bleed line productivity, with each stack being total productivity. a) and d): Simple Cell Recycle; b) and e) Feed-and-Bleed with outlet from bioreactor; c) and f) Feed-and-Bleed with outlet from recirculation loop. D=0.2176h^{-1}.

At both dilutions rate, each of the systems are comparable when product inhibition is absent. Permeate productivities are especially close when no product inhibition is present, with both Feed-and-Bleed arrangements being within 1% of the Simple arrangement. Both with and without product inhibition, the simple cell recycle arrangement is between the productivities for the other systems, for both permeate and total productivity. At low dilution rate, the Feed-and-Bleed with recirculation bleed (Figure 20 f1, f2) is the most productive, as the bleed line in this arrangement pulls the least amount of unconsumed substrate from the recirculation loop.

With inhibition and higher flow productivity is significantly decreased in all systems. This is due to the product inhibition slowing growth, so the ideal dilution rate for each system with inhibition would necessarily be below those given. A series of dilution rates need to be compared to properly examine the systems with inhibition. This is done below

where productivity is compared to dilution rate for total flow in Figure 22 and for permeate flow in Figure 23.

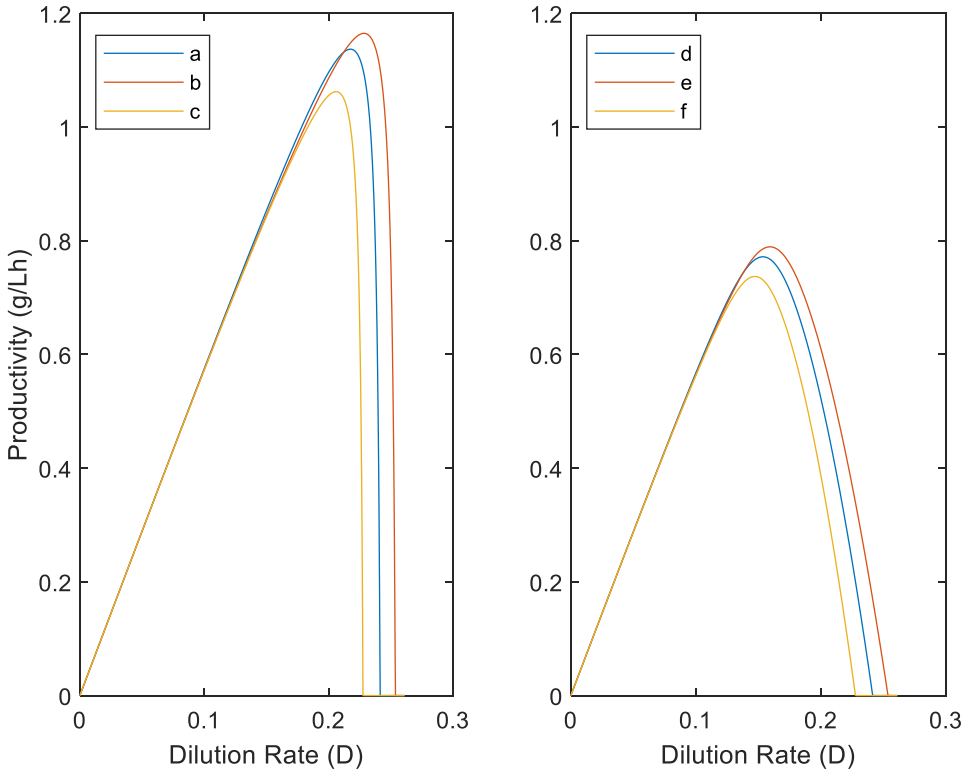

Figure 22: Productivity vs Dilution Rate for Total Flow. Simulations a-c are without product inhibition, d-f are with product inhibition a) and d): Simple Cell Recycle; b) and e) Feed-and-Bleed with outlet from bioreactor; c) and f) Feed-and-Bleed with outlet from recirculation loop.

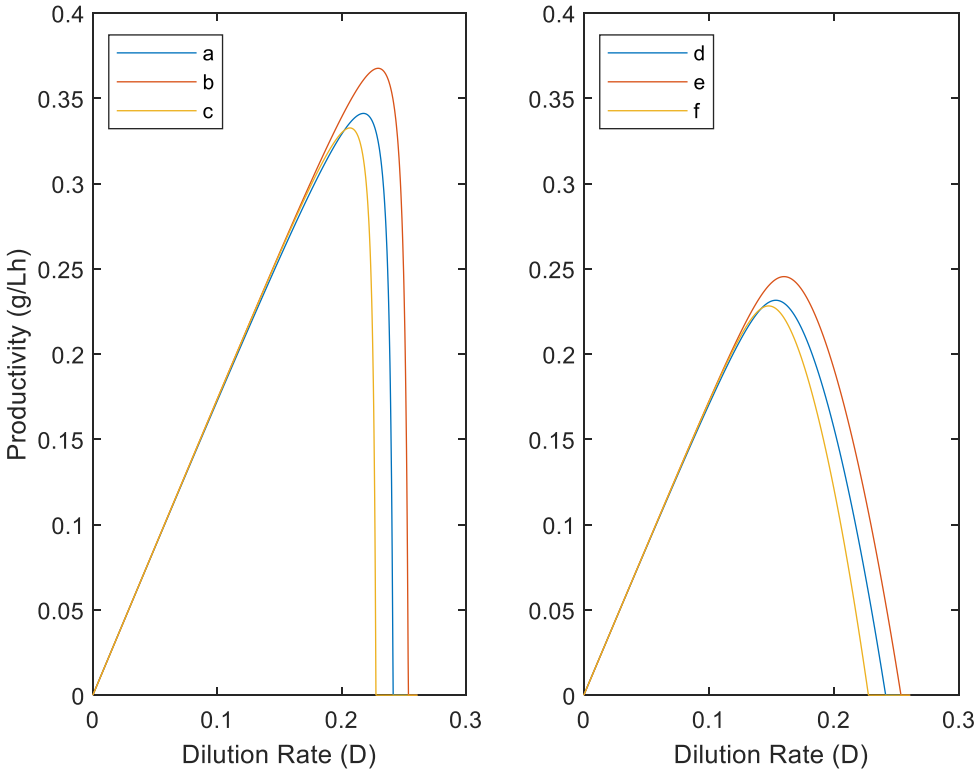

Figure 23: Productivity vs Dilution Rate for Permeate Flow. Simulations a-c are without product inhibition, d-f are with product inhibition. a) and d): Simple Cell Recycle; b) and e) Feed-and-Bleed with outlet from bioreactor; c) and f) Feed-and-Bleed with outlet from recirculation loop.

Figure 22 and Figure 23 show that at low dilution rates, the three systems all perform similarly, both with and without product inhibition. At higher flow rates the Feed-and-Bleed system with Recirculation Loop Bleed consistently underperforms compared to both other systems. Total productivity is close for both systems, but the Feed-and-Bleed with Bioreactor Bleed outperforms simple cell recycle in maximum productivity for both total flow and permeate flow. Maximum productivities are given in Table 14 below.

	Maximum Permeate Productivity (g/Lh)	Dilution Rate (h^{-1})	Maximum Total Productivity (g/Lh)	Dilution Rate (h^{-1})
Simple Cell Recycle	0.3411	0.2175	1.1370	0.2175
Feed-and-Bleed with Bioreactor Bleed	0.3676	0.2294	1.1649	0.2284
Feed-and-Bleed with Recirculation Loop Bleed	0.3326	0.2067	1.0623	0.2059
Simple Cell Recycle with Product Inhibition	0.2315	0.1536	0.7718	0.1536
Feed-and-Bleed with Bioreactor Bleed with Product Inhibition	0.2454	0.1602	0.7894	0.1591
Feed-and-Bleed with Recirculation Loop Bleed with Product Inhibition	0.2282	0.1479	0.7372	0.1471

Table 14: Maximum Productivities for Permeate and Total Flow for Bioreactor Arrangements

The maximum productivity for permeate flow under Feed-and-Bleed with Bioreactor Bleed is 8% and 6% higher than the Simple Cell Recycle without and with product inhibition respectively. The maximum productivity for total flow under Feed-and-Bleed with Bioreactor Bleed is 2% higher than the Simple Cell Recycle system both with and without product inhibition.

3.3.2 Limitations of Simulations

There are a few omissions from this work which may impact the results. Any cell death or stress associated with pump actions, shear stress, or substrate limitation are not considered. Given the similar volumes between the Simple Cell Recycle and Feed-and-Bleed arrangements, the impact of pumping and shear within the membrane and recirculation sections may be comparable, and any significant limitation from those effects would be present in any of the arrangements.

The effect of substrate limitation may be present in low dilution rates in the Feed-and-Bleed arrangements, and this could contribute an unstable population and a decrease in cell recycle effectiveness, however substrate never reaches zero, and under product inhibition conditions and low flow rates substrate concentrations remain over 1.5g/L for all bioreactor arrangements. So long as this substrate concentration is not below a minimum threshold for the organism, these models should be valid.

3.3.3 Recommended Bioreactor Configuration for Intensifying *Clostridium pasteurianum* at Lab Scale

The Feed-and-Bleed with Bioreactor Bleed under all conditions produces a higher maximum productivity, however this is not the only consideration. Assuming total flow would be used in a downstream process, then the increase in productivity is only 2%. This maximum productivity would also require a longer time to reach steady state as the dilution rate is higher. The Feed-and-Bleed arrangement is also more complicated, requiring additional pumping and piping, and requiring control of fermentation conditions such as temperature and pH in the recirculation loop.

The models used here also assume that there is no effect from changing fermentation conditions, such as substrate and product concentration, flow and shear, or temperature and pH. These conditions may differ in value or method of control from the bioreactor to the recirculation loop, and so may require the organisms to respond differently. These changed may result in different growth rates, product profiles or even a lag phase. This is both a limitation of the assumptions used here as well as the logistic models used in these simulations [14]. To accommodate these issues empirical testing is required for any scenario to be certain that these models will continue to apply.

Lastly, no examples of cell recycle work using the Feed-and-Bleed arrangement are present in the literature. While this does present an opportunity for increased productivity, there is no opportunity for comparison if cell recycle work is not initially performed using the Simple Cell Recycle arrangement.

It is recommended that initial cell recycle work for *Clostridium pasteurianum*, or any organisms which has not been studied in a cell recycle arrangement, be performed using

the Simple Cell Recycle arrangement for simplicity of design, build, and operation, and for the ability to compare to other cell recycle work.

3.4 Conclusions and Future Work

We found that the Feed-and-Bleed system with Bioreactor Bleed has a benefit of 6% or 8% increase in productivity in the permeate stream compared to simple cell recycling, depending on the presence or absence of product inhibition, and 2% increased productivity when both outlet streams are combined, regardless of inhibition. However, given that the Feed-and-Bleed system is more complex to implement than the Simple Cell Recycle system and does not currently have a body of comparable literature, initial studies of *Clostridium pasteurianum*, or any organism which has not been studied in a cell recycle arrangement, should be performed using the Simple Cell Recycle arrangement before studies are performed using the Feed-and-Bleed arrangement.

Future work on simulation of bioreactor arrangements for *Clostridium pasteurianum* should include derivation of analytical solutions of optimum dilution rate for product inhibition, optimization of bioreactor and recirculation loop sizing of bioreactor, and optimization of substrate concentration. Additionally, expansion of model variations to include different kinetic models for growth and expanding the equations used for product inhibition would expand this work to apply to other organisms.

Lastly, additional future modelling work on *in situ* extraction, inclusion of downstream processes, and expanded recycle streams for minimizing water requirements and maximizing yield would be beneficial for larger system design and moving towards commercialization.

Chapter 4

4 Design and Construction of Benchtop Bioreactor and Cell-Recycle System and Testing with DI Water

Intensification of bioreactor systems is useful for increasing productivity of fermentation systems, however off-the-shelf solutions do not exist for cell recycle systems. This chapter outlines the design, development, and construction of a benchtop bioreactor and cell recycle system. Materials chosen and design of outflow systems for passive level control are discussed, and flow testing of the system was performed using deionized water to show maximum flows and fluxes within operational limits.

4.1 Introduction and Background

Intensification of bioreactor systems is needed in cases with slow growing organisms, or organisms with slow metabolisms at conditions for product formation [26]. This intensification can be done in different arrangements, including settling, immobilization, and cell recycle via filtration [46, 26]. Certain methods are not available or as effective for smaller scale benchtop fermentations so separate design considerations need to be put in place than would be ideal for a commercial scale system.

In addition to intensification, the cell recycle system is also a stepping stone to a larger project with integrated pervaporation where cells are removed from the stream leading to the pervaporation unit [1]. Previous work on *Clostridium pasteurianum* has generally been focused on continuous fermentation or using genetic engineering on *Clostridium pasteurianum* as a solution to fermentation issues. This process engineering approach combines with these other approaches as an improvement over continuous systems and a system where the advantages of engineered organisms can be taken advantage of to a greater extent.

This work covers design considerations, construction, and testing with DI water of a benchtop scale single pass, single module cell recycle system [25]. This design is based on a minimum viable product approach using low cost materials for fast and easy construction of a benchtop system. This system will then be tested using DI water to

show maximum flow, membrane resistance, and to ensure general functionality as expected. This system is designed with its intended use with the anaerobic bacteria *Clostridium pasteurianum*, however the design should be general enough to be used with any microorganism, so long as appropriate sparging is performed for aerobic organisms.

4.2 Materials and Methods

4.2.1 Bioreactor and Pumps

The bioreactor that the system was built around was a Labfors 4 from Infors HT (Infors HT, Bottmingen/Basel, Switzerland, model: LabFors 4, 7L total volume). In order to most closely resemble fermentation conditions, the built-in controller was used to deliver pure nitrogen gas sparged at a rate of 0.60L/min, maintain temperature at 35^{o}C, and agitated with a Rushton impellor at 150 RPM.

Fluid was transferred from the bioreactor and through the membrane apparatus using a peristaltic pump (Watson-Marlow 620UN). This pump was chosen as peristaltic pumps are commonly used as they are less damaging to cells, and this pump meets the needed 10L/min flow rate recommended by Koch. Flow calibrations for this pump in the apparatus can be found in Appendix A. All other pumps were Masterflex Compact Drive peristaltic pumps with operating ranges between 5-100mL/min.

The membrane cartridge used was a Koch Romicon Pro microfiltratration unit (HF,1018-1.0-53-MF-0.5) with a pore size of 0.5mm, an internal volume of 40mL, and a total membrane area of 0.09m^2.

4.2.2 Choice of Materials

This design was built as a minimum viable product and development model, so cost and ease of availability of components was prioritized over long term use. Tubing used was made of polyvinylchloride (PVC), hard connectors for the filter cartridge section were made of polypropylene (PP), and tubes drawing and returning to the bioreactor were made of stainless steel. The PVC and PP materials were chosen for low cost and corrosion compatibility with sterilization with chlorine bleach, and the stainless steel materials were chosen due to need for hard materials connecting to the bioreactor and the

need for sterilization via autoclave. Sterilization procedures can be found in Appendix B. One connector piece for the return line from the membrane section to the bioreactor was made of nickel-plated brass, as sourcing of a NPT-to-PG stainless steel piece was prohibitively expensive, so this piece is a consumable as significant corrosion is expected to occur over long term use in fermentation.

4.2.3 Methods

Permeate flow was measured gravimetrically by measuring the time it took to fill a 1L graduated cylinder with deionized water. The mass of the cylinder was measured before and after on a standard balance, and the flow rate calculated assuming a density of water of 1.000g/L.

Pressure within the system was measured using McMaster-Carr stainless steel pressure gauges before and after the membrane, and on the permeate side. Values varied due to the duty cycle of the pump, so the average of minimum and maximum values for each gauge was used as the value for that gauge. Membrane Pressures are the average of the values for the gauges before and after the membrane.

4.3 Design of Outflow Systems for Volume Control

Volume control in benchtop systems can be difficult, certain methods are limited in accuracy due to the size of the system. If the density of the liquid is known, then pressure at the bottom of a tank can be used to determine liquid level. Additional common methods used for level sensing include floating level switches and imagine. None of these methods are appropriate for benchtop use to size or cost.

Methods commonly used on benchtop scale include using light sensing or conductance at the expected height of the liquid, however these methods are prone to failure from foaming at the top of the liquid, giving a falsely high measurement.

The above volume control methods require active control of the outflow, either by adjusting a valve or changing the setting on a pump. However, simpler methods are

available for benchtop scale bioreactors using passive control. An example of a simple outflow system is given in Figure 24 below.

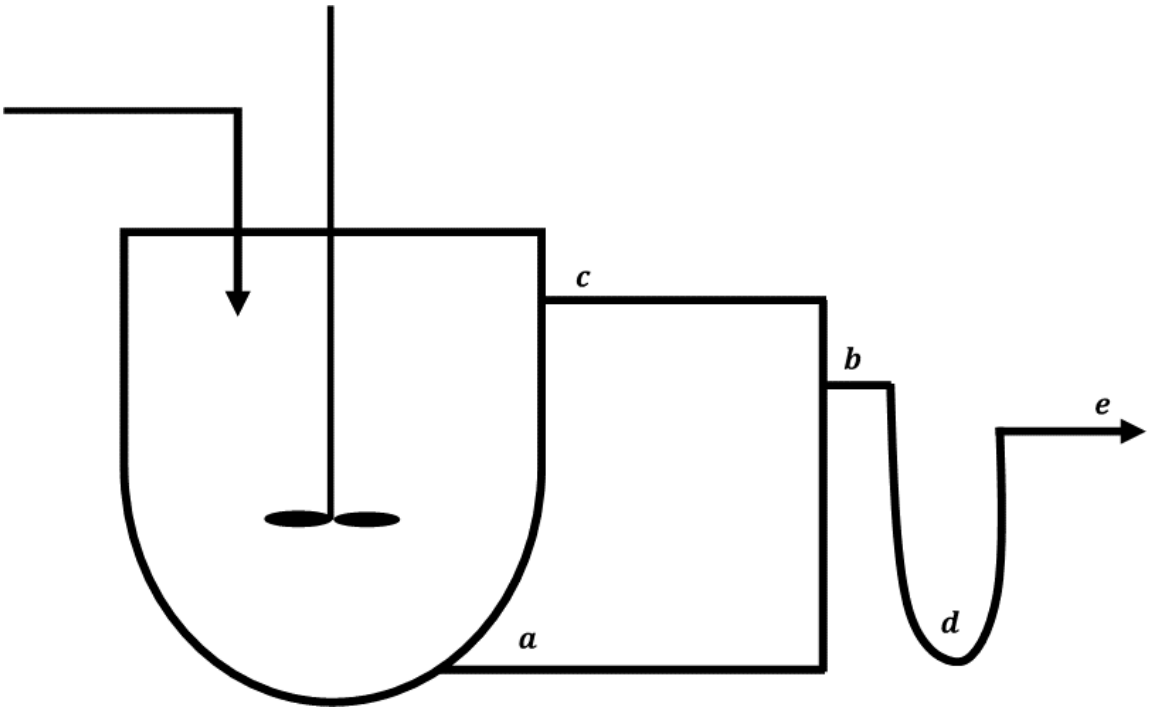

Figure 24: Diagram of Passive Outflow System. *a*) Bioreactor outlet. *b*) Gas-liquid junction and bioreactor liquid level. *c*) Gas pressure balance line. *d*) Fluid plug. *e*) Outlet system output.

In Figure 24, fluid leaves the bioreactor at *a* due to the pressure in the bioreactor, and rises to *b*. The Gas-liquid junction at *c* prevents siphoning through the outlet and allows pressures to equalize, meaning that the liquid level will be equal to the position at *b*. From *b*, liquid flows into the fluid plug loop at *d*, where the height of the fluid in the plug on the bioreactor side is equal to the height of *e* minus the effect of gas pressure. The height difference from gas pressure is the gauge pressure of the gas in the bioreactor divided by the density and force of gravity ($\Delta h = \frac{P}{\rho g}$). So long as the height from the bottom of *d* to *e* is greater than the height from gas pressure, then the liquid plug should remain in place and only liquid will leave via the outflow line, leaving any gas flow measurements accurate and allowing volume to be controlled passively while maintaining isolation from contamination.

In order to construct the system in Figure 24, a connection needs to be made through the side of the bioreactor, which is undesirable if it is not part of the initial construction, especially for jacketed bioreactors. To accommodate this, fluid can be drawn from the top of the bioreactor with a pump which runs at a higher rate than the expected outflow. This system is shown in Figure 25.

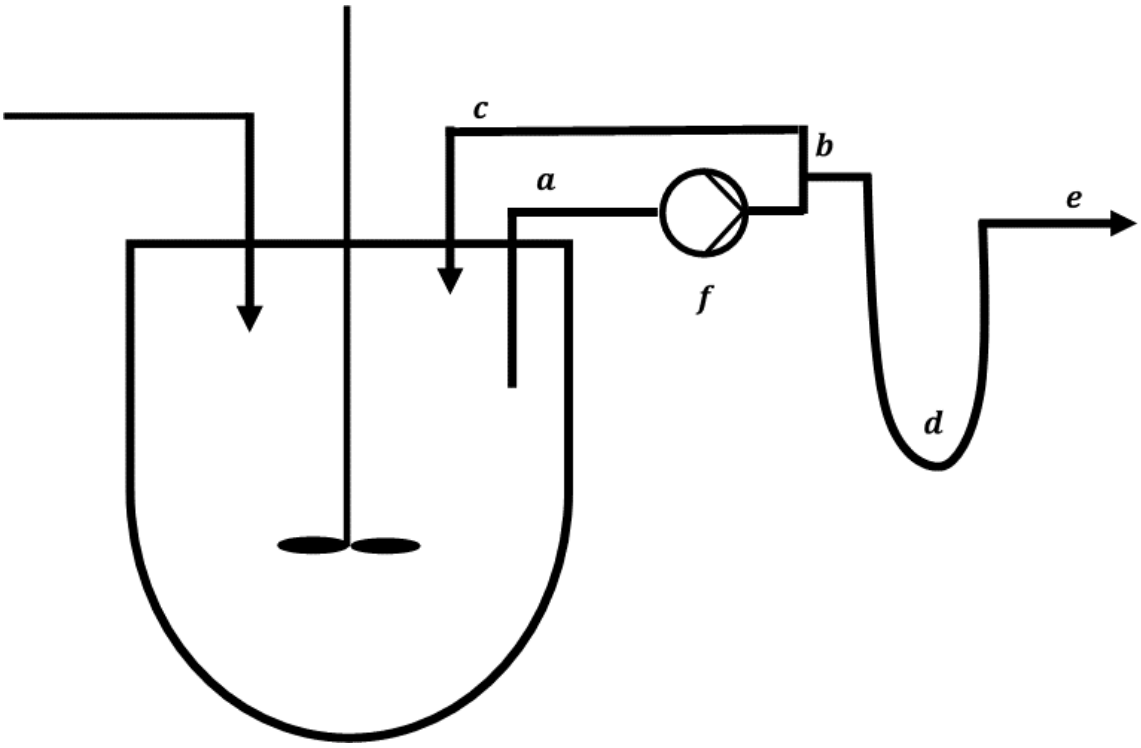

Figure 25: Diagram of Active-Passive Outflow System *a*) Bioreactor outlet. *b*) Gas-liquid junction. *c*) Gas pressure balance line. *d*) Fluid plug. *e*) Outlet system output. *f*) Outlet flow pump.

For the system in Figure 25, the bottom of the outlet line *a* in the bioreactor is the liquid level, and the pump runs faster than the flow in and out of the system. This will draw in gas, which will recirculate through *b* and back into the bioreactor via *c*. This way, liquid will flow from *b* out of the bioreactor in the same was as the passive system, but with simpler modification to the bioreactor.

One major limitation of the system in Figure 25 is that by drawing from the top of the bioreactor flow is limited by the pressure of the gas in the head space of the bioreactor. This gas is generally at or near atmospheric pressure, unless the bioreactor is specifically designed as a pressure vessel. This vacuum suction limits both the flow, the type of pump, and the type of tubing that is effective for this system. Silicone tubing and a

peristaltic pump were effective for controlling volume at flow levels under 20mL/min. Calculating the limitations of flow can be done by finding flow resistance at a given volumetric flow rate and pipe diameter on a per distance basis, which when combined with the pressure loss from gravity will give the maximum height from the liquid level any liquid in the pipe can reach. This is particularly important in the design of the membrane section of the bioreactor, as flows of 10L/min are recommended to minimize fouling.

Assuming the pressure inside the bioreactor is atmospheric, then the maximum pressure loss from gravity and friction is 1atm, or 101.325kPa, after which no flow can proceed. This limitation is fundamental, but in practice the limit would be lower due to any imperfections in the system, such as curves, or phase changes in the liquid. Flow resistance from friction can be calculated using the Darcy-Weisbach equation and the Colebrook-White Equation, seen below Table 15.

Colebrook-White Equation (Darcy-Weisbach friction factor, f)	$\frac{1}{\sqrt{f}} - 2\log\left(\frac{\varepsilon}{3.7D_h} + \frac{2.51}{Re\sqrt{f}}\right)$	**4-1**
Darcy-Weisbach Equation (pressure loss from friction)	$\frac{\Delta p}{L} = f\frac{\rho}{2}\frac{v^2}{D}$	**4-3**

Table 15: Pressure Loss from friction - Darcy-Weisbach and Coleman-White Equations. Where Re is Reynolds number, f is the Darcy-Weisbach friction factor, D is pipe diameter, $\boldsymbol{\rho}$ is density, $\boldsymbol{v}$ is superficial fluid velocity, $\boldsymbol{\varepsilon}$ is material roughness.

The total height of the unit is 46.5cm, so for both the bioreactor outlet and the line leading to the membrane section a height of at least 40cm needs to be overcome. Using non-linear methods to solve for f in the Colebrook-White equation in Table 15, and using parameter values for water, the pressure loss can be found. If this pressure loss is less than atmospheric pressure, then vertical vacuum suction should be effective at fluid transfer. For the 2mm tube which comes with the Infors unit this gives a possible flow of over 1L/min, well above what should be needed for that section. The membrane line however needs to be able to handle 10L/min of flow, according to the manufacturers recommendations to minimize fouling of the membrane. In order to accomplish this using

standard sizing, the tube needs to be ¼ inch or greater, and for this build a ½ inch tube was used to ensure no issues with flow.

4.4 Construction and Description of Cell Recycle System

The final construction of the system consists of a modified Labfors 4 bioreactor. A diagram of the modifications to the completed system can be seen in Figure 26 below.

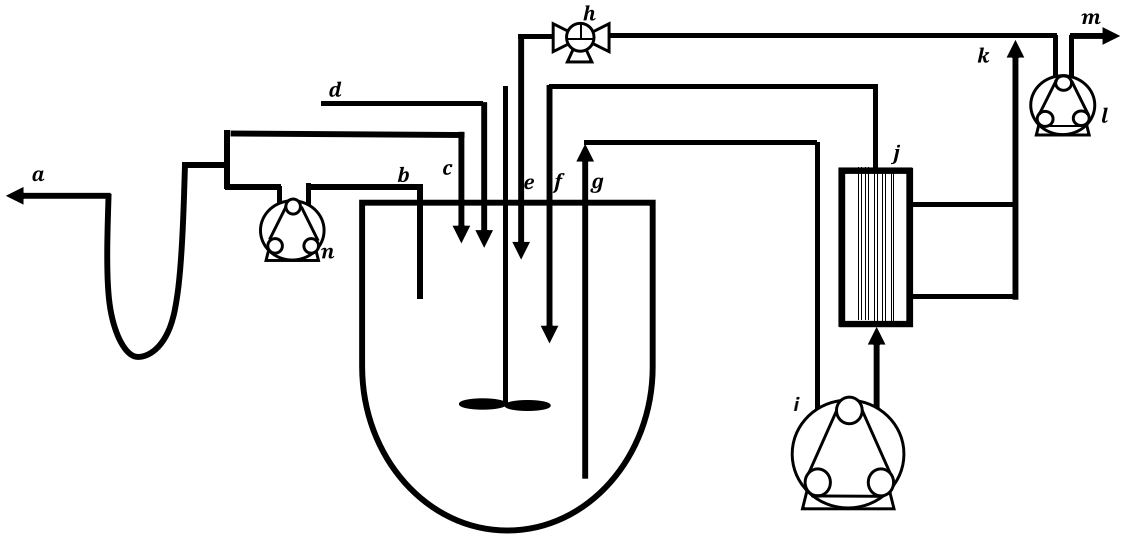

Figure 26: Diagram of full bioreactor system. *a*) Bleed system outlet (Outlet of active-passive system). *b*) Bioreactor draw to active-passive bleed system. *c*) Gas return for active-passive bleed system. *d*) Bioreactor Feed. *e*) Membrane Permeate return. *f*) Membrane Retentate return. *g*) Membrane Input draw. *h*) Three-way sample valve. *i*) Peristaltic Microfiltration Membrane input pump. *j*) Microfiltration membrane. *k*) Permeate line. *l*) Peristaltic Permeate outlet pump. *m*) Permeate outlet. *n*) Bleed pump.

Volume control and outflow consists of sections *a-c*, and is accomplished via the Active-Passive system shown in Figure 25 above. A 2mm tube extends down into the bioreactor at *b* and ends at the top of the liquid in the bioreactor. Tubing in low flow sections (*a-d, h, k, m*) all used 2mm ID silicone tubing. Pumps at *n* and *l* are small peristaltic pumps with a maximum flow of 100mL/min.

Flow to the membrane section was accomplished by extending a ½ inch stainless steel tube to 5cm above the bottom of the bioreactor. This leads to ¾ inch PVC tubing, which leads the Watson-Marlow peristaltic pump, which was placed on the ground roughly 1m below the bioreactor, to ensure appropriate net positive suction head for maintenance of

the internal tubing of the pump. After the pump the ¾ inch tubing leads to the membrane, then back to the bioreactor. A ½ inch stainless steel tube was lowered 20cm into the bioreactor, below the top of the liquid in the bioreactor, to decrease agitation from return flow. Operating flow into the membrane is approximately 10L/min as recommended by the manufacturer.

The permeate outflow pump, *l*, allows for control of permeate flow from the bioreactor, which gives a constant bleed ratio, β, and allows for the system to be predictable. The three-way value at *h* can be left open for maximum permeate flow, opened to sample to allow for measurement of total permeate flow, or can be left closed to limit permeate flow to the rate set on the pump. A lower flow of permeate reduces the amount of flow through the membrane and thus decreases the amount of fouling of the membrane [47]. This increases the amount of time an individual filter can be used in an operating system without needing to be taken offline for cleaning.

4.5 Flow Testing with DI Water

The system was tested to determine maximum flow with DI water, verify stability, operational range, linearity with respect to pressure, and to measure membrane resistance independent of media, biomass, and fouling. Both flow rate and pressure were varied. Flow rate was varied by changing RPM on the Watson-Marlow pump, and pressure was varied by changing flow resistance through opening or closing a globe value that was added between the membrane and the return line to the bioreactor, and measured using inline pressure sensors.

Permeate flow can be modelled either empirically for the region that data is available for, or by matching to a theoretical model of flux. Data below 150RPM and 5psi are not included in the curve fitting, as the sensors used to measure pressure did not have sensitivity below 2psi, so the actual average feed pressure was not able to be determined as the retentate stream had a pressure at or below 2psi. Similarly, in all cases permeate pressure is assumed to be 0psi, as permeate pressure was always at or below 2psi. The effect of this is an overestimation of membrane resistance, or an underestimation of expected flow, in all models.

Empirical equations for linear curve fitting one and two variable models, as well as an equation for theoretical resistance-in-series model, are given in Table 16 below [47].

Model	Equation	
Empirical Curve Fitting		
Two variable Model	$Y=\beta_0+ \beta_1X_1+ \beta_2X_2$	**4-7**
Single Variable Model	$Y=\beta_0+ \beta_1X$	**4-5**
Theoretical Flux Model		
Permeate Flux	$J = \frac{Q}{A_m} = \frac{TMP}{\mu(R_m + R_c + R_p)}$	**4-9**

Table 16: Empirical and Resistance-in-Series Models for permeate flux. Where J is membrane flux, Q is volumetric flow, TMP is transmembrane pressure, $\boldsymbol{A_m}$ is membrane area, μ is dynamic viscosity, $\boldsymbol{R_m}$ is membrane resistance, $\boldsymbol{R_c}$, is cake resistance, and $\boldsymbol{R_p}$ is resistance from pore blocking.

In the above model, resistance from cake and pore blocking can both be assumed to be zero or negligible, since in this case testing was performed using pure DI water. This leads to the theoretical model reducing to the equation given below, which in turn can be expressed as a least squares system for the purposes of curve fitting.

Permeate Flow Model	$Q = \frac{TMP(A_m)}{\mu(R_m)}$	**4-1**
Permeate Flow Model as a Least Squares System	$Y = \beta X$	**4-1**
	$Where: Y = Q; X = TMP;\ \beta = \frac{A_m}{\mu(R_m)};$	

Table 17: Theoretical and Least Squares Models for Permeate Flux

Permeate flow vs average pressure and RPM are shown in Figure 27 below.

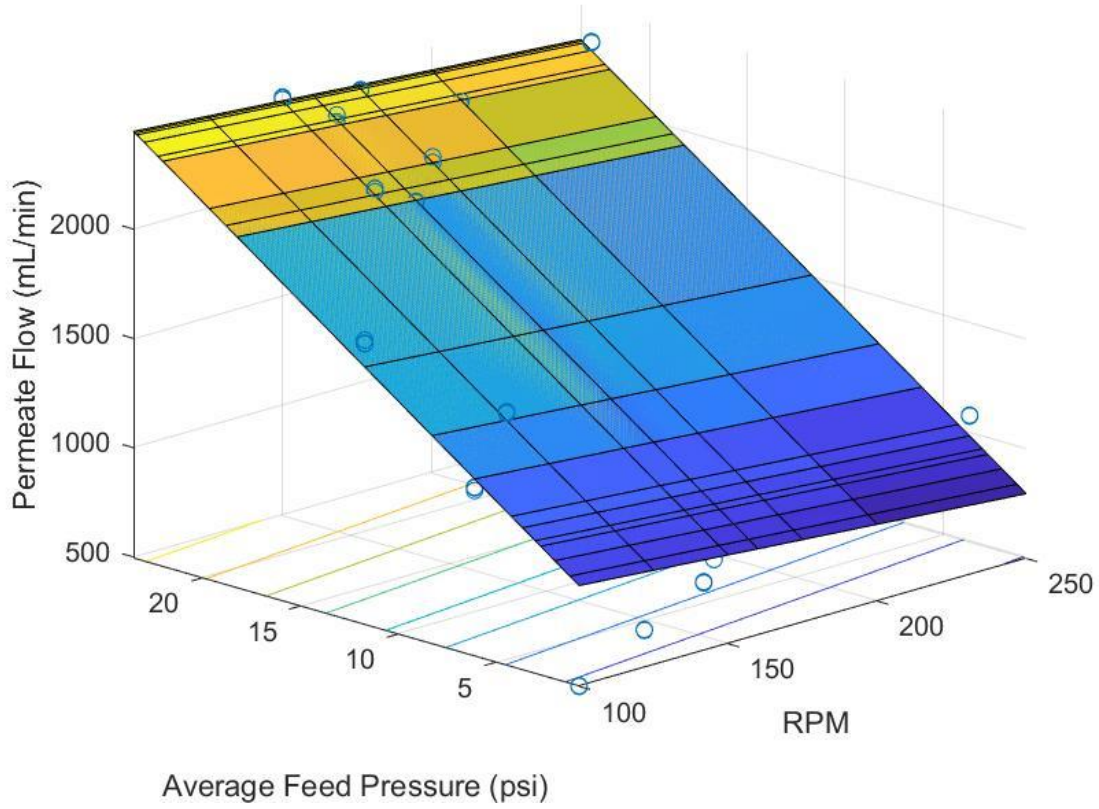

Figure 27: Permeate Flow vs RPM and Average Feed Pressure. Curve shown is a least-squares fit following the equation: $Y=\beta_0+\beta_1X_1+\beta_2X_2$, where Y is permeate flow in mL min^{-1}, X_1 is RPM, X_2 is Average Feed Pressure in psi. Values with 95% confidence interval: $\beta_0=1020\pm70$ mL min^{-1}, $\beta_1=-1.1\pm0.4$ mL min^{-1} RPM^{-1}, $\beta_2=65\pm2$mL min^{-1} psi^{-1}. $R^2=0.98$, RMSE=63mL min^{-1}, $p<0.01$.

Figure 27 shows the curve modelled by the two-variable empirical model shown in Table 16. This model has a strong fit for all values where pressure is greater than 5psi or RPM is greater than 150RPM, corresponding to approximately 9L/min, so operating parameters should stay within this boundary. The constant implies at no pressure or flow there would be roughly 1L/min of permeate flow, an obvious physical impossibility, therefore it is important to only use this model as an indication of flow within the applicable range.

Regardless of model used, if RPM is included as a predictive variable the p-value is significantly lower than those for the constant or pressure. Additionally, the effect size of the entire range of RPM is on roughly the same scale as the error for pressure. It is then

reasonable to eliminate RPM as a variable and only use psi as a predictive variable. Figure 28 below shows both a single variable empirical model and a theoretical model as shown in Table 16.

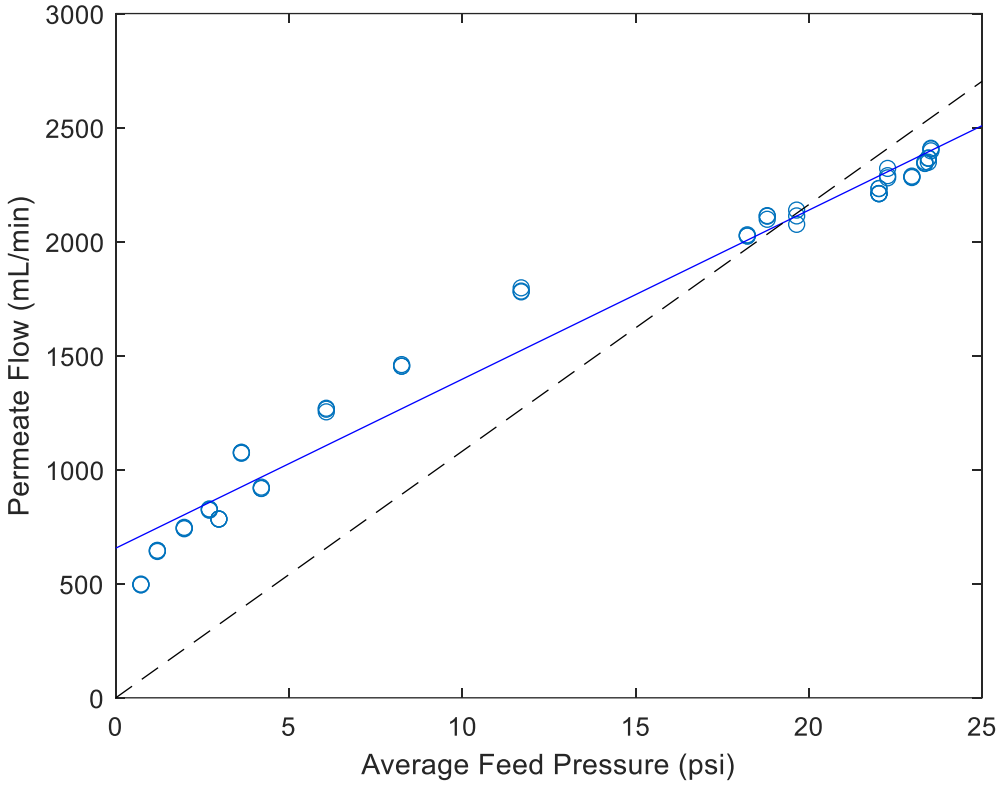

Figure 28: Average Feed Pressure vs Permeate Flow. Curves shown are based on equations for empirical curve (solid) and theoretical (dashed) from Table 16. Empirical curve shown is a least-squares fit following the equation: $Y=\beta_0+\beta_1X_1$, where Y is permeate flow in mL min^{-1}, X_1 is Average Feed Pressure in psi. Values with 95% confidence interval: β_0=660±40 mL min^{-1}, β1=74±3 mL min^{-1} psi^{-1}. R^2=0.97, RMSE=113mL min^{-1}, p<0.01. Theoretical curve shown is a least-squares fit following the equation: $Y=\beta_0X$, where Y is permeate flow in mL min^{-1}, X is Average Feed Pressure in psi. Values with 95% confidence interval: $\beta_0 = \frac{A_m}{\mu(R_m)}$ =108±5 mL min^{-1} psi^{-1}. RMSE=394 mL min^{-1}, p<0.01.

The curves shown in Figure 28 show that the empirical curve has a much better fit than the curve fit to the theoretical flux curve. Again, the empirical curve is only valid within the parameters shown, however the empirical curve was fit using all of the data obtained, and so is valid for average feed pressures from 1psi to 25psi, and RPM settings from 100RPM to 250RPM. The theoretical curve is forced through zero, as there would be no permeate flow at zero pressure. Using the dynamic viscosity of water at 35°C (μ=0.7185 mPa s), the membrane resistance is estimated to be $4.8x10^8$±0.2 $x10^8 m^{-1}$.

4.6 Conclusions and Next Steps

This work shows the outline of a modified design of a benchtop bioreactor unit to include a cell recycle system. In order for operation to be as predicable as possible, the unit should be operated with the pump running above 150RPM (~9L/min). All conditions tested gave permeate flows above 500mL/min, which is over an order of magnitude higher than would be needed given the maximum productive dilution rate shown in Chapter 2. However, this is for a system with no particulates or fouling, so this excess in open flow may be needed to accommodate actual fermentation conditions.

Further work is shown in Chapter 4, including initial fermentation, demonstration of concentrating cells and increased productivity. Future work for benchtop design and construction should include exploration of additional recycle streams on the cell bleed stream, *in situ* extraction processes, and active control of the system and of flow processes.

Chapter 5

5 Fermentation with Cell Recycle Apparatus

With design, construction, and initial flow testing of the cell recycle apparatus completed, the next step is to apply the system to actual fermentation. This chapter covers investigation into the system with active fermentation of *Clostridium pasteurianum*. The cell recycle system was operated with an active culture of *Clostridium pasteurianum* in a fed-batch mode and comparison to fed-batch growth without the cell recycle apparatus, demonstrating that not only can the cells withstand operation, but fermentation is not significantly different with the cell recycle than without it, showing minimum stress. The system was then operated continuously with an active culture of *Clostridium pasteurianum*. A maximum apparent Cell Dry Weight (CDW) of 3.14g/L was measured under low feed flow and low bleed flow, however not at steady state. Additionally, a maximum butanol productivity of 1.16g/Lh was measured under a high feed flow, the highest reported for wild-type *Clostridium pasteurianum* without genetic modification or immobilization, though also not at steady state. Productivity and efficiency of the system can be improved by increasing available fermentation time, which could be accomplished expanding the cell recycle system to include multiple membranes to be switched between or improving media composition to reduce fouling.

5.1 Introduction and Background

Intensification of fermentation processes can compensate for the low productivity of slow growing organisms, or decreased productivity due to product inhibition at high product concentrations by allowing for higher dilution rates, decreasing inhibitory compounds [1, 19, 20, 25]. *Clostridium pasteurianum* has been shown to be inhibited by butanol, so for butanol production to be industrially viable productivity needs to be as high as possible in order to prevent prohibitively large fermentation volumes, and one way to achieve this productivity gain is by retaining cells via a cell recycle system [6].

This chapter covers fermentation of *Clostridium pasteurianum* in parallel fed-batch, with one fermenter connected to a cell recycle system with permeate returned to the

bioreactor, and continuous cell recycle operation under two flow conditions. this is the first instance of wild type *Clostridium pasteurianum* in a cell recycle arrangement.

5.1.1 Previous Fermentation Work

Clostridium pasteurianum is a gram-positive bacteria, which can produce multiple valuable fermentation products, with most interest being in 1,3-propanediol and 1-butanol [6]. Previous work using mutant or engineered strains of *Clostridium pasteurianum* has been shown to increase productivity and yield, as has work using co-substrate fermentations with addition of sugars, acetic acid, or butyric acid [48, 49, 40]. This work has been performed mostly in batch, with few cases in fed-batch or continuous operation. Only one work has been done using cell recycle, and this was done using an engineered strain of *Clostridium pasteurianum*, so productivity increases cannot necessarily be generalized to wild-type *Clostridium pasteurianum* or other mutants [32]. Productivity values found in literature for *Clostridium pasteurianum* can be found in Table 18.

Strain	Mode	Substrate	Max Butanol Productivity (g/Lh)	Source
DSM 525	Batch	20 g/L Glycerol	0.98	[28]
DSM 525	Batch	50 g/L Crude Glycerol	0.119	[29]
DSMZ 525	Batch	80g/L glycerol, 20g/L glucose	0.96	[30]
DSMZ 525 (GMO)	Batch	80 g/L glycerol	0.29	[31]
MBEL_GLY2 (GMO)	Batch	80 g/L glycerol	0.43	[32]
DSMZ 525	Batch with gas stripping	111 g/L glycerol and crude glycerol	1.2	[34]
DSMZ 525 (MNO6)	Batch with gas stripping	105 g/L crude glycerol	1.8	[35]
DSMZ 525	Repeated batch with immobilized cells	60 g/L glycerol	3.08	[36]
DSMZ 525	Fed-batch with gas stripping	80 g/L glycerol	0.59	[37]
CT7	Fed-batch with pervaporation	100 g/L glycerol	0.21	[38]
DSM 525	Continuous	30 g/L Glycerol	1.07	[5]
DSMZ 525	Continuous, immobilized on corn stover	35 g/L Glycerol	4.2	[39]
MBEL_GLY2 (GMO)	Continuous with cell recycle	60 g/L Glycerol	7.8	[32]
DSMZ 525	Continuous with cell recycle	20 g/L Glycerol	1.16	This work
DSM 525	Batch	50 g/L Crude glycerol with 4 g/L butyrate	0.119	[29]
DSM 525	Batch	50 g/L Crude glycerol, 12 g/L Jerusalem Artichoke hydrolysate	0.74	[40]
DSMZ 525	Batch	50 g/L glycerol and 50 g/L biomass hydrolysate	1.1	[30]
CH4	Batch	60 g/L glycerol and 20 g/L glucose	0.28	[41]
CH4	Batch	60 g/L glycerol, 25 g/L bagasse hydrolysate	0.14	[41]

Table 18: Butanol Productivity for fermentations using *Clostridium pasteurianum*

5.1.2 Growth and Productivity in Cell Recycle Systems

Cell growth is assumed to follow Monod kinetics, and if the values for kinetic constants are known then mass balance can be performed and the system can be solved numerically [16, 25]. Equations describing cell recycle systems are given below [19, 20].

$$\mu = \frac{\mu_{max} S}{(K_s + S)} \quad \textbf{5-1}$$

$$\frac{dX}{dt} = \mu X - \beta D X \quad \textbf{5-2}$$

$$\frac{dS}{dt} = D(S_{in} - S) - \frac{1}{Y_{XS}} \mu X \quad \textbf{5-4}$$

$$\frac{dP}{dt} = \frac{Y_{PS}}{Y_{XS}} \mu X - DP \quad \textbf{5-5}$$

While some characteristics, like cell and product yield, are fairly consistent between fermentations, productivity and kinetic constants are heavily dependent on the specifi **5-7** fermentation characteristics and bioreactor arrangement, since Monod kinetics are empirical in nature [14]. As a result, kinetics cannot be assumed to be the same between fermentations unless the fermentations are very similar.

Butanol yield in *Clostridium pasteurianum* fermentations grown on only glycerol is generally around 0.3 grams of butanol per gram of glycerol [5, 33, 30, 31, 32]. Productivity, cell concentrations, and concentration of side products are not as consistent in the literature and much be measured and calculated. Equations for product yield, Y_{PS}, and productivity, p_P, are given below [19, 20].

$$Y_{PS} = \frac{\Delta P}{\Delta S}, \frac{g\ product}{g\ substrate} \quad \textbf{5-8}$$

$$p_P = DP \quad \textbf{5-9}$$

5.1.3 Fouling in Membrane Cell Recycle

Fouling of membranes in crossflow filtration comes from three mechanisms: concentration polarization, cake formation, and pore fouling. Conveniently, concentration polarization is negligible for pore sizes greater than 0.1µm, and so is also negligible at microfiltration scales of 0.5µm [22].

Cake formation is dependent on particle concentration, permeate flow, and crossflow fluid velocity. While cake formation for any given particle concentration proceeds at the same rate, the final cake depth is lower for high crossflow velocities. Permeate flow, however, increases both the rate of cake formation and final cake depth [22].

Pore fouling is fouling by the filling in of pores within the membrane. This can be a result of the deposition of organic material, such as dead cells of unconsumed media contents, or inorganic material, such as insoluble or minimally soluble compounds. Fouling from inorganic sources is also called scaling, and increases with concentration of species that are less soluble or likely to precipitate, such as calcium, magnesium, or iron in the presence of carbonate, sulfate, or phosphate. However, scale formation decreases with lower pH, so only the least soluble species should be of concern [22].

Pore fouling is only treatable by cleaning of the filter, with organic fouling being treated with caustic cleaning and inorganic fouling treated with acidic cleaning. Simple cleaning procedures can be seen in Appendix B.

These effects suggest that a high crossflow velocity is desirable to minimize long term cake depth, and that permeate flow should be held constant at the expected steady state flow, if that is known, to minimize the rate of fouling.

5.2 Materials and Method

5.2.1 Chemicals

Three solutions were used in fermentation: Reinforced Clostridium Medium, Modified Biebl Media, and SL7 micronutrient solution used in the Modified Biebl Media [5].

Reinforced Clostridium Medium (RCM) consisted of 3g/L Yeast extract, 10g/L Peptone from Fischer Scientific, Massachusetts, USA; 10g/L Beef Extract, BD-Becton, Dickinson and Company, New Jersey, USA; 1g/L Soluble Starch, 3g/L Sodium Acetate, 1mL/L Resazurin, Alfa Aesar, Ward Hills, MA, USA; 10g/L Dextrose, Amresco, Ohio, USA; 5g/L NaCl, 0.5g/L L-Cysteine added after sparging with nitrogen, BDH, Georgia, USA.

Modified Bieble Media consisted of 20g/L Glycerol, 0.5g/L KH_2PO_4, 0.5g/L K_2HPO_4, 5g/L Ammonium Sulfate, 1g/L Yeast Extract, Fischer Scientific, Massachusetts, USA; 0.02g/L $CaCl_2$, EMD Millipore, Massachusetts, USA; 0.2g/L $MgSO_4 \cdot 7H_2O$, Caledon Laboratory Chemicals, Georgetown, Ontario, Canada; 0.1g/L $FeSO_4 \cdot 7H_2O$, BDH, Georgia, USA; 0.2 mL/L Antifoam, Sigma-Aldrich, St. Louis, MO, USA; 2mL/L SL7 micronutrient solution.

SL7 micronutrient solution consisted of 1.5g/L $FeCl_2 \cdot 4H_2O$, dissolved in 25% HCl solution, 0.19 $CoCl_2 \cdot 6H_2O$, 0.1g/L $MnCl_2 \cdot 4H_2O$, 0.07g/L $ZnCl_2$, 0.062g/L H_3BO_3, 0.036g/L $Na_2MoO_4 \cdot 2H_2O$, 0024g/L $NiCl_2 \cdot 6H_2O$, 0.017 $CuCl_2 \cdot 2H_2O$, Sigma-Aldrich, St. Louis, MO, USA.

5.2.2 Culturing and Fermentation Conditions

Clostridium pastuerianum was purchased from DSMZ German Collection of Microorganisms and Cell Cultures in Braunschweig, Germany. Cultures were revived in an anaerobic chamber (Plas-Labs; Michigan, USA; model: 855-ACB-EXP) at 35^{o}C, on RCM, and stored at -80^{o}C with 20%v/v glycerol.

For fermentations with initial volumes of 5L, samples stored at -80^{o}C were revived by thawing in the anaerobic chamber and adding 0.5mL aliquots to 4.5mL of RCM, which were then incubated for 12 hours. This 5mL culture was then added to 45mL of RCM and

incubated for 8 hours, then the 50mL was added to 450mL and incubated until optical density (OD) measured between 1 and 1.3, approximately 8 hours. The 500mL of culture was then inoculated into 4.5L of fermentation media at the beginning of fermentation. For fed-batch fermentations with initial volumes of 3L, the same 10% v/v scale up procedure was performed, but with 0.3mL of thawed sample added to 2.7mL of RCM, 3mL of culture added to 27mL RCM, and 30mL culture added to 270mL RCM, with the 300mL of culture then added to 2.7L of media at inoculation.

All fermentations were carried out in an Infors HT bioreactor (Infors HT, Bottmingen/Basel, Switzerland, model: LabFors 4, 7L total volume) at pH 5, controlled using the onboard PID controlled on the Infors unit using 3M KOH and 1.5M H_2SO4 and 35^oC. Anaerobic conditions were maintained by sparging 0.6L/min N_2 gas into the bottom of the fermenters, which had passed through a sterilized filter. Sparging began at least 30 mins before in order to ensure that fermentation media was anaerobic before inoculation. Flow was controlled using the flow control built into the Infors bioreactor. Agitation was performed with a Rushton impeller at 150RPM.

All fermentations used the modified Biebl media described above in 5.2.1. This media used a concentration of 20g/L glycerol in order to avoid instability in fermentation and toxicity from butanol [50].

5.2.3 Analytical Methods

Fermentation products in broth were determined by High Performance Liquid Chromatography (HPLC), measured via refractive index (RI). The HPLC system was from Waters (Waters Corp. Milford, USA) and included an autosampler (Waters model 2707) and isocratic pump (Waters model 1515). Samples were separated using Hi-Plex-H guard and column (Agilent Technologies, Santa Clara, USA), held at 45^oC, and measured using a refractive index detector (Waters model 2414), held at 55^oC. The system was calibrated using a 5-point calibration for each component. A 5mM H_2SO_4 solution was used as mobile phase at a flow rate of 0.8mL/min.

Redox potential, pH, and fermentation gas content (CO_2 and H_2) were measured during fermentation. The pH probe was using a Hamilton EasyFerm Plus K8 325 (Hamilton; Reno, NV, USA) and the redox probe was using a Mettler Toledo Ingold probe (Mettler-Toledo; Wilmington, DE, USA). H_2 on bioreactor 1 was measured using a BlueSens BCP-H_2 gas analyzer (BlueSens; Herten, Germany). CO_2 and H_2 on bioreactor 2 was measured using a BlueSens BlueVary (Herten, Germany) equipped with CO2 and H2 sensors (Sensor ID: CO2—30783; H2—31068).

Labfors software (Iris V5 Pro) was used for datalogging of all online data.

Cell dry weight (CDW) was calculated by using lab vacuum to filter a 5mL sample of bioreactor media though a pre-weighed cellulose filter with average pore size of 0.2µm. The sample was then rinsed with 20mL of DI water, and the filter was then dried to a constant weight, and concentration was determined by difference from the final weight.

5.2.4 Modified Bioreactor with Cell-Recycle

An Infors HT bioreactor was modified to include a recirculation loop with a cross-flow microfiltration membrane unit to act as a cell-recycle apparatus. The membrane cartridge used was a Koch Romicon Pro microfiltratration unit (HF,1018-1.0-53-MF-0.5) with a pore size of 0.5mm, an internal volume of 40mL, and a total membrane area of 0.09m^2. A Watson-Marlow pump (Watson-Marlow 620UN) was used to recirculate media from the bioreactor, through the loop, and back to the bioreactor. All other pumps were Masterflex Compact Drive peristaltic pumps with operating ranges between 5-100mL/min. Tubing was made of either PVC, for the main recirculation loop, or silicone for all other streams. Components connecting the streams were made of polypropylene or stainless steel. A diagram of the bioreactor setup is given in Figure 29 below.

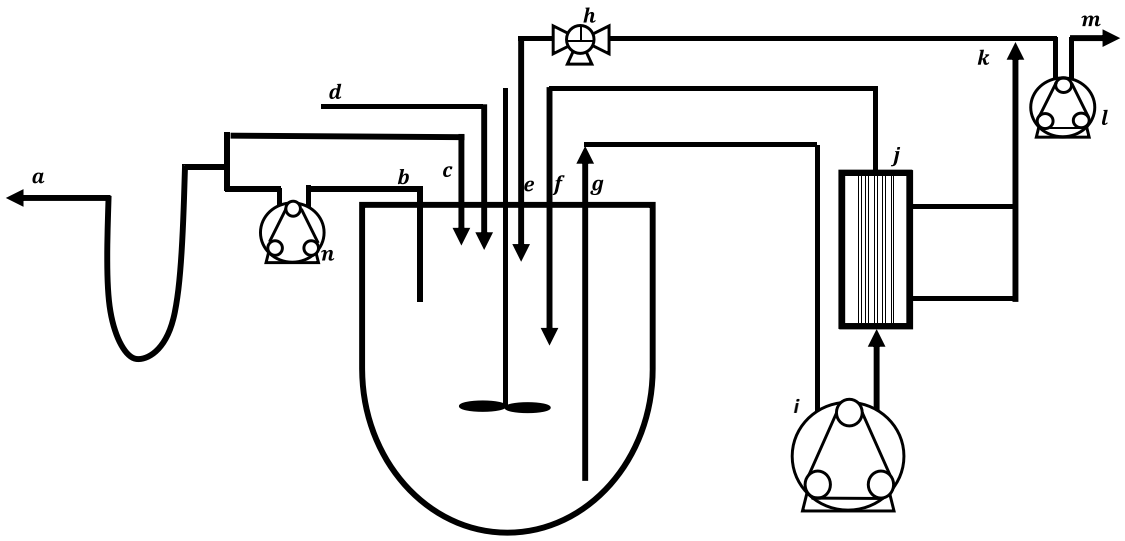

Figure 29: Diagram of full bioreactor system. *a*) Bleed system outlet (Outlet of active-passive system). *b*) Bioreactor draw to active-passive bleed system. *c*) Gas return for active-passive bleed system. *d*) Bioreactor Feed. *e*) Membrane Permeate return. *f*) Membrane Retentate return. *g*) Membrane Input draw. *h*) Three-way sample valve. *i*) Peristaltic Microfiltration Membrane input pump. *j*) Microfiltration membrane. *k*) Permeate line. *l*) Peristaltic Permeate outlet pump. *m*) Permeate outlet. *n*) Bleed pump.

5.2.5 Fed-Batch Fermentations

Fed-batch fermentations were carried out in parallel using the modified Biebl media described above. Initial fermentation was done in batch until products in fermentation gas reached a maximum, after which media was added at a rate of 1.3mL/min. Feed flows with Masterflex pumps were determined by difference in mass of feed bottles over time. Fermentations started with 20g/L glycerol, with initial volume of 5L in the cell recycle system (Bioreactor 1), and 3L in control (Bioreactor 2). Fermentations were run until the bioreactors were filled, each taking 4L of media and taking roughly 70 hours total fermentation time.

5.2.6 Continuous Fermentations

Continuous fermentations were carried out using modified Biebl media as described above. The first continuous condition was a low feed flow, low bleed (β) flow fermentation to target a high cell concentration. The feed flow was set at 5.9mL/min from 18.8h to 98.8h ($D=0.06h^{-1}$, $\beta=0.01$), however at low flow the pump used was inconsistent so flow was increased to 11.4mL/min ($D=0.14h^{-1}$, $\beta=0.48$) from 98.8h to the end of

fermentation. Permeate flow was not monitored over this fermentation, and decreased over the course of the run, so values for β are assumed based on permeate pump flow calibrations, and are approximate at best.

The second continuous fermentation condition was performed at a flowrate of 22mL/min ($D=0.26h^{-1}$). Permeate flow pump was set sufficiently high so that flow was a result of membrane performance, not the pump setting, so that maximum permeate flow could be monitored.

Feed and Permeate flow in all cases was measured by filling a pre-weighed 15mL centrifuge tube with approximately 10mL of permeate, measuring the time taken to the nearest second, and weighing the filled tube.

5.3 Comparison of Fed-Batch Fermentations With and Without Cell Recycle

Fed-batch fermentations were initially carried out in order to demonstrate that *Clostridium pasteurianum* cells can survive the stresses associated with cell recycle. Figure 30 and Figure 32 show results from two sets of parallel fermentations, where Bioreactor 1 has the integrated membrane cell recycle connected, with permeate returning to the bioreactor.

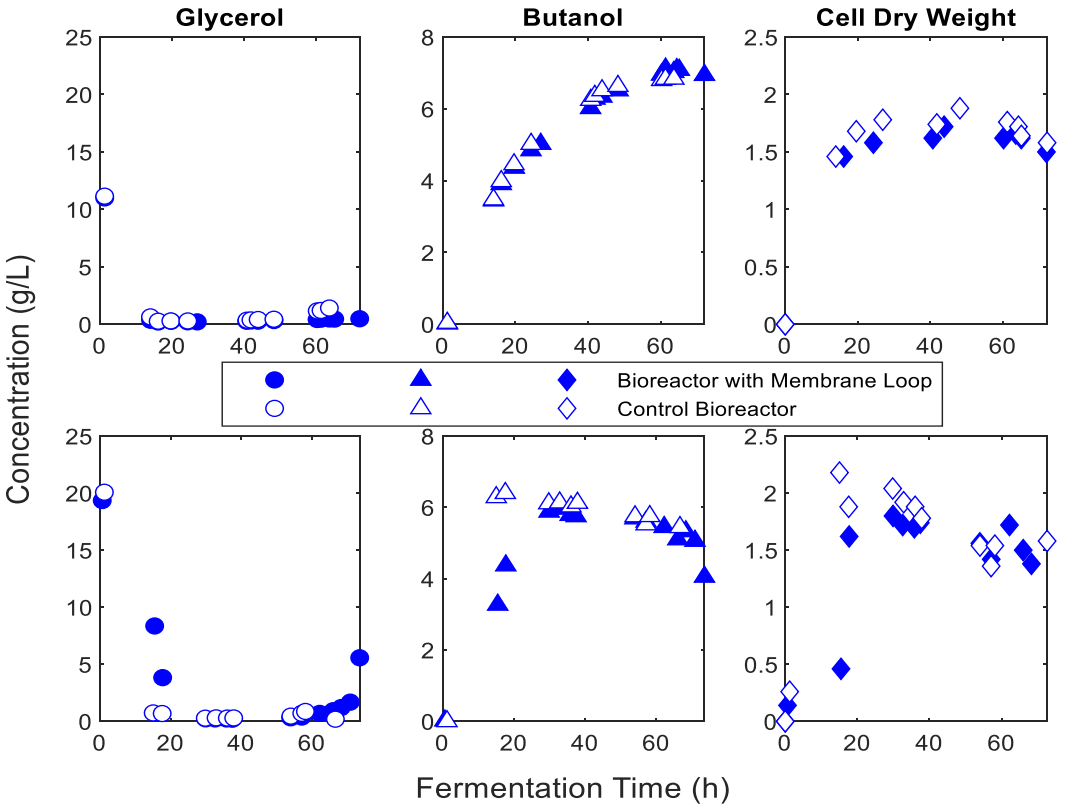

Figure 30: Glycerol, Butanol, and Cell Dry Weight (CDW) for Parallel Fed-Batch Fermentations. Each row represents a separate fermentation. Values for Bioreactor 1, with cell recycle apparatus, are shown with solid symbols, Bioreactor 2, the control, is shown by hollow symbols. Circles – Glycerol, Triangles – Butanol, Diamonds – Cell Dry Weight. All measurements are in g/L.

Bioreactor 1 has greater total volume and thus greater total initial glycerol than Bioreactor 2, the control, however since the feed flow is quite low the glycerol concentration also remains quite low after the batch phase and is comparable across all fed-batch fermentations. Also, both bioreactors have very similar butanol concentrations

throughout fermentation, and tend towards similar cell mass as measured by CDW. While Bioreactor 1 has a lower average measured CDW than Bioreactor 2 in both runs, this difference is not significant, so either there is no difference in expected cell yield or the difference is negligible. The same pattern can be seen in side products, acetate, butyrate, and 1,3-propanediol, seen below in Figure 31.

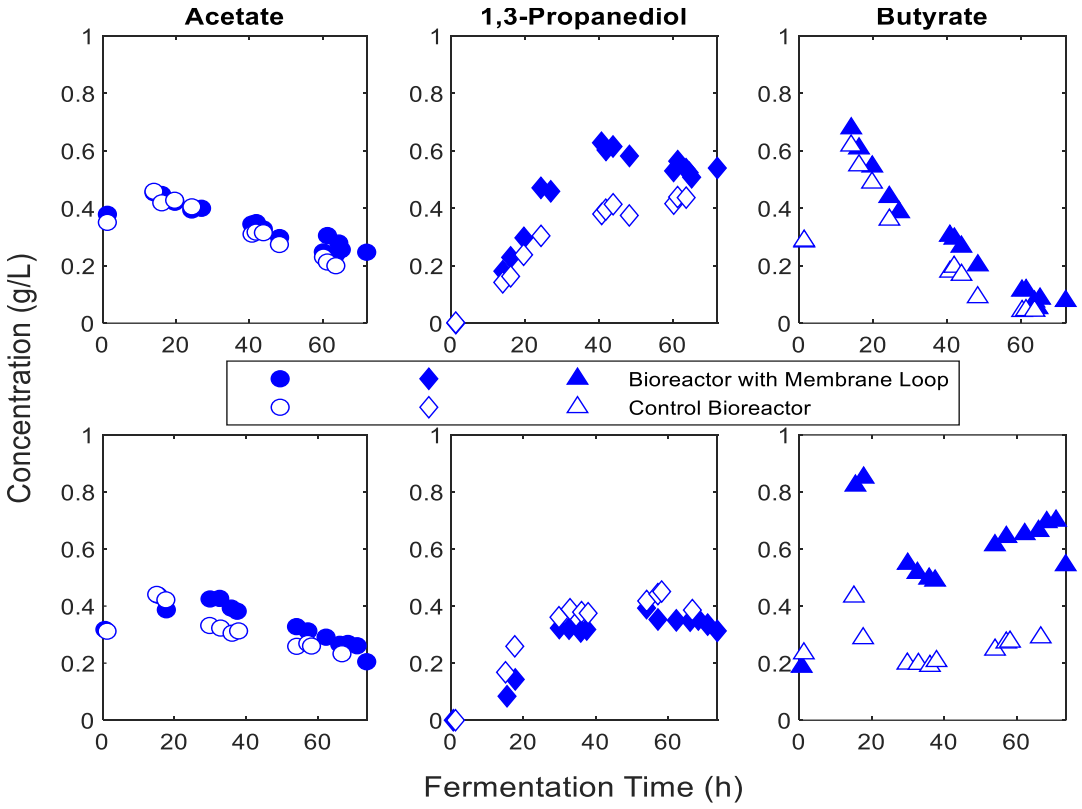

Figure 31: Acetate, 1,3-Propanediol, and Butyrate for Parallel Fed-Batch Fermentations. Each row represents a separate fermentation. Values for Bioreactor 1, with cell recycle apparatus, are shown with solid symbols, Bioreactor 2, the control, is shown by hollow symbols. Circles – Acetate, Triangles – 1,3-Propanediol, Diamonds – Butyrate. All measurements are in g/L.

Both parallel runs show that acetate and 1,3-propanediol have very similar results, both in value and how the values change during fermentation. Butyrate is closer in the first trial, however the changes in concentration in the second trial are in the same direction for both bioreactors. It should also be noted that the scale of these measurements is significantly lower, so differences are exaggerated.

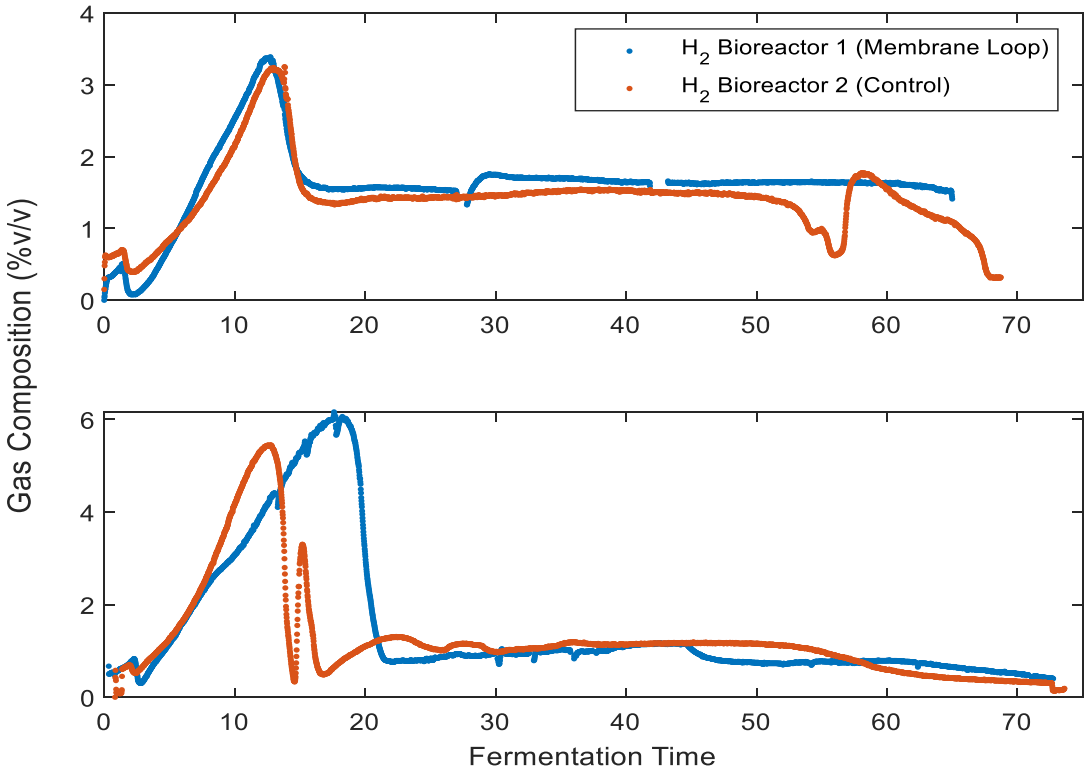

Figure 32: Hydrogen Gas Concentration in Off-Gas for Parallel Fed-Batch Fermentations.

Hydrogen gas concentration in the fermentation off gas was very similar between the two fermenters in both trials. There is a stable region between roughly 25h and 50h, where in both cases the difference in hydrogen concentration was less than 0.2%.

The comparable fermentation characteristics between the parallel bioreactors with and without the integrated membrane cell recycle suggest that the setup should be successful in continuous fermentation.

5.4 Continuous Fermentation with Cell Recycle

Two continuous fermentation were carried out with the integrated cell recycle. A low feed flow, low bleed (β) flow fermentation intended to maximize cell concentration, and high feed flow fermentation intent ended to maximize productivity.

5.4.1 Low Feed Flow, Low Bleed Flow Fermentation

The first fermentation, shown in Figure 33 and Figure 34, was a low feed flow, low bleed (β) flow fermentation, intended to produce a high cell concentration.

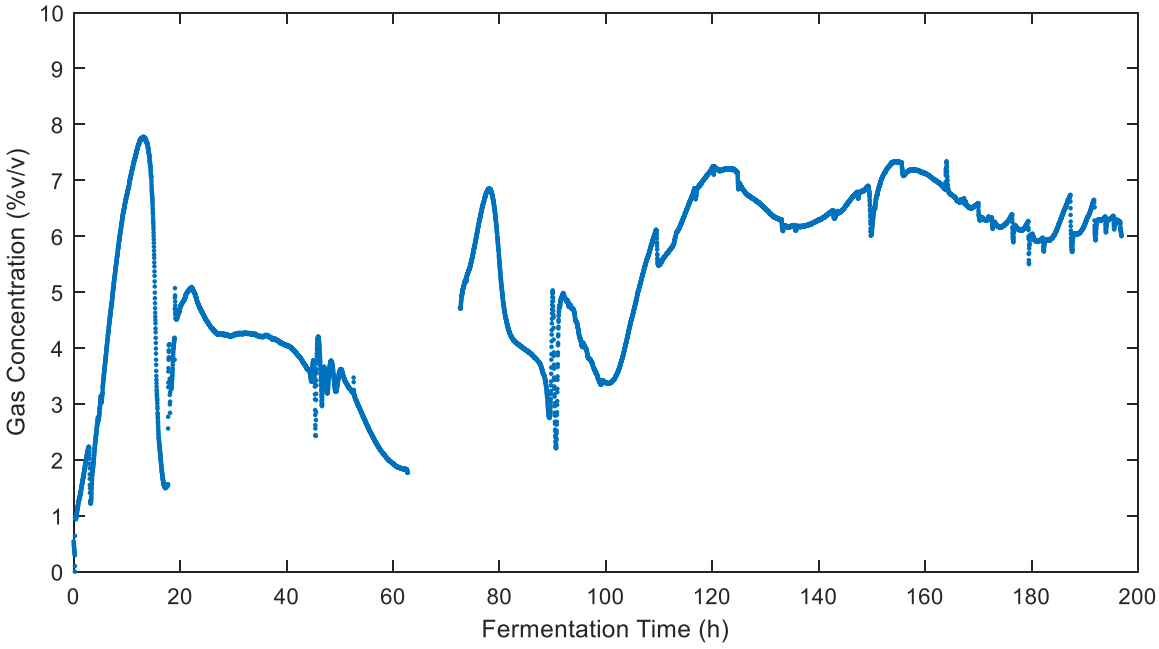

Figure 33: Hydrogen Gas Concentration in Off-Gas for Low Feed Flow, Low Beta Continuous Fermentation

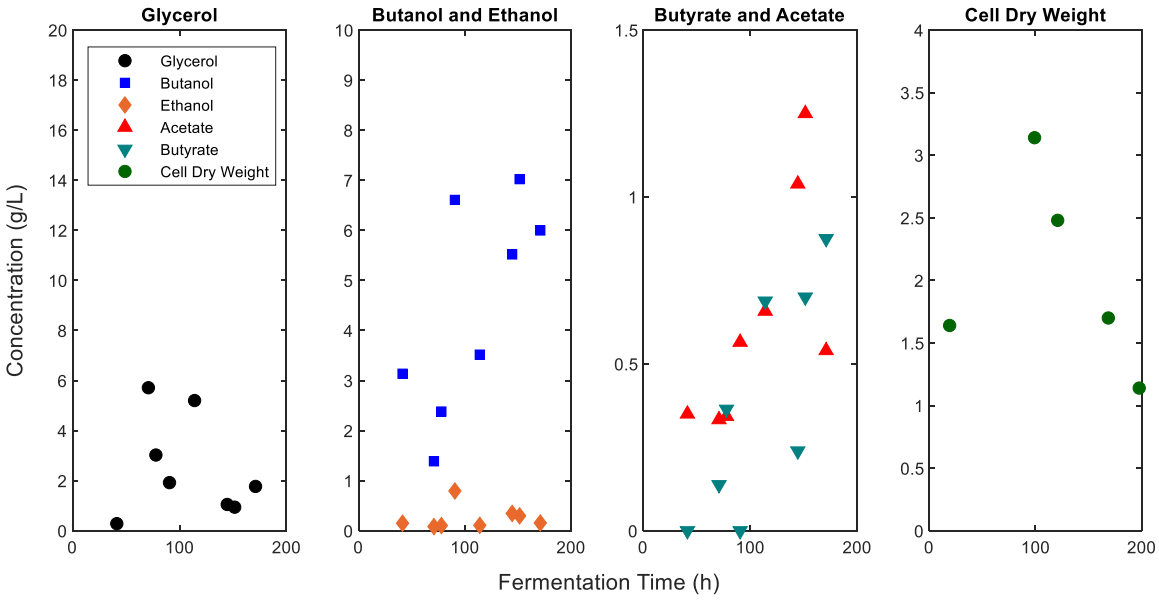

Figure 34: Glycerol, Butanol, Ethanol, Acetate, Butyrate Concentration and Cell Dry Weight for Low Feed Flow, Low Beta Continuous Fermentation

Despite the inconsistent feed and permeate flow, a high measured CDW of 3.14g/L was achieved at 99h. This is higher than literature values for continuous fermentations, and batch fermentations have achieved this cell concentration when much higher substrate concentrations were used (Table 19). Permeate CDW measurements were negligible at all measurements.

Strain	Mode	Substrate	Max CDW (g/L)	Source
DSMZ 525	Batch	10 g/L glycerol	1.3	[33]
DSMZ 525	Batch	80 g/L glycerol	3.2	[30]
DSMZ 525	Batch	70 g/L Glucose	13.2	[30]
DSMZ 525	Batch	50 g/L glycerol, 50 g/L glucose	6.1	[30]
DSMZ 525	Batch with gas stripping	105 g/L pure and crude glycerol	2.1	[34]
DSMZ 525	Continuous	10 g/L glycerol, D=0.07	0.75	[33]
DSMZ 525	Continuous with cell recycle	20g/L glycerol, D=0.06	3.14	This work

Table 19: Cell Dry Weight of *Clostridum pasteurianum* in literature

While a steady state was not achieved due to membrane fouling and operational issues, fermentation continued without issue up to and after the maximum CDW, suggesting that

cell concentration does not affect the ability for fermentation to continue in continuous operation up to that point. Additionally, with literature values extending up to over 13g/L CDW further suggests high cell concentration should not hinder fermentation [30].

5.4.2 High Feed Flow Fermentation

The second continuous fermentation was performed at a higher flowrate of 22mL/min (D=0.26), and with higher permeate flow, which was measured over fermentation to monitor fouling. Permeate flow for the second fermentation can be seen in Figure 35.

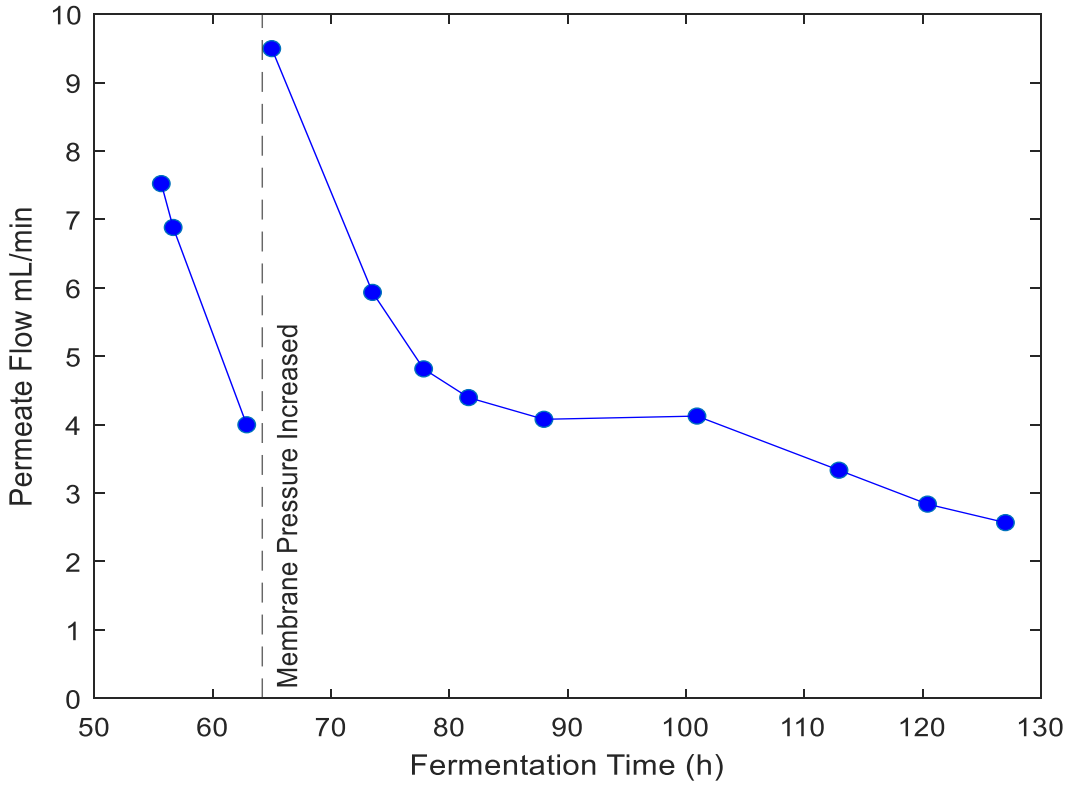

Figure 35: Permeate Flow over Duration of Fermentation with High Feed Flow, High Beta.

Pressure was increased at 64.2 hours to the maximum rated pressure for the membrane (30psi at inlet) in order to increase permeate flow and extend fermentation at higher productivity. Both permeate and feed flow were started at 55.7h into fermentation, after the peak gas concentration was reached. Hydrogen concentration in off gas was used as an indicator of fermentation and can be seen Figure 36.

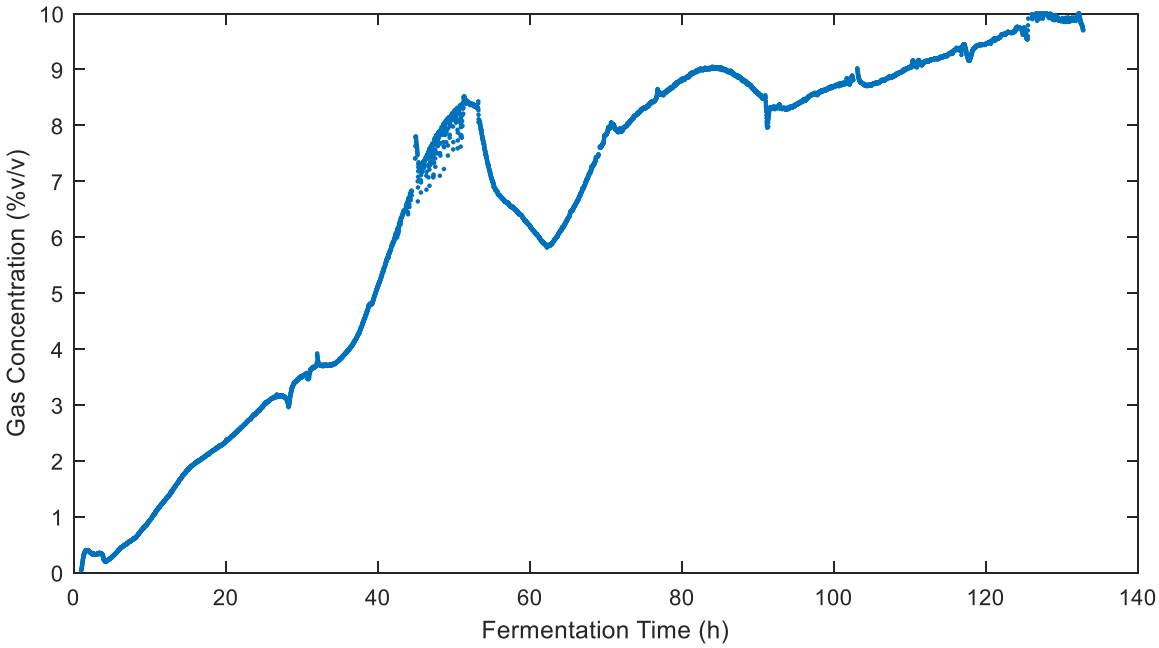

Figure 36: Hydrogen Gas Concentration in Fermentation Off-Gas in High Feed Flow, High Beta Continuous Fermentation.

After feed flow was started, glycerol concentration increased and all other concentrations decreased slightly due to dilution (Figure 37). Cell concentration also decreased after membrane pressure was increased, possibly due to increased stress on cells from the ball value. However, as fermentation continued cell concentration increased slightly and appeared to stabilize after 81h at 1.53±0.06g/L.

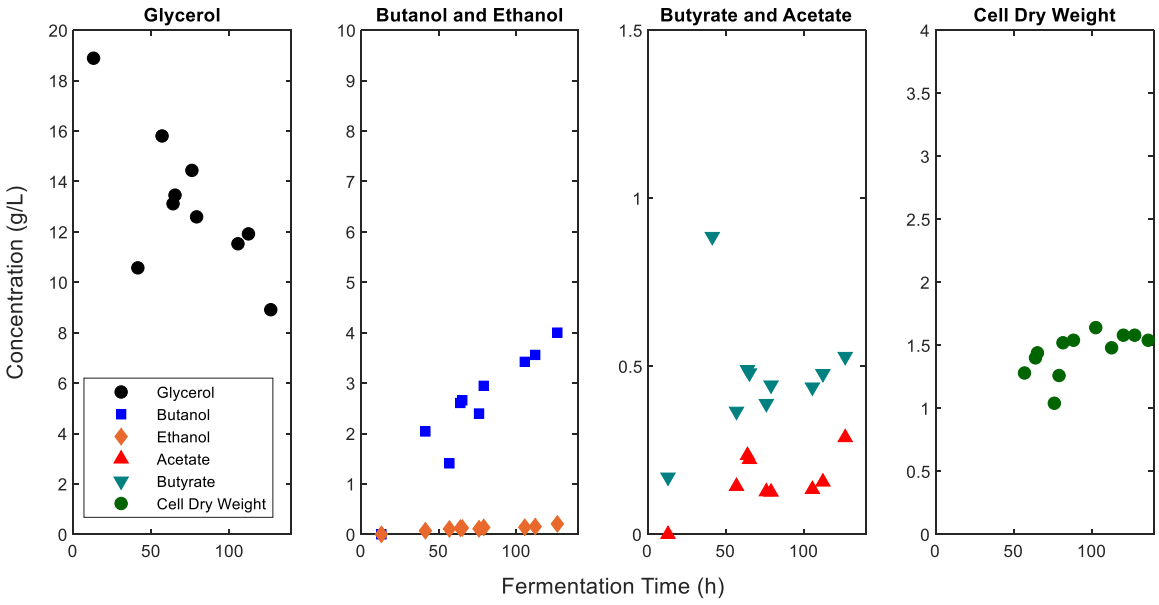

Figure 37: : Glycerol, Butanol, Ethanol, Acetate, Butyrate Concentration and Cell Dry Weight for High Feed Flow, High Beta Continuous Fermentation

As fermentation continued, even though CDW appeared to stabilize, glycerol continued to decrease and butanol continued to increase. It is not clear whether cell mass had reached steady state before glycerol and fermentation products, if the CDW was artificially high earlier in fermentation due to insoluble precipitates, such as iron or magnesium phosphates, or if another mechanism is occurring.

The increase in butanol concentration drives the productivity of the system, as it was operated at a constant flow rate. The maximum productivity reached during this fermentation was 1.16g/Lh.

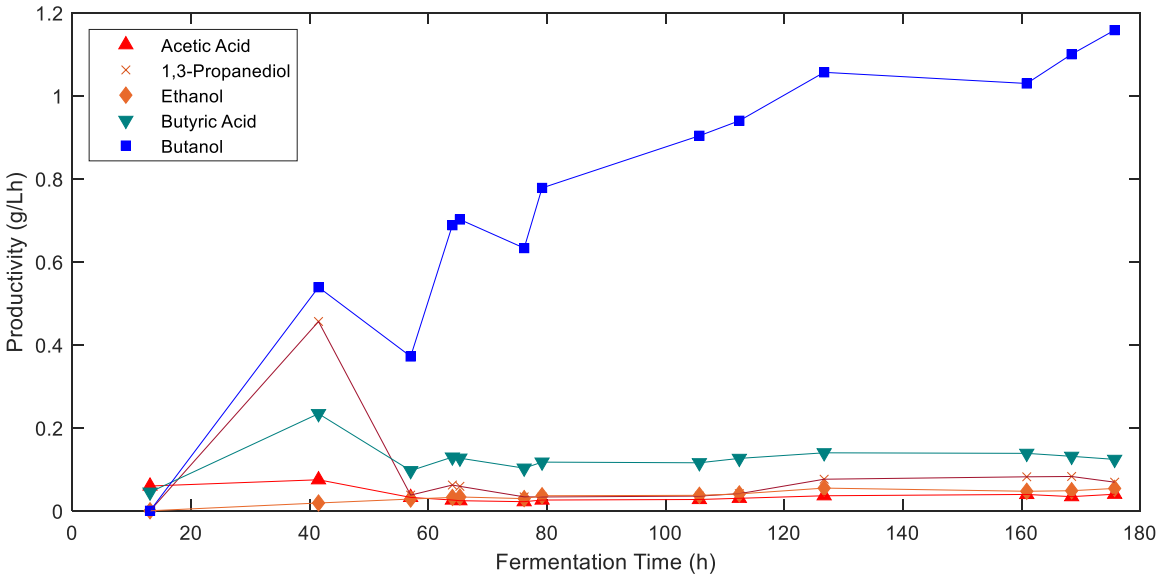

Figure 38: Productivity over Duration of Fermentation with High Feed Flow, High Bleed.

As shown in Table 18, the maximum productivity produced in this work is slightly higher than most sources, but pales in comparison to the highest values. However, all sources with higher productivities have higher substrate concentrations, genetically engineered strains, alternative process improvements, or a combination of those three. Additionally, steady state was not reached in this system, and productivity increased throughout operation, as seen in Figure 38. This work is the first to show the wild-type *Clostridium pasteurianum* in a continuous membrane cell recycle system.

The biggest hindrance to this work was the fouling of the membrane over the course of fermentation. In both continuous fermentations, lack of permeate flow was the reason for stopping the fermentations. At the end of each fermentation flow through the membrane was dominated by fermentation gas, rather than media. This is not due to the volume of gas produced, as the amount of gas production seen at the end of the low feed flow fermentation was reached in the batch phase of all fermentations, including the fed-batch fermentation, as well as midway through the high feed flow fermentation, all without gas taking over the permeate flow. This implies that the gas flow through the membrane seen at the end of both continuous fermentations is a result of the fouling of the membrane. As fouling through pore blocking proceeds, the resistance through each pore increases. When the resistance from the pore size is sufficiently high, due to the pores becoming

sufficiently small, gas transfer is favoured as the gasses have significantly lower viscosity and are more able to flow through such a significant restriction.

In studies of colloids, which can be used as an approximation of live cells, mass deposited on the membrane increases linearly with time, so long as conditions are consistent, and the rate of flux decline is linear with both transmembrane pressure and particle concentration. Additionally, porosity is similar, if not constant, with deposited mass. The result, in colloidal systems, is a decrease in flux towards a lower asymptote. As cell concentration increases, this asymptote is pushed further down [22].

In the high flow fermentation, permeate flow appears to approach an asymptote from 80h to 100h, after which permeate appears to decrease linearly. This suggests that initial fouling up to 100h is dominated by cake formation, and fouling after this is likely from pore fouling, as the only other form of resistance to flow is from the resistance of the membrane itself, which is constant. Depressurization of the membrane may help alleviate fouling from cake formation, but will not affect pore fouling [22].

Pore fouling in fermentation systems comes from two sources: organic and inorganic fouling. Organic fouling is a result of biomass, whether parts of dead cells or live cells, fouling the system through caking on the surface of the membrane and entering and blocking pores. Inorganic fouling, also known as scaling, is through the deposition of inorganic material on surfaces or within the pores.

After the first fed-batch fermentations the membrane was cleaned using a 0.5g/L NaOH solution for 1h, then rinsed with DI water. This procedure would clean organic fouling, however flow was still blocked when tested with DI water. After sitting in storage with DI water, the DI water the membrane was stored in took on a light-green colour, similar to the media the fermentation was done in, and similar to the colour of dissolved Fe^{2+}. Subsequent fermentations added a step after the caustic cleaning of a pH 2.5-3 wash using sulfuric acid. This increased permeate flow substantially after cleaning, suggesting that at least one main source of fouling is inorganic.

Iron and magnesium are necessary nutrients for butanol production, but both also precipitates with phosphate, which is also necessary [28]. It is likely that deposition of minimally soluble or insoluble iron and magnesium species are the source of inorganic fouling that resulted in the clogging of the membrane. Decreasing the phosphate concentration and optimizing the concentrations of iron and magnesium in this environment may increase the amount of time that the membrane can operate. Additionally, maintaining a low pH environment while mixing media may help keep phosphate partially hydrogenated and help maintain solubility.

Another possible way to increase the productivity of the system, even if fouling occurs at the same rate, is to increase the rate of initial biomass growth and decrease the amount of time until continuous operation is reached. This could be accomplished by having glucose in the initial media during the batch phase, as *Clostridium pasteurianum* grows faster on glucose than glycerol [41].

5.5 Conclusions and Future Work

This work is a part of a larger project, and is only one of many steps in developing this system, with the goal of building a system that both maximizes productivity and yield by integrating an *in situ* extraction process, such as pervaporation, with an intensified process, such as the work shown here with membrane cell recycle.

This work demonstrates the initial viability of the membrane cell recycle as a method for intensifying fermentation of *Clostridium pasteurianum* on glycerol to produce butanol. The bacteria grew in fed-batch operation with membrane cell recycle operating while permeate was returning to the bioreactor with no significant difference in cell growth as compared to a control fermentation.

Continuous operation was operated under low feed flow, low bleed flow for just under 200h before membrane fouling ceased permeate flow, and concentrated cells up to 3.14g/L, the highest cell concentration shown in the literature for a continuous fermentation, while removing all cells from the permeate. Under high flow conditions maximum productivity of 1.16g/Lh was achieved, which is higher than the literature

values in batch or continuous operation with wild-type *Clostridium pasteuriaum*, however studies with immobilized cells or genetically engineered strains of *Clostridium pasteuriaum* have had higher productivity. Additionally, under high flow conditions it was shown that *Clostridium pasteuriaum* can not only withstand pressure up to 30psig, but can withstand a system where pressures vary from atmospheric up to 30psig.

Future work on this should begin with media optimization to reduce membrane fouling and to create a media that would resemble what might be used industrially. Additional membrane units can be added to switch between and allow for online cleaning of membrane units for long term operation. From there, integration of pervaporation on the permeate stream will complete the benchtop scale unit. Lastly, investigating the completed system on engineered strains of *Clostridium pasteuriaum* would likely allow for further advances beyond what can be accomplished by process engineering.

On scale-up of the system, use of a decanter centrifuge for cell recycle would likely be a preferable option to the microfiltration membrane, as this would be less susceptible to fouling.

References

[1] E. Johnson, T. Sarchami, S. Kießlich, G. Munch and L. Rehmann, "Consolidating biofuel platforms through the fermentative bioconversion of crude glycerol to butanol," *World Journal of Microbiology and Biotechnology,* pp. 32-103, 2016.

[2] M. Sauer, "Industrial production of acetone and butanol by fermentation-100 years later," *FEMS microbiology letters,* vol. 363, no. 13, p. fnw134, 2016.

[3] P. Dürre, "Biobutanol: An attractive biofuel," *Biotechnology Journal,* vol. 2, no. 12, pp. 1525-1534, December 2007.

[4] Industry Arc, "N-Butanol Market - Forecast(2020 - 2025)," Industry Arc, Hyderabad, 2019.

[5] H. Biebl, "Fermentation of glycerol by Clostridium pasteurianum — batch and continuous culture studies," *Journal of Industrial Microbiology and Biotechnology,* vol. 27, pp. 18-26, 2001.

[6] T. Sarchami, G. Munch, E. Johnson, S. Kießlich and L. Rehmann, "A Review of Process-Design Challenges for Industrial Fermentation of Butanol from Crude Glycerol by Non-Biphasic Clostridium pasteurianum," *fermentation,* pp. 2-33, 2016.

[7] K. Gao, V. Orr and L. Rehmann, "Butanol fermentation from microalgae-derived carbohydrates after ionic liquid extraction," *Bioresource Technology,* vol. 206, pp. 77-85, 2016.

[8] Y. Tashiro, K. Takeda, G. Kobayashi, K. Sonomoto, A. Ishizaki and S. Yoshino, "High Butanol Production by Clostridium saccharoperbutylacetonicum N1-4 in Fed-Batch Culture with pH-Stat Continuous Butyric Acid and Glucose Feeding

Method," *Journal of Bioscience and Bioenginieering,* vol. 98, no. 4, pp. 263-268, 2004.

[9] C. Hansen, A. Hernandez, B. P. Mullan, K. Moore, M. Trezona-Murray, R. H. King and J. R. Pluske, "A chemical analysis of samples of crude glycerol from the production of biodiesel in Australia, and the effects of feeding crude glycerol to growing-finishing pigs on performance, plasma metabolites and meat quality at slaughter," *Animal Production Science,* no. 49, pp. 154-161, January 2009.

[10] Grand View Research, "Glycerol Market Size, Share & Trends Analysis Report By Source (Biodiesel, Fatty Acids, Fatty Alcohols, Soap), By Type (Crude, Refined) By End Use (Food & Beverage, Pharmaceutical), By Region, And Segment Forecasts, 2020 - 2027," Grand View Research, San Francisco, USA, 2020.

[11] F. Yang, M. A. Hanna and R. Sun, "Value-added uses for crude glycerol–a byproduct of biodiesel production," *Biotechnology for Biofuels,* vol. 5, no. 13, pp. 1-10, 2012.

[12] A. Rodrigues, J. C. Bordado and R. G. dos Santos, "Upgrading the Glycerol from Biodiesel Production as a Source of Energy Carriers and Chemicals—A Technological Review for Three Chemical Pathways," *Energies,* vol. 10, no. 1817, pp. 1-36, 2017.

[13] P. F. Verhulst, "Recherches mathématiques sur la loi d'accroissement de la population," *Nouveaux Mémoires de l'Académie Royale des Sciences et Belles-Lettres de Bruxelles,* vol. 18, p. 1–42, 1845.

[14] M. Schasechter, "A Brief History of Bacterial Growth Physiology," *Frontiers in Microbiology,* vol. 6, p. 289, 21 April 2015.

[15] J. Monod, Recherches sur la Croissance des Cultures Bactériennes, Paris: Hermann & Cie, 1942.

[16] J. Monod, "The Growth of Bacterial Cultures.," *Annu. Rev. Microbiol.,* vol. 3, p. 371–394., 1949.

[17] L. Michaelis and M. L. Menten, "Die Kinetik der Invertinwirkung," *Bio-chem. Zeitsch.,* vol. 49, pp. 333-369, 1913.

[18] J. M. Lee, "Cell Growth Measurement," in *Biochemical Engineering*, 2.1 ed., Pullman, Washington: Washington State University, 2002, pp. 5-29-33.

[19] J. M. Lee, Biochemical Engineering, Version 2.1 ed., Pullman: Department of Chemical Engineering Washington State University, 2001.

[20] M. L. Shuler, F. Kargi and M. DeLisa, Bioprocess Engineering Basic Concepts, Third Edition ed., Boston: Pearson Education Inc., 2017.

[21] C. F. Wan, T. Yang, G. G. Lipscomb, D. J. Stookey and T.-S. Chun, "Design and fabrication of hollow fiber membrane modules," *Journal of Membrane Science,* vol. 538, pp. 96-107, 2017.

[22] S. Hong, R. S. Faibish and M. Elimelech, "Kinetics of Permeate Flux Decline in Crossflow Membrane Filtration of Colloidal Suspensions," *Journal of Colloid and Interface Science,* vol. 196, no. 2, pp. 267-277, 1997.

[23] H. Choi, H.-S. Kim, I.-T. Yeom and D. D. Dionysiou, "Pilot plant study of an ultrafiltration membrane system for," *Desalination,* vol. 172, pp. 281-291, 2005.

[24] M. S. Rappé, S. A. Connon, K. L. Vergin and S. J. Giovannoni, "Cultivation of the ubiquitous SAR11 marine bacterioplankton clade," *Nature,* vol. 418, pp. 630-633, 2002.

[25] W. J. Groot, R. G. J. M. van der Lans and K. C. A. M. Luyben, "Process engineering for a membrane recycle fermentor," *Bioprocess and Biosystems Engineering,* vol. 8, no. 5, pp. 235-246, 1993.

[26] P. Pal, R. Kumar, J. Nayak and S. Banerjee, "Fermentative production of gluconic acid in membrane-integrated hybrid reactor system: Analysis of process intensification," *Chemical Engineering & Processing: Process Intensification,* vol. 122, pp. 258-268, 2017.

[27] M. Dworkin and D. Gutnick, "Sergei Winogradsky: a founder of modern microbiology and the first microbial ecologist," *FEMS Microbiology Reviews,* vol. 36, no. 2, pp. 364-379, 1 March 2012.

[28] C. Moon, C. H. Lee, B.-I. Sang and Y. Uma, "Optimization of medium compositions favoring butanol and 1,3-propanediol production from glycerol by Clostridium pasteurianum," *Bioresource Technology,* vol. 102, pp. 10561-10568, 2011.

[29] R. Gallardo, M. Alves and L. Rodrigues, "Modulation of crude glycerol fermentation by Clostridium pasteurianum DSM 525 towards the production of butanol," *Biomass and Bioenergy,* vol. 71, pp. 134-143, 2014.

[30] W. Sabra, C. Groeger, P. N. Sharma and A.-P. Zeng, "Improved n-butanol production by a non-acetone producing Clostridium pasteurianum DSMZ 525 in mixed substrate fermentation," *Applied Microbiology and Biotechnology*, vol. 98, pp. 4267-4276, 2014.

[31] R. Gallardo, M. Alves and L. Rodrigues, "Influence of nutritional and operational parameters on the production of butanol or 1,3-propanediol from glycerol by a mutant Clostridium pasteurianum," *New Biotechnology*, vol. 34, pp. 59-67, 2017.

[32] A. Malaviya, Y.-S. Jang and S. Y. Lee, "Continuous butanol production with reduced byproducts formation from glycerol by a hyper producing mutant of Clostridium pasteurianum," *Applied Microbiology and Biotechnology,* vol. 93, pp. 1485-1494, 2012.

[33] S. Kalafatakis, I. V. Skiadas and H. N. Gavala, "Determining butanol inhibition kinetics on the growth of Clostridium pasteurianum based on continuous operation and pulse substrate additions," *Journal of Chemical Technology and Biotechnology,* vol. 94, pp. 1559-1566, 2019.

[34] T. Ø. Jensen, T. Kvist, M. J. Mikkelsen, P. V. Christensen and P. Westermann, "Fermentation of crude glycerol from biodiesel production by Clostridium pasteurianum," *Journal of Industrial Microbiology and Biotechnology,* vol. 39, pp. 709-717, 2012.

[35] T. O. Jensen, T. Kvist, M. J. Mikkelsen and P. Westermann, "Production of 1,3-PDO and butanol by a mutant strain of Clostridium pasteurianum with increased tolerance towards crude glycerol," *AMB Express,* vol. 2, no. 44, pp. 1-7, 2012.

[36] V. Krasnan, M. Plz, A. C. Marr, K. Markosová, M. Rosenberg and M. Rebros, "Intensified crude glycerol conversion to butanol by immobilized Clostridium pasteurianum," *Biochemical Engineering Journal,* vol. 134, pp. 114-119, 2018.

[37] C. Groeger, W. Sabra and A.-P. Zeng, "Simultaneous production of 1,3-propanediol and n-butanol by Clostridium pasteurianum: In situ gas stripping and cellular metabolism," *Engineering in Life Sciences,* vol. 16, pp. 664-674, 2016.

[38] T. Chen, F. Xu, W. Zhang, J. Zhou, W. Dong, Y. Jiang, J. Lu, Y. Fang, M. Jiang and F. Xin, "High butanol production from glycerol by using Clostridium sp. strain CT7 integrated with membrane assisted pervaporation," *Bioresource Technology,* vol. 288, no. 121530, pp. 1-4, 2019.

[39] A. Gallazzi, B. Branska, F. Marinelli and P. Patakova, "Continuous production of n-butanol by Clostridium pasteurianum DSM525 using suspended and surface-immobilized cells," *Journal of Biotechnology,* vol. 216, pp. 29-35, 2015.

[40] T. Sarchami and L. Rehmann, "Increased Butanol Yields through Cosubstrate Fermentation of Jerusalem Artichoke Tubers and Crude Glycerol by Clostridium pasteurianum DSM 525," *ACS Omega,* vol. 4, pp. 15521-15529, 2019.

[41] W.-C. Kao, D.-S. Lin, C.-L. Cheng, B.-Y. Chen, C.-Y. Lin and J.-S. Chang, "Enhancing butanol production with Clostridium pasteurianum CH4 using sequential glucose–glycerol addition and simultaneous dual-substrate cultivation strategies," *Bioresource Technology,* vol. 135, pp. 324-330, 2013.

[42] Mathworks, "Solve nonstill differential equations - medium order method - MATLAB ode45," Mathworks, [Online]. Available: https://www.mathworks.com/help/matlab/ref/ode45.html. [Accessed 15 March 2020].

[43] J. R. Dormand and P. J. Prince, "A family of embedded Runge-Kutta formulae," *Journal of Computational and Applied Mathematics,* vol. 6, no. 1, pp. 19-26, 1980.

[44] Mathworks, "Solve system of nonlinear equations - MATLAB fsolve," Mathworks, [Online]. Available: https://www.mathworks.com/help/optim/ug/fsolve.html. [Accessed 26 April 2020].

[45] Mathworks, "Unconstrained Nonlinear Optimization Algorithms - MATLAB," Mathworks Inc, [Online]. Available: https://www.mathworks.com/help/optim/ug/unconstrained-nonlinear-optimization-algorithms.html#f3137. [Accessed 05 05 2020].

[46] E. Elbeshbishy, B. R. Dhar, H. Hafez and H.-S. Lee, "Acetone–butanol–ethanol production in a novel continuous flow system," *Bioresource Technology,* vol. 190, pp. 315-320, 2015.

[47] W. J. Lewis, T. Mattsson, Y. J. Chew and M. R. Bird, "Investigation of cake fouling and pore blocking phenomena using fluid dynamic gauging and critical flux models," *Journal of Membrane Science,* vol. 533, pp. 38-47, 18 March 2017.

[48] G. Munch, J. Mittler and L. Rehmann, "Increased Selectivity for Butanol in Clostridium Pasteurianum Fermentations via Butyric Acid Addition or Dual Feedstock Strategy," *Fermentation,* vol. 6, no. 67, pp. 1-14, 2020.

[49] L. Regestein, E. W. Doerr, A. Staaden and L. Rehmann, "Impact of butyric acid on butanol formation by Clostridium pasteurianum," *Bioresource Technology,* vol. 196, pp. 153-159, 2015.

[50] E. E. Johnson and L. Rehmann, "Self-Synchronizing Oscillatory Metabolism in Clostridium pasteurianum in Continuous Culture," *Processes,* vol. 8, no. 137, pp. 1-17, 2020.

Appendices

Appendix A: Pump Calibrations

Watson-Marlow 620UN Peristaltic Pump

Measurements for total flow were taken with the full cell recycle apparatus connected. Curves for these measurements can be seen below in Figure 39 and Figure 40. These show that above 200RPM the response of the pump is non-linear, but between 100 and 200RPM there is a linear flow curve, following the equation $Q = 0.0569RPM + 0.5679$. This curve was used to find the flow setting of 165RPM, targeting roughly 10L/min of flow used in fermentations.

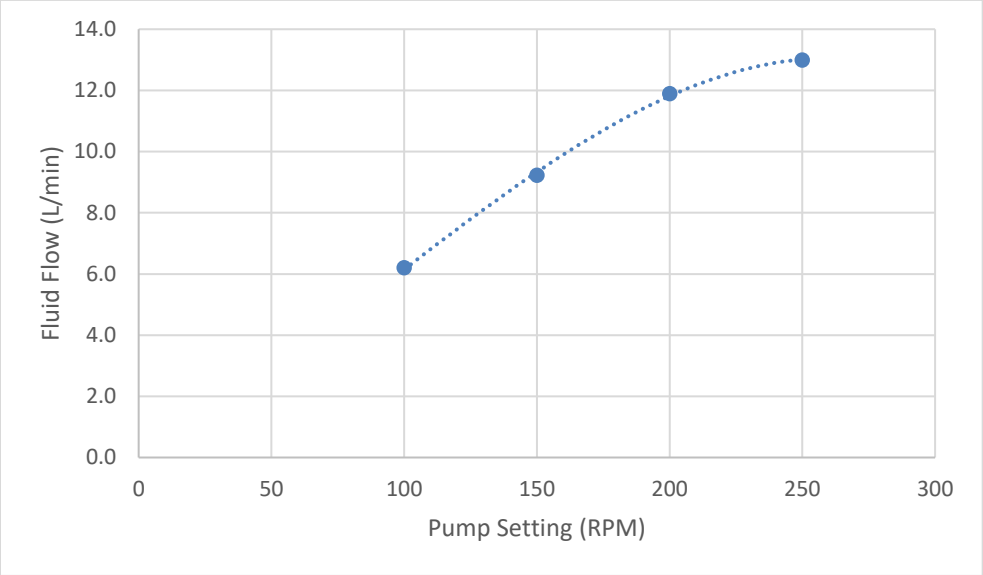

Figure 39: Watson-Marlow 620UN Flow Measurements

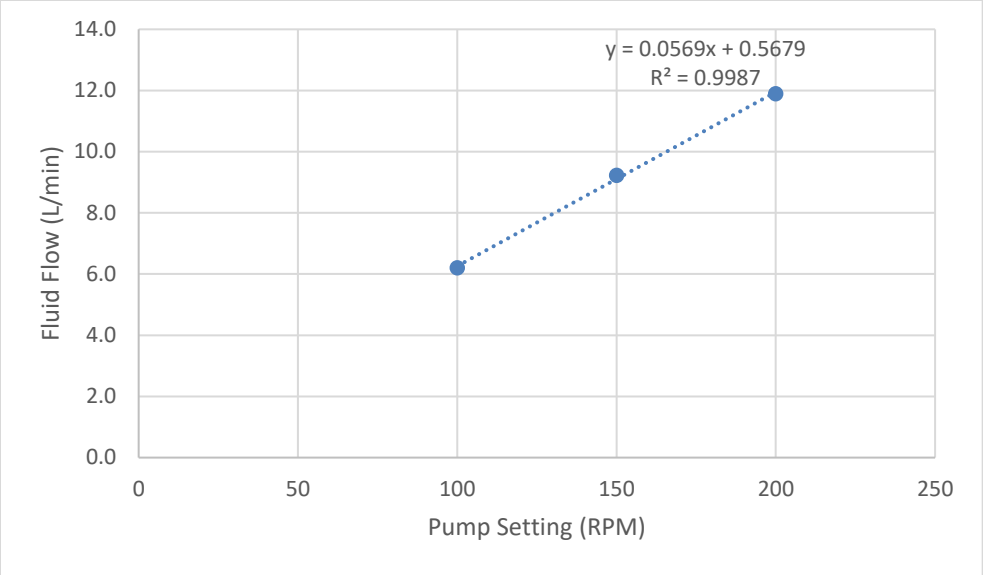

Figure 40: Watson-Marlow 620UN Calibration Curve

Appendix B: Operating Procedures for Cleaning and Sterilization of Cell Recycle Apparatus

Cleaning of Cell Recycle unit

1) Prepare 3-5L of CIP solution by at 0.5g/L NaOH
2) Recirculate CIP solution through filter at high flow rate (10L/min→160RPM on WatsonMarlow) for 60 minutes

DI Water Flush

3) 10gal DI water to drain
4) 5gal DI water recirculate through system for 15min then drain
5) 5gal DI water recirculate through system then flush out permeate, alternating between top and bottom port (5 min each, 2 flushes each), remainder of DI water to drain via retentate
6) Repeat 5

Sterilize system after CIP.

Sterilization of Cell Recycle unit

1) Prepare 3-5L of Sterilization solution by at 0.01g/L NaOH targeting 10-10.5pH and 100-200ppm sodium hypochlorite (bleach)
2) Recirculate sterilization solution through filter at high flow rate (10L/min→160RPM on WatsonMarlow) for 60 minutes
3) Flush with 3L sterilized DI water
4) Flush with 3L sterile metabisulfite solution (0.5g/L)
5) Flush with 5L sterilized DI water

NOTE: 200ppm hypochlorite is the maximum concentration, and must be used with a pH of 10-10.5. pH must never go below 9.5 with hypochlorite in solution.

Curriculum Vitae

Name:	Colin Couper
Post-secondary Education and Degrees:	University of Guelph Guelph, Ontario, Canada 2004-2012 B.Engg.
Related Work Experience	**Teaching Assistant** **The University of Western Ontario** **2018-2019**
	Quality Laboratory Technician/Coordinator **IGPC Ethanol Inc** **2012-2017**